UPPSALA
UNIVERSITET

Digital Comprehensive Summaries of Uppsala Dissertations from the Faculty of Science and Technology 1720

Magnetism in Transition Metal Systems

Interplay between structure, dimensionality and electron correlation

SAMARA KESHAVARZ HEDAYATI

ACTA
UNIVERSITATIS
UPSALIENSIS
UPPSALA
2018

ISSN 1651-6214
ISBN 978-91-513-0438-0
urn:nbn:se:uu:diva-357525

Dissertation presented at Uppsala University to be publicly examined in Polhemsalen, 10134, Ångströmlaboratoriet, Lägerhyddsvägen 1, Uppsala, Friday, 26 October 2018 at 09:15 for the degree of Doctor of Philosophy. The examination will be conducted in English. Faculty examiner: Professor Tamio Oguchi (Institute of Scientific and Industrial Research, Osaka University, Japan).

Abstract

Keshavarz Hedayati, S. 2018. Magnetism in Transition Metal Systems. Interplay between structure, dimensionality and electron correlation. *Digital Comprehensive Summaries of Uppsala Dissertations from the Faculty of Science and Technology* 1720. 94 pp. Uppsala: Acta Universitatis Upsaliensis. ISBN 978-91-513-0438-0.

In this thesis, an *ab initio* study of electronic structures and magnetic properties of transition metal systems has been presented, covering bulk, interface and surface geometries. Among them are Fe, Co, Ni, $CaMnO_3$, Co_2MnSi, a ferromagnetic Heusler alloy, as well as double-perovskites oxides such as $Sr_3(Fe_{1.25}Ni_{0.75})O_6$ and Nd_2NiMnO_6.

Their electronic structures have been obtained within the framework of the density functional theory (DFT) in combination with Hubbard type interaction such as the static correction evaluated within the Hartree-Fock method (DFT+*U*) or within the more sophisticated method of dynamical mean-field theory (DFT+DMFT). Using many-body approaches enables us to treat the correlation effects such as non-quasiparitcle states above the Fermi level for Co_2MnSi and in the half-metallic side of the Co_2MnAl/CoMnVAl heterostructure.

Based on the converged electronic structure, the magnetic excitations were mapped onto the Heisenberg Hamiltonian. Among various ways to extract exchange parameters, in this Thesis the method of infinitesimal rotation of the spins has been applied in the framework of the local magnetic force approach. It is shown that the exchange interactions on the surface of transition metals can be substantially different from those in the corresponding bulk. At the same time, the dynamical correlations lead to a slight renormalization of the magnetic couplings. For $CaMnO_3$, we demonstrated the crucial role of the atomic relaxations defining the magnetic order on the surface atoms. We were also able to extract the orbital decompositions, which helped identify the main contributions to the total exchange. For the double-perovskite systems, the extracted exchange parameters were then used to evaluate the ordering temperature using Monte-Carlo simulations, and the calculated critical temperatures were found to be in good agreement with our experimental measurements.

In a more technical investigation, the influence of the spin polarization of the DFT exchange-correlation functional on the extracted exchange parameters has been investigated. We found a very good correspondence between the computed total energies and the parametrized Heisenberg model for LDA+*U* calculations, but not for LSDA+*U*. This means that for the extraction of the exchange parameters based on total energy differences, LDA+*U* is more appropriate.

Finally, a systematic study of the emergence of the local minima in DFT+*U* calculations has been performed for the bulk of NiO, FeO, CoO and UO_2. We extended the use of the occupation matrix control method to randomly generate density matrices which help better monitor the local minima and explore the energy landscape. The effect of the Hubbard *U* and the double-counting in introducing the local minima are discussed.

Samara Keshavarz Hedayati, Department of Physics and Astronomy, Materials Theory, Box 516, Uppsala University, SE-751 20 Uppsala, Sweden.

ISSN 1651-6214
ISBN 978-91-513-0438-0
urn:nbn:se:uu:diva-357525 (http://urn.kb.se/resolve?urn=urn:nbn:se:uu:diva-357525)

to my father
1939-2014

List of papers

This thesis is based on the following papers, which are referred to in the text by their Roman numerals.

I Layer-resolved magnetic exchange interactions of surfaces of late 3d elements: Effects of electronic correlations
S. Keshavarz, Y. O. Kvashnin, I. Di Marco, A. Delin, M. I. Katsnelson, A. I. Lichtenstein, and O. Eriksson
Phys. Rev. B 92, 165129 (2015)

II Exchange interactions of $CaMnO_3$ in the bulk and at the surface
S. Keshavarz, Y. O. Kvashnin, D. Rodrigues, M. Pereiro, I. Di Marco, C. Autieri, L. Nordström, I. V. Solovyev, B. Sanyal, and O. Eriksson
Phys. Rev. B 95, 115120 (2017)

III First principle studies of the Gilbert damping and exchange interaction for half-metallic Heuslers alloys
J. Chico, S. Keshavarz, Y. O. Kvashnin, M. Pereiro, I. Di Marco, C. Etz, O. Eriksson, A. Bergman, and L. Bergqvist
Phys. Rev. B 93, 214439 (2016)

IV Half-metallicity and magnetism in the Co_2MnAl/CoMnVAl heterostructure
I. Di Marco, A. Held, S. Keshavarz, Y. O. Kvashnin, L. Chioncel
Phys. Rev. B 97, 035105 (2018)

V Magnetic properties of $Sr_{3-x}Y_x(Fe_{1.25}Ni_{0.75})O_{7-\delta}$: a combined experimental and theoretical investigation
S. Keshavarz, S. Kontos, D. Wardecki, Y. O. Kvashnin, M. Pereiro, S. K. Panda, B. Sanyal, O. Eriksson, J. Grins, G. Svensson, K. Gunnarsson, P. Svedlindh
Phys. Rev. Materials 2, 044005 (2018)

VI Curious magnetic states in double perovskite Nd_2NiMnO_6
S. Pal, S. Jana, G. Sharada, B. Pal, S. Mukherjee, S. Keshavarz, D. Thonig, Y. Kvashnin, M. Pereiro, R. Mathieu, J. Freeland, O. Eriksson, O. Karis, and D. D. Sarma
In manuscript

VII Electronic structure, magnetism and exchange integrals in transition metal oxides: role of the spin polarization of the functional in DFT+*U* calculations
S. Keshavarz, J. Schött, A. J. Millis, and Y. O. Kvashnin
Phys. Rev. B 97, 184404 (2018)

VIII A systematic study of the local minima in L(S)DA+*U*
S. Keshavarz and P. Thunström
In manuscript

Reprints were made with permission from the publishers.

Publications not included in this thesis:

- Magnetism at the surface of Heusler semiconductors
  S. Keshavarz, Y. O. Kvashnin, D. Thonig, I. Di Marco, O. Eriksson
  In preparation

- Surface magnons and critical temperatures of Ni surfaces on Cu
  D. Rodrigues, S. Keshavarz, Y. O. Kvashnin, A. Klautau, O. Eriksson, B. Hjörvarsson, A. Bergman
  In manuscript

Contents

1. Introduction

Human beings are members of a whole,
in creation of one essence and soul.

Saadi, 13th century

Our modern understanding of the electronic structure of solids is based on the concepts of charge and spin. Historically, the first experimental observation of spin quantization emerged in the year 1922 through the *Stern-Gerlach* experiment [1], where a beam of silver atoms from an oven passed through an inhomogeneous magnetic field. The screen revealed two discrete points of accumulation rather than one continuous distribution, due to the quantum nature of spin. Later on, during a short important period from 1925 to 1928, the concept of spin was theoretically developed by Uhlenbeck, Goudsmit, Heisenberg, Pauli, and Dirac. The aim was understanding of atomic spectra by means of quantum theory. In this process, two of the most important concepts in modern physics emerged, *exchange* and *spin-orbit* coupling. Moreover, analog to the classical interaction of the spin moments with an external magnetic field introduced additional concept known as *Zeeman effect*. The interplay between the exchange, the spin-orbit, and the Zeeman interactions has been the essence of magnetism research since then. In particular, they play a key role in all of condensed matter physics which is based on the concepts of charges, spins and orbital moments and their interactions [2]. Without exchange there would be no spontaneous magnetization. It determines the spin arrangement in magnetic materials, i.e., the existence of parallel (ferromagnetic), antiparallel (antiferromagnetic) spin alignment. On the other hand, the spin-orbit interaction generates orbital magnetism and couples the spin to the lattice. Through this interaction spin and charge can talk to each other through exchanging energy and angular momentum. The Zeeman interaction is used to align magnetic materials. In particular, if one needs to align a magnetic material in a specific direction the Zeeman interaction has to overcome the spin-orbit interaction which determines intrinsic spin direction, i.e. easy axis. This is because the external field in Zeeman interaction can act on both spin and orbital moments, despite the exchange interaction which is isotropic thus it only acts on the spin.

This Thesis comprises a theoretical study of magnetic materials based on $3d$ elements, so we shall put a particular emphasis on the exchange interaction because it is the largest magnetic interaction in these systems and the most difficult one to treat theoretically. Throughout this thesis, a semi-classical treatment of magnetism has been employed, where the parameters of a classical

Heisenberg model are obtained from a quantum mechanical *ab initio* calculations.

This Thesis is segmented in three main parts: Introduction, theoretical background and the contributions and outlook. In the first chapter, I expose the origin of exchange and different types of exchange mechanism in magnetic materials. In the second part in chapter 2, the electronic structure methods of this Thesis has been discussed from single- to many-body approaches. This is followed by chapter 3 where different ways to extract exchange parameters has been discussed with a special focus on the formalism used in this Thesis. Finally in the last part, I present my contributions through chapter 3−8, followed by chapter 9 where I conclude my results.

1.1 Origin of exchange

Exchange interaction is at the heart of the phenomenon of long range magnetic order and the Heisenberg Hamiltonian is the basis of most theoretical studies of magnetism in determination of the exchange interaction parameters J_{ij}. These microscopic parameters define most of macroscopic magnetic properties such as the Curie temperature (T_c), magnon dispersion curves and the magnetic response function to an external field [3, 4]. Therefore, a good knowledge of exchange parameters and the mechanisms generating them (direct exchange, super exchange, etc.) for real materials is desired [5, 6].

In order to understand the basic mechanism behind the exchange interaction, let us consider a very simple model with just two electrons with spatial coordinates $\mathbf{r}_1$ and $\mathbf{r}_2$ on atom a and atom b, as shown in Fig. 1.1 (known as Heitler-London model for the H_2 molecule [7]). The total wave function for the joint state (2-particle wavefunction) should be antisymmetric (for fermions). So, the spin part of the wave function can be either an antisymmetric singlet state χ_S (S=0), in the case of a symmetric spatial state or a symmetric triplet state χ_T (S=1), in the case of an antisymmetric spatial state. Hence, the wave functions of the singlet and triplet states can be written as

$$\begin{aligned} \Psi_S &= \tfrac{1}{\sqrt{2}}[\phi_a(\mathbf{r}_1)\phi_b(\mathbf{r}_2) + \phi_a(\mathbf{r}_2)\phi_b(\mathbf{r}_1)]\chi_S, \\ \Psi_T &= \tfrac{1}{\sqrt{2}}[\phi_a(\mathbf{r}_1)\phi_b(\mathbf{r}_2) - \phi_a(\mathbf{r}_2)\phi_b(\mathbf{r}_1)]\chi_T, \end{aligned} \tag{1.1}$$

where $\phi(\mathbf{r})$ is the single electron state. Then, the energies of the two possible states are

$$E_S = \int \Psi_S^* \hat{H} \Psi_S d\mathbf{r}_1 d\mathbf{r}_2, \qquad E_T = \int \Psi_T^* \hat{H} \Psi_T d\mathbf{r}_1 d\mathbf{r}_2. \tag{1.2}$$

It is possible to separate the spin-dependent part of the energy from the rest. In this respect, the Hamiltonian can be rewritten in the form of an effective

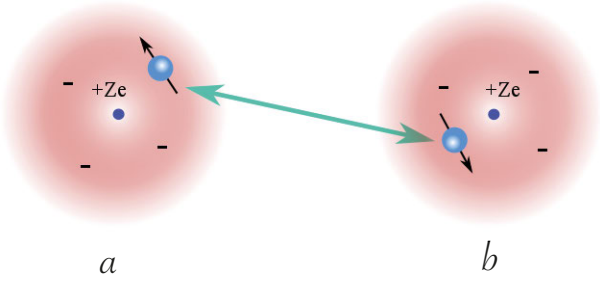

Figure 1.1. Symmetric representation of a two-particle model which illustrates the phenomenon of the direct exchange. Two electrons feel each other through Coulomb interaction between the corresponding electron densities and exchange interaction which appears for indistinguishable fermionic wavefunctions.

Hamiltonian [6]

$$\hat{H}_{eff} = \frac{1}{4}(E_S + 3E_T) - (E_S - E_T)\mathbf{S}_1 \cdot \mathbf{S}_2. \tag{1.3}$$

For a singlet state $\mathbf{S}_1 \cdot \mathbf{S}_2 = -\frac{3}{4}$, while for a triplet state $\mathbf{S}_1 \cdot \mathbf{S}_2 = \frac{1}{4}$. By inserting these values into Eq. (1.3) we can obtain energies compatible with Eq. (1.2). Now, the Eq. (1.3) is the sum of a constant term and a term which depends on the spins. The spin-dependent term in Eq. (1.3) can be used to define the exchange constants (exchange integrals). Hence, the effective spin Hamiltonian can be simply rewritten as

$$\hat{H}^{spin} = -J\mathbf{S}_1 \cdot \mathbf{S}_2. \tag{1.4}$$

Since $\hat{H}^{spin}$ depends on the scalar product of the spin moments, it will favor parallel spins if J is positive and antiparallel if J is negative. Of course, this depends on the convention used for the minus sign, but in the rest of this thesis we will adopt this definition. The equation (1.4) is relatively simple for two electrons, but generalizing it to a many body system is far from trivial. However, this equation can still be applied for atoms in a real material and leads to the Heisenberg model:

$$\hat{H} = -\sum_{ij} J_{ij}\mathbf{S}_i \cdot \mathbf{S}_j, \tag{1.5}$$

where J_{ij} is the exchange constant between the ith and jth spins. The calculations of exchange integrals in many body systems are in general complicated. Here we present a brief overview of some types of exchange interaction arising from the direct or indirect Coulomb interaction between the electrons from two different ions. For more details, we refer the interested readers to the books by Ashcroft [5] and Fazekas [8].

Next, we discuss different types of exchange mechanism that can exist in magnetic systems:

Direct exchange:
In the previous section we explained a two-particle system where the one-particle bases $\phi_a(\mathbf{r})$ and $\phi_b(\mathbf{r})$ are orthogonal, i.e., the overlap matrix is zero

$$\mathscr{O} = \int \phi_a^*(\mathbf{r})\phi_b(\mathbf{r})d\mathbf{r} = 0. \tag{1.6}$$

In this case the value of J in Eq. (1.5) only depend on the exchange integral [8]. However, if the one-particle bases are not orthogonal, Eq. (1.6) will have a finite value of $\mathscr{O} > 0$. In this case, not only the exchange integral but also the Coulomb integral will contribute in the calculation of the exchange parameters. To be more clear, let us define two quantities as following: Coulomb integral (U_{ab}) and exchange integral (J_{ab}) in orthogonal basis

$$U_{ab} = \int \phi_a^2(\mathbf{r}_1)\left(\frac{1}{R_{ab}} + \frac{1}{r_{12}} - \frac{1}{r_{r_{a1}}} - \frac{1}{r_{b2}}\right)\phi_b^2(\mathbf{r}_2)d\mathbf{r}_1 d\mathbf{r}_2, \tag{1.7}$$

$$J_{ab} = \int \phi_a^*(\mathbf{r}_1)\phi_b^*(\mathbf{r}_2)\left(\frac{1}{R_{ab}} + \frac{1}{r_{12}} - \frac{1}{r_{r_{a1}}} - \frac{1}{r_{b2}}\right)\phi_a(\mathbf{r}_2)\phi_b(\mathbf{r}_1)d\mathbf{r}_1 d\mathbf{r}_2. \tag{1.8}$$

where R_{ab} is the proton-proton distance, r_{12} is the electron-electron distance, and $r_{a1}(r_{b2})$ is electron-proton distance. The exchange parameter J in Eq. (1.5) can be defined as follows (a complete derivation can be found in the book by Fazekas [8])

$$J = \begin{cases} J_{ab} & \text{Orthogonal basis} \\ \frac{J_{ab} - \mathscr{O}^2 U_{ab}}{1-\mathscr{O}^4} & \text{Non-orthogonal basis} \end{cases} \tag{1.9}$$

At sufficiently large overlap, the exchange coupling J tend to be antiferromagnetic. Note that the value of the true observed exchange parameter does not depend on the choice of orbitals, as it is a physical interaction.
To conclude, direct exchange interaction is based on the overlap of electronic wavefunctions and are very short-ranged, confined to electrons in orbitals on the same atom (intra-atomic exchange) or nearest neighbor atoms. In the former, the single-electron wavefunctions are orthogonal and the coupling is strictly ferromagnetic. This is a so-called Hund's intra-atomic exchange.

Indirect exchange in metals:
This form of exchange interaction is known as the Ruderman, Kittel, Kasuya and Yosida (RKKY) interaction. RKKY is the dominant magnetic coupling between rare-earth ions in their elemental phases and intermetallic compounds. The basic idea of RKKY mechanism is that the exchange interaction between localized moments can be mediated by conduction electrons. A

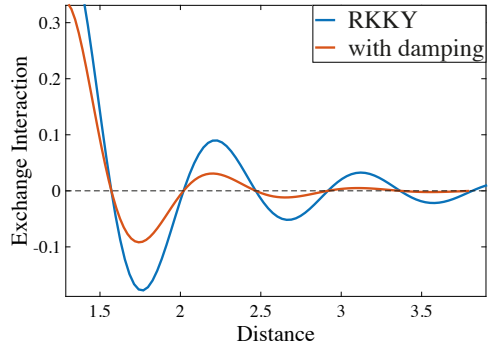

Figure 1.2. Indirect exchange in metals. Depending on the strength of ferromagnetism in the system, RKKY (Eq. 1.11) or damping (Eq. 1.12) character can be pronounced in long range.

localized magnetic moment induces the spin polarization to the conduction electrons and this polarization in turn couples to another localized magnetic moment at a distance **r** from it. The exchange interaction, in this case, is indirect because it does not involve the direct overlap of the wavefunctions. The RKKY exchange coupling has a peculiar asymptotic behavior at large distances and, as explained in Ref. [9], it can also occur in transition metal systems. In the limit of large distance (R_{ij}) between the two atoms i and j, the exchange interaction (J_{ij}) takes the form of

$$J_{ij} \propto \mathrm{Im}\frac{\exp[i(\mathbf{k}_F^{\uparrow}+\mathbf{k}_F^{\downarrow})\cdot\mathbf{R}_{ij}]}{R_{ij}^3}, \tag{1.10}$$

where $\mathbf{k}_F^{\uparrow}(\mathbf{k}_F^{\downarrow})$ is the Fermi wave vector for the spin up (down) channel. If both majority and minority spin bands are partially occupied, both Fermi wave vectors are real and one obtains

$$J_{ij}(r) \propto \frac{\sin[(\mathbf{k}_F^{\uparrow}+\mathbf{k}_F^{\downarrow})\cdot\mathbf{R}_{ij}]}{R_{ij}^3}. \tag{1.11}$$

The materials which show this kind of exchange interaction are called *weak ferromagnets*. As is clear from Eq. (1.11), this interaction has an oscillatory dependence on the distance between the magnetic moments (Fig. 1.2). Hence, depending on the distance it may be either ferromagnetic or antiferromagnetic. On the other hand, for an ideally strong ferromagnet; a material in which the majority spin band is fully occupied, the Fermi level lies in a band gap for this spin-channel. Therefore, we get an imaginary $\mathbf{k}_F$ for this spin-projection, i.e.,

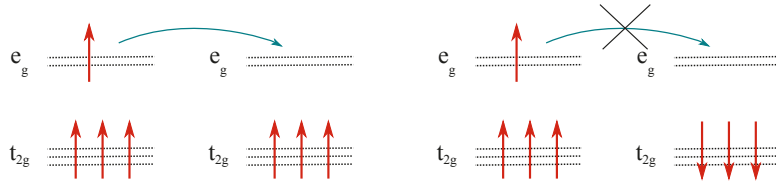

Figure 1.3. The double exchange interaction gives rise to ferromagnetic coupling between Mn^{+3} and Mn^{+4} ions, if neighboring atoms are ferromagnetically aligned.

$k_F^{\uparrow} = i\kappa_F^{\uparrow}$.[1] In this case the exchange interaction takes the form

$$J_{ij}(r) \propto \frac{\sin(\mathbf{k}_F^{\downarrow} \cdot \mathbf{R}_{ij}) \exp(-\kappa_F^{\uparrow} \cdot \mathbf{R}_{ij})}{R_{ij}^3}. \tag{1.12}$$

Therefore, for a weak ferromagnet like Fe, we expect a more pronounced RKKY interaction, while for strong ferromagnets like Co and Ni this type of interaction is more suppressed [4].

Double exchange:
In some oxides, the ions display mixed valence states (multiple oxidation states of the same element). For example, some compounds contain Mn ions in valence state 3 and 4, i.e. as Mn^{4+} and Mn^{3+}. Then it is possible to have a ferromagnetic exchange interaction, due to the double exchange mechanism as shown in Fig. 1.3. The e_g electron on a Mn^{3+} ion can hop to a neighboring site only if there is an empty orbital of the same spin (since hopping proceeds without spin-flip). If the neighbor is a Mn^{4+} ion which has no electron in its e_g shell, this should not present any problem. However, there is a strong intra-atomic exchange interaction between the e_g electron and the three electrons in the t_{2g} level. This interaction corresponds to the first Hund's rule and it wants to keep all spins aligned in the same direction. Thus it is not energetically favorable for an e_g electron to hop to a neighboring ion in which the t_{2g} spins are antiparallel to the e_g electron. Therefore, the system aligns ferromagnetically to save energy. Moreover, the ferromagnetic alignment allows the e_g electrons to hop through the crystal and the material becomes metallic.

Indirect exchange in ionic solids (superexchange):
There is a number of ionic solids, like transition metal oxides, where the ground states is magnetic. In these materials the direct overlap between d-

[1] In ideally strong ferromagnets, there is a gap in one of the spin channels. Thus, the Fermi surface is not well-defined. However, one can compute the Fermi velocity and it will become imaginary, because the states in the gap exponentially decay; the gap acts as a barrier for electrons to move.

orbitals is generally so small that d-electrons can only move through hybridization with the ligand atoms (e.g oxygen $2p$-bands). This hybridization provides a type of exchange mechanism known as superexchange [10]: an indirect exchange interaction between non-neighboring magnetic ions mediated by a non-magnetic ion (e.g. O) which is placed in between the magnetic ions (see Fig.1.4). The interaction arises due to the competition between the kinetic exchange energy and the Coulomb repulsion [11]. The Hamiltonian used to describe this kind of interaction is the Hubbard Hamiltonian

$$H = \sum_{ij} t_{ij} c^{\dagger}_{i\sigma} c_{j\sigma} + U \sum_{i} \hat{n}_{i\uparrow} \hat{n}_{i\downarrow}. \tag{1.13}$$

The first term is the kinetic term; t_{ij} stands for the electron hopping between two different atoms and c_σ ($c^{\dagger}_{\sigma}$) represents the annihilation (creation) operator of an electron with spin σ. The second term is the Coulomb intra-atomic repulsion with U being the energy cost of having two electrons with opposite spins on the same atom. More discuss about this Hamiltonian is given in the next chapter. Here we only mention that in itinerant systems (metallic state) the first term dominates ($t_{ij} >> U$), while in localized systems (insulator) two different situations can happen which affect the strength of the superexchange. For example, in *early* transition metal oxides with cubic symmetry, t_{2g} states are partially filled while e_g states are empty. Hence, the hybridization with O is relatively small (because t_{2g} orbitals point away from the $2p$ oxygen orbitals). As a result, super-exchange interaction becomes quite weak. On the other hand, in *late* transition metal oxides the e_g manifold start getting occupied and since these states point to the *2p* states of O, their hybridization is stronger. As a result, the superexchange mechanism is more important mechanism in late transition metal oxides than for early ones. It is usually antiferromagnetic, but in some situations it can be ferromagnetic.

Empirically, the sign is determined by *Goodenough-Kanamori-Anderson rules* [12, 10, 13]. They are based on the symmetry relations and electron occupancy of the overlapping atomic orbitals. According to these rules:

- A 180° superexchange of two magnetic ions with partially filled d shells is AFM if the virtual electron transfer is between the overlapping orbitals that are each half-filled, but it is FM if the virtual electron transfer is from a half-filled to an empty orbital or from a filled to a half-filled orbital.
- A 90° superexchange interaction is FM and much weaker.

For example, in the case of $CaMnO_3$ bulk; the nearly 180° Mn-O-Mn bridge shows an AFM coupling as a result of the electron transfer from the half-filled t^3_{2g} of one Mn ion to the half-filled t^3_{2g} of another Mn (Paper II). While in the case of $NdNiMnO_6$, the Ni-O-Mn shows a FM coupling due to the electron transfer from the half-filled e^3_g of Ni to the empty e^0_g states of Mn (Paper VI).

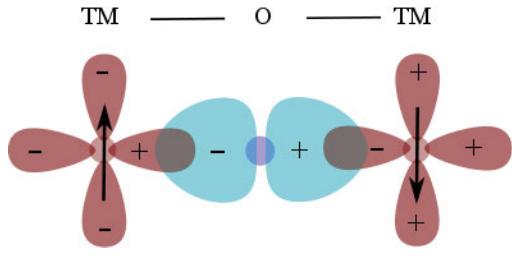

Figure 1.4. Superexchange or indirect coupling in a magnetic oxide as a result of the overlap of magnetic orbitals with a non-magnetic orbitals like the *p* states of O atom.

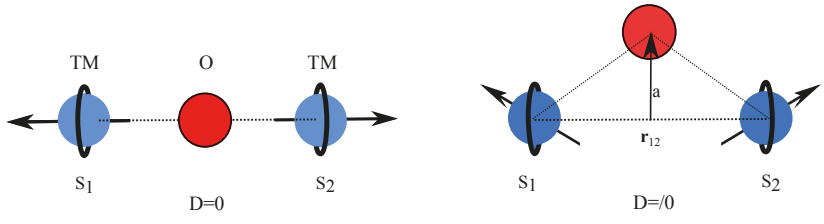

Figure 1.5. Schematic representation of anisotropic exchange interactions due to the lack of inversion symmetry.

Anisotropic exchange interactions:
It is also possible for the spin-orbit interaction to play a role similar to what oxygen atoms do in superexchange. This happens for certain compounds, like $MnCO_3$ and $CoCO_3$, where lack of inversion symmetry together with spin-orbit coupling gives rise to the antisymmetric anisotropic exchange interaction called Dzyaloshinski-Moriya (DM) interaction. For example, the DM interaction between two spins has the following form

$$H_{DM} = \mathbf{D}_{12} \cdot \mathbf{S}_1 \times \mathbf{S}_2 \qquad \mathbf{D}_{12} \sim \lambda \mathbf{a} \times \mathbf{r}_{12}. \tag{1.14}$$

The DM interaction is characterized by a vector $\mathbf{D}$, proportional to the spin-orbit coupling constant λ. In most cases, it depends on, e.g., the position $\mathbf{a}$ of the O ion between the two magnetic transition metal ions (see Fig. 1.5). The vector $\mathbf{D}$ vanishes when the crystal has an inversion symmetry with respect to the center between the two magnetic ions.

To conclude, in Fig. 1.6 we show a schematic representation of all these exchange mechanisms. Depending on whether the materials are metals or insulators and which type of magnetic atoms (rare earth or transition elements) are involved one or more of the exchange mechanisms can emerge. The most complicated situation is seen in 3*d* transition metals. In these materials, 3*d* electrons are partially localized on the atomic sites and also partially delocalized into the crystal. Furthermore, these two aspects can not be distinguished

completely due to correlated features of the 3d electrons.
Although these types of exchange mechanisms are suggested for different cases and can be applied to various situations appropriately, there are no clear borderlines between them. They are related to each other, and there are overlaps of their regimes of applicability.

Empirical values of the exchange parameters for ferromagnetic materials can be estimated from specific heats and from spin-wave spectra, whereas their theoretical estimation has been one of the most challenging problems in magnetism. Beside attempts based on combining electronic structure calculations with model Hamiltonian methods, the biggest obstacle is that, in comparison to the orbital interactions which lead to chemical bonding, the spin interactions between magnetic ions responsible for magnetic properties are closely packed in energy (of the order of meV or less), which makes it impossible to understand the magnetic properties of a system by focusing only on one or a few magnetic energy levels. Indeed, what is needed is a spectrum of the magnetic excitation energies. This can be described by a spin Hamiltonian which in a very general form has been defined as

$$\hat{H} = -\sum_{ij} J_{ij}\hat{S}_i \cdot \hat{S}_j + \sum_{ij} \vec{D}_{ij} \cdot (\hat{S}_i \times \hat{S}_j) + \sum_i A_i(\hat{S}_i)^2 + \sum_{ij} K_{ij}(\hat{S}_i \cdot \hat{S}_j)^2, \quad (1.15)$$

where the first term represents the symmetric exchange interactions, the second term the antisymmetric exchange interactions, the third term the single-ion (magnetocrystalline) anisotropy, and the last term is the biquadratic interaction. The symmetric exchange is known as the Heisenberg exchange, and the antisymmetric exchange as the DM interaction. DM interaction together with the single-ion interaction are a consequence of the relativistic corrections due to spin-orbit coupling.

For the materials studied in this thesis the first term is investigated. Because in most magnetic materials such as many of transition metals compounds, the first term is the leading term in the Hamiltonian due the strong local magnetic moment, while the remaining terms are supposed to be relatively small. The method used for the calculations of exchange parameters is explained in chapter 3. But before that a discussion on the theory and methods used to study the electronic structure of the materials in this Thesis is presented, which will come in the next chapter.

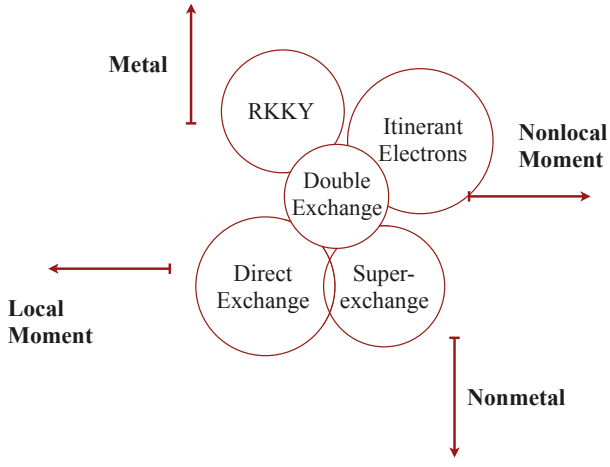

Figure 1.6. Different exchange interaction mechanism. In real materials, it is possible to have several exchange interactions coexist.

2. Electronic structure

In this chapter we explain the theory of electrons in solids. Atoms, molecules, clusters or solids are systems composed of mutually interacting electrons and nuclei. The non-relativistic time-dependent Hamiltonian of a system with mutual interaction through Coulomb forces, can be defined via the Schrödinger equation as [5, 14]

$$H_{tot} = \sum_i \frac{\mathbf{p}_i^2}{2m_e} + \sum_I \frac{\mathbf{P}_I^2}{2M_I} + \sum_{Ii} \frac{z_I e^2}{|\mathbf{R}_I - \mathbf{r}_i|} + \frac{1}{2}\sum_{i\neq j} \frac{e^2}{|\mathbf{r}_i - \mathbf{r}_j|} + \frac{1}{2}\sum_{I\neq J} \frac{z_I z_J e^2}{|\mathbf{R}_I - \mathbf{R}_J|}, \tag{2.1}$$

wherein $\mathbf{r}_i$ ($\mathbf{R}_I$) are the coordinates of the electrons (nuclei), $\mathbf{p}_i$ ($\mathbf{P}_I$) the momenta of the electrons (nuclei), m_e the mass of the electrons, M the mass of the nuclei and z_I the charge of the nuclei.
The first and obvious hint to attack this Hamiltonian is suggested by the large difference between the electron and the nuclear masses, which makes the nuclei less mobile than the electrons. Born-Oppenheimer approximation suggests to drop the kinetic energy of the nuclei in Eq. (2.1). This implies that the nuclear positions become classical variables and the nuclei can be considered as fixed in a given selected configuration; most often "fixed" means the equilibrium configuration. Consistently, this approximation goes even further by considering the nuclear repulsion (the last term in the above Hamiltonian) as a constant for any fixed configuration. Although the neglected terms can be very important to determine the total energy of a system or its cohesive energy, we can first ignore them and then take them into account when needed.

2.1 Density functional theory

For a many-body system consisting of N particles, the total wavefunction is a function of all the spatial degrees of freedom of the particles (3N) times the spin degrees of freedoms. For a real material with N close to the Avogadro number, finding the exact wavefunction becomes impossible. Density functional theory (DFT) has provided a good way to circumvent this problem, since its introduction in the 1960s [15, 16].
The basic idea in DFT is to shift the attention from the ground state *many-body* wavefunction to the much more manageable ground state *one-body* electron density n($\mathbf{r}$), which is a function of only 3 variables plus spin-degrees of freedom. In this way the ground state energy of a many-body system can be

expressed as a functional of the one-body density such that minimization of this functional in principle allows the determination of the actual ground state density. This idea originates from the Hohenberg-Kohn theorem [17], which together with the Kohn-Sham formalism forms the basis of DFT.

2.1.1 Hohenberg-Kohn theorems

The rules of quantum mechanics state that an external potential (V_{ext}) determines all the properties of an interacting system, including the density. But it is not clear if knowing the density is sufficient to obtain the external potential. The Hohenberg-Kohn theorems give the answer to this question. These theorems are summarized in three statements [17].

Statement 1 (*Uniqueness*): the ground state expectation value of any operator is a unique functional of the ground state density n(**r**). Hence, if we know the density, we can uniquely determine the ground state observables without finding the many-body wavefunctions. According to this statement, the ground state energy of a system can be expressed as a functional, as follows

$$E[n] = \langle \Psi[n] | T + V_{ee} + V_{ext} | \Psi[n] \rangle \,, \tag{2.2}$$

where T is the kinetic energy of electrons, V_{ee} is the electron-electron interaction and V_{ext} is the external potential experienced by the electrons from nuclei. Since the external potential uniquely defines the Hamiltonian, this statement implies that no two Hamiltonians and therefore no two external potentials can give the same ground state density, i.e., there is a one-to-one correspondence between $v_{ext}(\mathbf{r})$ and $n(\mathbf{r})$ (Fig. 2.1). Thus, all the quantities in the right hand side of Eq. 2.2 are functions of only density, e.g., $E[n]$, $T[n]$, $V_{ee}[n]$ and $V_{ext}[n]$. There are several ways to prove this theorem that can be found in the literature regarding density functional theory [15, 17, 18].

Statement 2 (*Variational Principle*): The exact ground state density minimizes the total energy functional in equation (2.2). This statement makes it possible to derive a scheme to find the ground state charge density. We will discuss this scheme in the next section.

For the third statement, we consider that the part of the energy functional associated with the external potential can be singled out and the remaining terms can be included in a new functional $F[n]$ containing the kinetic energy and the electron-electron interaction energy. The total energy functional can then be written as

$$E[n] = F[n] + \int d\mathbf{r} v_{ext}(\mathbf{r}) n(\mathbf{r}). \tag{2.3}$$

where $V_{ext} = \sum_i v_{ext}$.

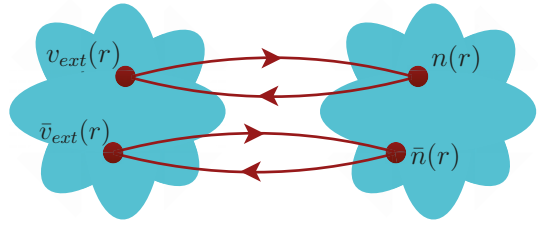

Figure 2.1. There is a one-to-one correspondence between the ground state density of an N electron system and the external potential acting on it.

Statement 3 (*Universality*): The functional $F[n]$ is *universal* in the sense that it does not depend on $V_{ext}(r)$, i.e., it is the same functional for all electronic structure problems and can be written as

$$F[n] = T_0[n] + \frac{1}{2}\int d\mathbf{r}d\mathbf{r}' \frac{n(\mathbf{r})n(\mathbf{r}')}{|\mathbf{r}-\mathbf{r}'|} + E_{xc}[n], \tag{2.4}$$

where $T_0[n]$ is the kinetic energy of a non-interacting electron gas with the density $n(\mathbf{r})$, and the second term is recognized as the classical Coulomb interaction. The functional $E_{xc}[n]$ is called the exchange and correlation energy. All many-particle effects are contained in $E_{xc}[n]$, i.e., the many-particle contribution to the kinetic energy and the effects due to the Pauli exclusion principle.

2.1.2 Kohn-Sham formalism

Although the Hohenberg-Kohn (KS) theorem gives a very comfortable way to address the many-body problem, it does not give an explicit method to find the ground state density. This, however, is given by the Kohn-Sham formalism [19]. The main idea of this formalism is to find an auxiliary non-interacting system exposed to an effective potential V_{eff}, such that this system gives the same density as for the interacting system with the external potential V_{ext}. Then the new Hamiltonian of the non-interacting system is

$$H_{eff} = T_0 + V_{eff} \tag{2.5}$$

and its energy functional becomes

$$E_{eff}[n] = T_0[n] + \int d\mathbf{r} v_{eff}(\mathbf{r})n(\mathbf{r}). \tag{2.6}$$

Since the effective system is non-interacting, we can obtain the ground state density by first solving the Schrödinger-like single-particle Kohn-Sham equations

$$\left(-\frac{1}{2}\nabla^2_{\mathbf{r}} + v_{eff}(\mathbf{r})\right)\psi_i(\mathbf{r}) = \varepsilon_i\psi_i(\mathbf{r}), \tag{2.7}$$

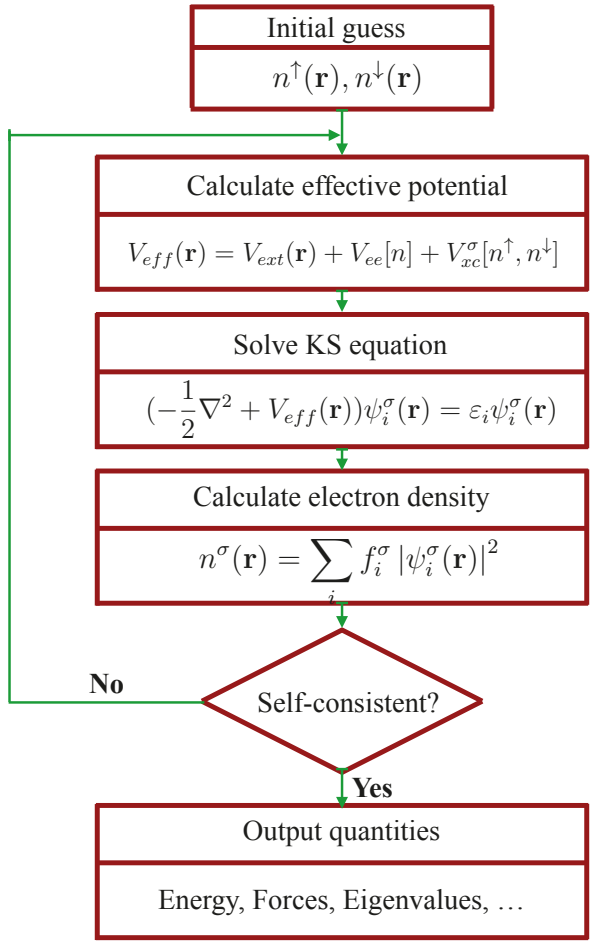

Figure 2.2. Schematic representation of the iterative procedure to follow in density functional theory.

where the ψ_i are single-electron KS orbitals with no physical meanings, but they give the ground state density as

$$n_{eff}(\mathbf{r}) = \sum_{i=1}^{occ} |\psi_i(\mathbf{r})|^2. \tag{2.8}$$

Now, we want the non-interacting density of the effective system to be equal to the interacting density of the original system. According to the Hohenberg-Kohn theorem, the ground-state density should minimize the energy functional. This must be done under the constraint that the number of particles must be conserved. Knowing this, the Euler-Lagrange equation associated with the minimization of the energy functional is expressed as

$$\mu = \frac{\delta E[n]}{\delta n(\mathbf{r})} = \frac{\delta T_0[n]}{\delta n(\mathbf{r})} + v_{eff}(\mathbf{r}) \tag{2.9}$$

where μ is a Lagrange multiplier acting as the chemical potential. The variation of the total energy functional for the original interacting system in Eq. (2.3) gives

$$\frac{\delta E[n]}{\delta n(\mathbf{r})} = \frac{\delta T_0[n]}{\delta n(\mathbf{r})} + v_{ext}(\mathbf{r}) + \int d^3r' \frac{n(\mathbf{r}')}{|\mathbf{r}-\mathbf{r}'|} + \frac{\delta E_{xc}[n]}{\delta n(\mathbf{r})}. \tag{2.10}$$

By comparing Eq. 2.10 and Eq. 2.6, we can derive the effective KS potential as

$$v_{eff}(\mathbf{r}) = v_{ext}(\mathbf{r}) + \int d^3r' \frac{n(\mathbf{r}')}{|\mathbf{r}-\mathbf{r}'|} + \frac{\delta E_{xc}[n]}{\delta n(\mathbf{r})}. \tag{2.11}$$

The last term in equation (2.10) is called the exchange-correlation potential

$$v_{xc}(\mathbf{r}) \equiv \frac{\delta E_{xc}[n]}{\delta n(\mathbf{r})}. \tag{2.12}$$

The combination of the Hohenberg-Kohn theorems and the Kohn-Sham formalism leads to the Kohn-Sham equations, Eq. (2.6) and (2.11), that can be solved in a self-consistent manner.
Theis self-consistent scheme is as follows: First a guess is made for a starting density n(**r**) which is used as input in Eq. (2.11) and (2.12). The potential $v_{eff}(\mathbf{r})$ is then used to solve the Kohn-Sham equation (2.7). The obtained single-particle orbitals ψ_i are used to construct a new density from Eq. (2.8). A fraction of this new density is then mixed with a fraction of the old density and then used as input in Eq. (2.11) to get a new potential. This cycle is repeated until self-consistency is reached (see Fig. 2.2). The final density will then not only be the correct ground state density for the non-interacting system, but also for the interacting system by construction.
The procedure is formally exact. However, no explicit form for the exchange-correlation potential $v_{xc}(\mathbf{r})$ is known, and one has to obtain it approximately.

One of the most common approximations is the local density approximation (LDA) and its extension for a spin-polarized density (LSDA). In these approximations the exchange-correlation functional E_{xc} is assumed to be local and the exchange-correlation energy per electron corresponds to a uniform electron gas which can be parametrized in various ways, i.e., through the popular parameterization suggested by Perdew and Wang [20]. For other approximations to the exchange-correlation potential the reader is referred to the literature [21, 22, 23].

2.1.3 Relativistic effects

The Schrödinger equation is a non-relativistic equation which is taken as a starting point for electronic structure calculations. In some systems, the relativistic effects can become very important such that they need to be taken into account to have a reasonable description of the system. In such cases, we should start from the 4-vector Dirac equation [24], which describes both electrons and positrons with spin up and spin down. This approach leads to a fully relativistic (FR) treatment of the electronic structure problem. However, it is also common to take into account the relativistic effects in a perturbative manner by using a two-component wavefunction for the electrons. In this way, we can rewrite the single-particle Kohn-Sham Hamiltonian in Eq. (2.7) in the following form

$$H = \frac{\mathbf{p}^2}{2m_e} + V_{eff}(\mathbf{r}) - \frac{\mathbf{p}^4}{8m_e^3c^2} + \frac{\hbar^2}{8m_e^2c^2}\nabla^2 V_{eff}(\mathbf{r}) + \frac{\mathbf{S}\cdot(\nabla V_{eff}(\mathbf{r})\times\mathbf{p})}{2m_e^2c^2}, \quad (2.13)$$

where $\mathbf{S} = \sigma/2$ is the spin of the electron [25, 26]. The first two terms represent the non-relativistic Hamiltonian used in the Schrödinger equation. The third term is the relativistic mass correction to the electronic kinetic energy. The fourth term is the Darwin term and is a correction due to the quantum fluctuations and it only affects the s orbitals, since the wave function of an electron with $l > 0$ vanishes at the origin. The last term represents the spin-orbit coupling, which stems from the interaction of the electron spin with the magnetic field caused by its own orbital motion. The mass enhancement term together with Darwin term are called the scalar relativistic (SR) corrections to the Schrödinger equation. The spin-orbit term, on the other hand, couples the spin and orbital degrees of freedom and therefore it is a vector quantity.
Relativistic effects become important when heavy elements are involved. This is due to the fact that the Darwin term ($\nabla V_{eff}(\mathbf{r})$) is larger for electrons in heavy elements, specially the ones which are close to the nucleus, than for electrons in light elements. Here we bring a brief explanation for one of the corrections that is caused by relativistic motion of electrons.

Spin-orbit coupling

The most significant corrections due to relativistic effects, is the spin-orbit coupling (SOC). If we assume that the potential V_{eff} is spherically symmetric, the SOC term can be written as

$$H_{soc} = -\frac{e}{2c^2 m_e^2 r}\frac{dV_{eff}(\mathbf{r})}{dr}\mathbf{S}\cdot\mathbf{L} = \xi \mathbf{S}\cdot\mathbf{L}, \tag{2.14}$$

where $\mathbf{L} = \mathbf{r}\times\mathbf{p}$ is the orbital angular momentum operator and ξ is the SOC constant. In solids, the SOC determines the magneto-crystalline anisotropy (MCA). The MCA is a measure of how strong the spin is locked into a special lattice direction through the spin-orbit coupling. The MCA, thus, depends on the magnetization direction in the crystal lattice. If we define the magnetization direction $\hat{M}$ with respect to the z axis as $\hat{M} = (\sin\theta\cos\phi, \sin\theta\sin\phi, \cos\theta)$ then we can expand the MCA for a uniaxial system (like hcp Co) as [27]

$$E_{MCA} = K_1 \sin^2\theta + K_2 \sin^4\theta + K_3 \sin^6\theta + K_4 \sin^6\theta\cos 6\phi + ..., \tag{2.15}$$

where K_i are anisotropy constants.

If we are interested in transition metals systems, where the SOC constant ξ is much smaller than the band width of the d orbitals and also smaller than the exchange splitting, it is quite common to consider the SOC term as a simple perturbation. The change in the energy due to the SOC to the second-order is given by[1]

$$\Delta E_{soc} = \xi^2 \sum_{n\neq m} \frac{|\langle n|\mathbf{L}\cdot\mathbf{S}|m\rangle|^2}{\varepsilon_n - \varepsilon_m}, \tag{2.16}$$

where ε_n and ε_m are the eigenvalue energies of the occupied and unoccupied eigenstates of the unperturbed Hamiltonian. A rough estimate of K_1 in Eq. (2.15) for a uniaxial system, like ultrathin film ferromagnet, is

$$K_1 \sim \xi^2/W \tag{2.17}$$

Given that $\xi \approx 75$ meV and the bandwidth of the d states is W≈ 5 eV, one obtains $K_1 \approx 1$ meV·atom^{-1}. However, for cubic systems the second-order perturbation term gives zero contribution and one needs to go to higher order perturbation terms, which lead to orders of magnitude smaller contributions and hence, the magnitude of $\sim 1\mu$eV·atom^{-1} is appropriate for K_1.

2.1.4 DFT basis set

Practical implementations of the self-consistent Kohn-Sham equations (represented in Fig. 2.2) require a basis set for the computations. According to

[1] The first order is zero due to the cancellation in summation.

quantum mechanics, the wavefunction $|\psi_i\rangle$ of a system can be expanded via a complete basis set

$$|\psi_i\rangle = \sum_l c_l |\chi_l\rangle , \tag{2.18}$$

Inserting this equation into Eq. (2.7) gives

$$\sum_l c_l H_{eff} |\chi_l\rangle - \varepsilon_i \sum_l c_l |\chi_l\rangle = 0. \tag{2.19}$$

Multiplying this equation from the left with $\langle\chi_k|$, we get

$$\sum_l c_l \langle\chi_k| H_{eff} |\chi_l\rangle - \varepsilon_i \sum_l c_l \langle\chi_k|\chi_l\rangle = 0. \tag{2.20}$$

By defining the matrix elements of the Hamiltonian as $H_{kl} \equiv \langle\chi_k| H^{eff} |\chi_l\rangle$ and the overlap integrals as $O_{kl} \equiv \langle\chi_k|\chi_l\rangle$, the secular equation is written as

$$\sum_l c_l (H_{kl} - \varepsilon_i O_{kl}) = 0. \tag{2.21}$$

The Kohn-Sham equation (2.7) has been transformed from a differential eigenvalue equation to a linear algebraic equation. By solving this equation, we can obtain the Kohn-Sham energies of the system. This equation is generally solved iteratively. Therefore, first we choose a basis set. Then, by making use of the Rayleigh-Ritz procedure and standard numerical diagonalization routines, we calculate the eigenvalues of Eq. (2.21) without iterations. The self-consistent potential is of course iterated, and in this process the basis functions are at each step optimized to be the best for this potential. In our studies, we use the relativistic spin polarized toolkit (RSPt) code in order to solve the Kohn-Sham equations [28]. Below we explain the construction of the basis set that is implemented in this code.

2.1.5 Linear muffin-tin orbital method

The full-potential linear muffin-tin orbital (FP-LMTO) method, associated with site-centered basis functions, is a specific implementation of DFT. A brief introduction to this approach is given below, while for an extensive review we refer to the book by J. M. Wills et al. [28]. This method is based on the division of the space between the atoms into two regions: non-overlapping muffin-tin (MT) spheres centred on each atom and an interstitial region. For simplicity we can illustrate the method for a potential that is spherically symmetric close to the nuclei. In this respect, the external potential V_{ext} defined in Eq. (2.11) in the unit cell is represented as

$$V(\mathbf{r}) = \begin{cases} V_{MT}(\mathbf{r}) & , |\mathbf{r}| < r_{MT} \\ V_I(\mathbf{r}) & , |\mathbf{r}| \geq r_{MT} \end{cases} \tag{2.22}$$

where MT stays for muffin-tin region and I for interstitial region.
The site-centered basis functions start from the MT spheres (*heads* of the basis), and penetrate into the interstitial regions (*tails* of the basis). The shape of the basis functions depend on some parameters defined for the system. The discussion on these parameters is given in the next part, but first we explain the construction of the LMTOs inside and outside the MT sphere.

MT basis functions:
Typically the basis functions inside the MT spheres are defined in local coordinates with respect to the center of the site τ and are composed of two terms, a modified spherical harmonic times a radial function, i.e.

$$\chi_{\tau,L}(\varepsilon,\mathbf{r})|_{|r|<r_{MT}} = \mathscr{Y}_L(\hat{\mathbf{r}})\phi_l(\varepsilon,r), \tag{2.23}$$

where $L=(l,m_l)$ defines orbital quantum numbers. $\mathscr{Y}_L = i^l Y_{l,m}$, $\hat{\mathbf{r}}$ is the angular part of the coordinate and r is the distance from the center of the site τ. After some algebraic manipulation one gets the radial function ϕ_l by solving the radial Schrödinger equation

$$\frac{\partial^2(r\phi_l(\varepsilon,r))}{\partial r^2} = \left(\frac{l(l+1)}{r^2} + V_{MT}(\mathbf{r}) - \varepsilon\right) r\phi_l(\varepsilon,r). \tag{2.24}$$

In order to remove the energy dependence from the basis function, the radial functions can be expanded (usually to the first order) around some linearization energy ε_ν as follows

$$\phi_l(\varepsilon,r) = \phi_l(\varepsilon_\nu,r) + (\varepsilon-\varepsilon_\nu)\dot{\phi}_l(\varepsilon_\nu,r) \tag{2.25}$$

where the function and its derivative are orthogonal to each other.
Now a linear combination of the function $\phi_l(\varepsilon_\nu,r)$ and $\dot{\phi}_l(\varepsilon_\nu,r)$ can be made as a Taylor expansion of the energy dependence around the energy ε_ν for the l shell. This linear combination should be chosen in a way that the basis functions inside the MT spheres connect to the basis functions in the interstitial in a continuous and differentiable way. The interstitial basis functions are given by Hankel or Neumann functions and will be described in the next paragraph.

Interstitial basis function:
Each basis function in this region consists of a Hankel or Neumann function. Formally, each basis function in the interstitial is defined as a spherical harmonic times a spherical wave with some quantum number κ. This quantum number is a measure of the kinetic energy and is defined as $\kappa^2 = V_I - \varepsilon$, where V_I is the interstitial potential. The basis function takes the form

$$\chi_{I,L}(\varepsilon,\kappa r) = \mathscr{Y}_L(\hat{\mathbf{r}})y_l(\kappa r), \tag{2.26}$$

where the spherical waves (y_l) are the solutions of the Helmholtz equation

$$\left(-\frac{d^2}{dr^2}+\frac{l(l+1)}{r^2}-\kappa^2\right) r y_l(\kappa r)=0. \tag{2.27}$$

For a positive κ^2, the $y_l(\kappa r)$ obtained in this way is either of the two linearly independent spherical Bessel functions $j_l(\kappa r)$ or Neumann functions $n_l(\kappa r)$. For a negative value of κ^2 the solution of Eq. (2.26) is a first type Hankel function. The full basis function after matching with the function inside the MT, is defined as

$$\chi_{\tau,L}(\varepsilon_\nu,\kappa,r)=\mathscr{Y}_L(\hat{r})\begin{cases}\phi_l(\varepsilon_\nu,r)+\kappa cot(\eta_l)J_l(\kappa,r) & r<r_{MT}\\ \kappa N_l(\kappa,r) & r\geq r_{MT},\end{cases} \tag{2.28}$$

where J_l and N_l are the augmented versions of the spherical Bessel and Hankel functions,[2] and are related to the Bessel and Neumann functions as

$$N_L(\kappa,\mathbf{r})=n_l(\kappa r)\mathscr{Y}_L(\hat{\mathbf{r}}) \tag{2.29}$$

$$J_L(\kappa,\mathbf{r})=j_l(\kappa r)\mathscr{Y}_L(\hat{\mathbf{r}}). \tag{2.30}$$

In order to achieve a high precision in the electronic structure, it is more convenient to use a basis with several κ for each l. For example, for disperse valence bands like s and p, it is common to use 3 tails (3κ or 3 basis), and for the narrower d and f bands 2 tails. The reason for using several tails for each orbital is that in the formulation of LMTO, the interstitial region can not be accurately described by a single tail. In the atomic sphere approximation (ASA) of LMTO this problem can be solved by using large overlapping spheres such that the interstitial region can be ignored. However, in full-potential LMTO, the MT spheres do not overlap. To solve this problem, one needs to use multiple tails with different κ values. However, there are some cases which limit the number of tails applied in the calculations. More explanation on this case is given in section (2.2.5). Here, we only say that the choice of tail energies would affect the total energy value. The total energy is also determined by the number of k-points used in sampling the Brillouin zone, and hence a choice of basis functions must be accompanied by a choice of a k-point grid. This effect is more pronounced in non closed-packed structures, e.g. surface calculations. As an example, in Fig. (2.3) the total energy convergence with respect to the number of k-points for different tails are shown for a 15-layer slab of bcc Fe (for the z direction which is perpendicular to the surface only one k-point is used since we sample the two-dimensional Brillouin zone). By comparing the

[2] For $\kappa>0$, N_l is a Neumann function instead of Hankel function.

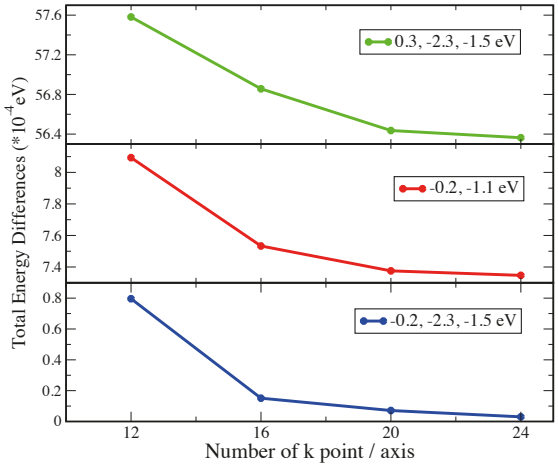

Figure 2.3. K-point dependence of the total energy is shown for different values of tail energies shown in the legend (κ). Using positive tails can produce less accurate results than having smaller basis set with negative tails. Nevertheless the total energy for any choice of tails is converged to within 6 meV/simulation cell (15 atoms).

total energy differences, one can see that in the case of three tails, of which one is positive, tail energies leads to at most 6 meV per simulation cell which is very small when compared to any energy that is relevant for a solid, e.g. the cohesive energy. Note that positive tail energies in the system can freely extend to outside of MT spheres, which in the case of a surface is vacuum. Therefore, surface atoms usually do not require basis functions with positive tail energies. However, positive tail energies can sometimes be helpful due to faster convergence.

Choosing a Basis Set:

In our LMTO-based code (RSPt), the range of energies considered in a normal calculation extends from the $1s_{1/2}$ deep core state to well above the Fermi energy E_f. The localized states in the core region are calculated separately. The variational basis functions are designed to represent the highest energy atomic valence configuration and the next highest energy configuration as well. For example, for Al with atomic configuration of $3s^2\ 3p^1$, the valence basis would contain $3s\ 3p$ and $3d$ LMTOs. A good choice would have three s and p orbitals with different interstitial kinetic tail energies and two d orbitals with different kinetic tail energies. We write this as

• $3\times(3s,3p)$, $2\times 3d$

The basis set must also be flexible enough to describe energy levels derived from atomic states, i.e., the states with different principal quantum numbers but the same angular momentum quantum number. For example, for describ-

ing the properties of actinides at any pressure, a basis with both *6p* and *7p* character is required. Similarly, a more precise calculation of the structural properties of transition metal oxides requires both semi-core and valence *s* and *p* states on the transition metal ions. Therefore, in LMTO-based methods it is common to perform calculations using both semi-core and valence states. For example, in the case of NiO under pressure one can define the valence basis as follows

• $3\times(3s,3p)$, $2\times(4s,4p)$, $2\times(3d)$

In this way the description of the evolution of semi core states from localized to itinerant under pressure can be achieved. In the next chapter we will show an example of different results one can obtain from different basis size.

2.2 Localized electrons and model Hamiltonians

Density functional theory and its formal extensions give an excellent parameter-free description of ground state properties of magnetic metals, such as bulk structures, surfaces, interfaces and disordered alloys [17, 29, 30]. However, besides many successes, there is a large class of materials for which these methods fail [31, 32, 33, 34]. This class contains systems with not fully occupied (or unoccupied) shells of localized electrons such as *d* and *f* orbitals. The motion of electrons in these orbitals is strongly entangled such that DFT with an exchange-correlation functional based on a homogeneous electron gas can not well describe the kinetic and the Coulomb energy associated with these electrons. Therefore, one needs to search for methods treating these electrons in a different manner. In parallel with the development of density functional theory, model Hamiltonian methods have been also used to study the many-body electronic structure problem. The aim of these methods is to simplify the electronic Hamiltonian in Eq. (2.1) while still keeping the physics of interest. Although model Hamiltonians look quite simple, their solutions might still be quite difficult. We refer the interested readers to the book by Yamada for a review of some of the most popular model Hamiltonians [35]. One of the famous examples is the Hubbard model [36], in which the interaction between electrons is assumed to be purely local as

$$\hat{H}_{hub} = -\sum_{\mathbf{R},\mathbf{R}',\sigma} (t_{\mathbf{R},\mathbf{R}'}\hat{c}^{\dagger}_{\mathbf{R},\sigma}\hat{c}_{\mathbf{R}',\sigma} + h.c.) + U\sum_{\mathbf{R}} \hat{n}_{\mathbf{R},\uparrow}\hat{n}_{\mathbf{R},\downarrow}. \tag{2.31}$$

Here $t_{\mathbf{R},\mathbf{R}'}$ is the energy an electron gains by jumping from site $\mathbf{R}$ to site $\mathbf{R}'$, $\hat{c}^{\dagger}(\hat{c})$ is the creation (annihilation) operator, and $\hat{n}_{\mathbf{R},\sigma}$ is the number operator for spin up and down at site $\mathbf{R}$. The amplitude of t is proportional to the dispersion (the bandwidth) of the valence electronic states and represents the single-particle term of the total energy. In the case of strong localization, the partially screened Coulomb repulsion affects mainly the electrons on the same atom through a term that is proportional to the product of the occupation

numbers. The strength of this term is the "Hubbard U". In other words, U is the price to pay for having two electrons with opposite spins on the same site. For systems with metallic character, when single-particle terms dominate ($t >> U$), DFT can still be used as a reliable approximation. Instead, in the regime dominated by short-range Coulomb interactions ($t << U$) like systems with insulating character, one needs to search for another method.
The main features described by the Hubbard model can be included into DFT, in the form of an explicit correction. This procedure will be discussed in the following.

2.2.1 DFT+U Hamiltonian

One of the failures of DFT is the description of Mott insulators [17, 19, 37]. In such systems the insulating character is due to the strong Coulomb repulsion between electrons which dominates over their kinetic energy, forcing the electrons to be localized on atomic-like orbitals (Mott localization) [38]. To describe this behavior more precisely, one needs to have a better account of the wavefunction than in DFT, where the focus is on the non-interacting KS quasi-particles..

The DFT+U approach [31, 32] is a correction to DFT functionals in order to improve their accuracy. This makes it possible to describe the ground state of correlated systems and sometimes even the excited states [39, 40, 41]. The idea is to use the Hubbard Hamiltonian for a better description of "strongly correlated" electronic states (typically, localized d or f orbitals). The other valence electrons can still be treated at the level of the "standard" exchange-correlation functional. In this approach, the DFT energy (E_{DFT}) is corrected with a static Hartree-Fock term to give

$$E_{DFT+U} = E_{DFT}[n^{\sigma}] + E_{hub}[n^{R,\sigma}_{\xi\xi'}] - E_{dc}[n^{R,\sigma}], \tag{2.32}$$

where n is the density, ξ index stands for the atomic quantum numbers $|lm\sigma\rangle$, $n^{R,\sigma}_{\xi\xi'}$ refers to the atomic orbital occupations, e.g., occupation matrix and $n^{R,\sigma} = \mathrm{Tr}(n^{R,\sigma}_{\xi\xi'})$ is the total spin-projected occupation of the localized states.
The Hubbard correction (second term) contains the electron-electron interactions as modelled in the Hubbard Hamiltonian. These interactions have already been partially taken into account when evaluating the DFT energy functional E_{DFT}. Therefore, it is necessary to eliminate the "double-counted" contributions, which are defined in the third term. We will discuss this term in more detail later, in section 2.2.4.

As can be seen from the Eq. (2.32), the Hubbard correction is a functional of the occupation matrix ($n^{R,\sigma}_{\xi\xi'}$). This matrix is obtained as projections of

the one-particle density matrix of the Kohn-Sham orbitals.[3] The projection to the localized states should be made such that the LDA+U energy becomes invariant under the rotation of the atomic orbital basis set. Because in general the choice of the localized basis set is not unique. Some of the most popular choices are atomic orbitals or maximally localized Wannier functions [42]. We refer the interested readers to section 2.2.5 or Ref. [33] for more details.

The practical procedure to arrive to Eq. (2.32) involves first the choice of the localized basis $|R,\xi\rangle$. Then the Hubbard interaction is explicitly added to the DFT Hamiltonian in the most general form as

$$\hat{H}_{hub} = \frac{1}{2}\sum_{R}\sum_{\xi_1\xi_2\xi_3\xi_4} U_{\xi_1\xi_2\xi_3\xi_4}\hat{c}^{\dagger}_{R\xi_1}\hat{c}^{\dagger}_{R\xi_2}\hat{c}_{R\xi_4}\hat{c}_{R\xi_3}. \tag{2.33}$$

The U-matrix represents the effective interaction which should take into account the screening effects. Assuming that atomic states (e.g., d or f) are chosen as a localized basis, the next step is the construction of the U-matrix as defined in Eq. (2.33). If we consider only the intra-site interactions for a given shell l, the U-matrix will take the form

$$U_{\xi_1\xi_2\xi_3\xi_4} = \delta_{l_1l_2l_3l_4}U_{m_1\sigma_1m_2\sigma_2m_3\sigma_3m_4\sigma_4}. \tag{2.34}$$

Although the experssion of Eq. 2.32 seems quite simple, implementation of the Hubbard term in a DFT code might be crucial. The reason is that there is no unique way for the choice of the localized basis set. Liechtenstein et al. [43] and Dudarev et al. [44] have suggested two methods which are both rotationally invariant.

In Liechtenstein approach, the orbital dependence of the Hubbard term is taken from the atomic Hatree-Fock

$$\begin{aligned} E_{hub}[n^{R\sigma}_{mm'}] = &\sum_{R,m,\sigma}\langle m_1,m_3\,|V_{ee}|\,m_2,m_4\rangle\, n^{R\sigma}_{m_1m_2}n^{R-\sigma}_{m_3m_4} \\ &+\left(\langle m_1,m_3\,|V_{ee}|\,m_2,m_4\rangle - \langle m_1,m_3\,|V_{ee}|\,m_4,m_2\rangle\right) n^{R\sigma}_{m_1m_2}n^{R\sigma}_{m_3m_4} \end{aligned} \tag{2.35}$$

with

$$U_{m_1m_2m_3m_4} = \langle m_1,m_3\,|V_{ee}|\,m_2,m_4\rangle\,, \tag{2.36}$$

[3] If $\psi^{\sigma}_{k,\nu}$ represents the occupied Kohn-Sham orbitals and $|R,\xi\rangle$ are the states of a localized basis set, then

$$n^{R,\sigma}_{\xi\xi'} = \sum_{k,\nu} f^{\sigma}_{k,\nu}\left\langle \psi^{\sigma}_{k,\nu}|R\xi'\right\rangle\left\langle R\xi|\psi^{\sigma}_{k,\nu}\right\rangle,$$

where $f^{\sigma}_{k,\nu}$ is the Fermi-Dirac occupation of Kohn-Sham states, k is the k-point, ν is band index.

they can be computed from the expansion of the bare Coulomb repulsion in terms of spherical harmonics

$$\langle m_1, m_3 | V_{ee} | m_2, m_4 \rangle = \sum_{k=0}^{2l} a_k(m_1, m_2, m_3, m_4) F^k, \tag{2.37}$$

where l is the angular moment of the localized manifold, with $-l \leq m \leq l$. The a_k factors can be obtained as products of Clebsh-Gordan coefficients:

$$a_k(m_1, m_2, m_3, m_4) = \frac{4\pi}{2k+1} \sum_{q=-k}^{k} \langle lm_1 | Y_{kq} | lm_2 \rangle \langle lm_3 | Y_{kq}^* | lm_4 \rangle . \tag{2.38}$$

Mathematically, it can be proved that the a_k factors are non-zero only when k is even and smaller than $2l$. The radial Slater integrals F^k are defined as

$$F^k = \int_0^\infty \int_0^\infty dr dr' r^2 r'^2 |\phi(r)|^2 |\phi(r')|^2 \frac{r_<^n}{r_>^{n+1}}, \tag{2.39}$$

where $r_<$ and $r_>$ are the lesser and the greater variable of r and r', and ϕ represents the radial part of the atomic wavefunction. For d electrons only F^0, F^2 and F^4 are needed to compute the matrix elements of Eq. (2.37), since for higher k values the corresponding a_k vanishes. The f electrons also require F^6. However, due to the screening, these integrals can not be calculated directly. It is, however, common to relate them to the direct and exchange integrals of the screened interaction U and J, which can be obtained semi-empirically. For d orbitals, this relation is defined as follows

$$U = \frac{1}{(2l+1)^2} \sum_{m_1 m_2} U_{m_1 m_2, m_1 m_2} = F^0 \tag{2.40}$$

$$J = \frac{1}{2l(2l+1)} \sum_{m_1 \neq m_2} U_{m_1 m_2, m_2 m_1} = \frac{F^2 + F^4}{14}. \tag{2.41}$$

These equations are often used to evaluate screened Slater integrals F^k from the values of U and J, with the assumption that F^2/F^4 and F^4/F^6 (for f electrons) have the same values as in isolated atoms [22]. Although these equations are strictly valid for atomic states and unscreened Coulomb interactions, they can be still accurate for solids if the localized orbitals keep their atomic character. Therefore, the determination of the 4-index matrix is reduced to only two parameters U and J.

In the second method, Dudarev proposed that based on the above expressions derived by Liechtenstein *et al.*, one can approximate U and J to be spherical averages, then the total energy in DFT+U will have a form as [44]

$$E_{DFT+U} = E_{DFT} + \frac{U-J}{2} \sum_{\sigma} \left[\sum_{m_1} n_{m_1 m_1}^{\sigma} - \sum_{m_1, m_2} n_{m_1 m_2}^{\sigma} n_{m_2 m_1}^{\sigma} \right]. \tag{2.42}$$

The main difference between the Dudarev approach and the Liechtenstein formalism is that the extra correlations in the former depends only on $U - J$ in isotropic screened on-site Coulomb interaction and is equivalent to the Liechtenstein approach with $J = 0$.

Choice of U

In theoretical studies, the U parameter is often chosen to fit one or several properties of the system under study. For instance, the band gap or the magnetic moment of the system is studied for different values of U and then the one yielding the closest agreement with experiment can be chosen for the rest of the study. In reality, the value of U should not be a fitting parameter as it corresponds to a physical property: strength of a screened electron-electron interaction. Therefore, several ways have been proposed in order to determine which U value should be used. Among them are constrained DFT (cDFT) and the improvements beyond that [45, 46, 47, 48] and also constraint random phase approximation (cRPA) [49]. In cDFT, a supercell is adopted in which the occupation of the localized orbitals of one atom is constrained and is decoupled from all the other atoms in the supercell. Then, the Hubbard U is calculated from the total energy variation with respect to the occupation number of the localized orbitals. On the other hand, in cRPA the static values from the dynamical polarization is extracted. However, these two methods do not yield the same results for the screened interaction. The reason is that the RPA includes responses from both on-site and inter-site $3d$ electrons, whereas the cDFT only takes into account the responses coming from on-site $3d$ electrons to an external perturbation. In this thesis, since the focus was not on the calculation of Hubbard U, these computational methods were not used, but the U values for different system were simply taken from the literature.

Before closing this section, we need to mention some differences between the DFT+U approach and the Hartree-Fock (HF) method which also uses a single Slater determinant as wavefunction [5]. First of all, the effective interaction in DFT+U is *screened* rather than the *bare* Coulomb kernel (as in HF). Second, DFT+U only acts on the localized atomic orbitals rather than all the states in the system. To express things shortly, DFT+U applies a screened HF to a sub-group of KS single particle orbitals. In reality, however, when the electrons are strongly localized, their motion becomes correlated and their wavefunction acquires many-body character. Thus, the HF or DFT+U methods which describe the ground state with an optimized single determinant can not capture the physics of, e.g., paramagnetic Mott insulators.

In the next section we will discuss a method which uses DFT as the single-particle starting point and is able to describe several properties of strongly correlated systems in a dynamical way based on many body approach. The

problem of the local minima and other failures which do exist in any single-particle approach, in principle, should not happen in this approach, unless due to technical problems and difficulties in the implementations which sometimes are unavoidable. Before that, we would like to give a brief introduction to two important objects in many-body physics; the self-energy and the Green's function.

The self-energy of particles:
Suppose we have an electron moving from point x at time t to point x' at time t'. Then the one electron Green's function $G(xt;x't')$ gives the probability amplitude that a particle inserted in the space-time (xt) propagates to the space-time $(x't')$. Now, consider the Green's function of an electron in an interacting environment like a solid. During the journey from (xt) to $(x't')$, the particle will experience many-body scattering processes. The self-energy is the sum of the amplitude of all these intermediate scattering processes into a single entity, represented by the symbol $\Sigma(x,t)$. For example, in case of Fermi-liquid the self-energy describes the cloud of particle-hole excitations surrounding the propagating electron and "dressing" it into a quasiparticle. The relation between the bare and the dressed propagating electrons (often denoted by non-interacting $\mathscr{G}_0$ and interacting Green's function G) is given by the Dyson equation which states that

$$\Sigma = \mathscr{G}_0^{-1} - G^{-1}. \tag{2.43}$$

Although we presented this relation for a Fermi-liquid, it is a general result for any interacting system.
In general, the self-energy has both a real and an imaginary component. While the real part can influence the Fermi surface of the solid and renormalize the effective mass of the particle, the imaginary part defines the finite life-times that the excitations acquire because of electron-electron interactions. It also gives us some information about non-quasiparticle peaks in the spectra of the system (Fig. 2.4). For more information, we refer to the book by Mahan [50].

2.2.2 Dynamical mean field theory

After the discovery of high T_c superconductivity, a need for methods which can handle dynamical aspects of many-body effects and temperature became more urgent. In strongly correlated systems where the on-site Coulomb interaction U is larger than the bandwidth, the LDA+U method [40] can be applied to study magnetic moments and spin wave spectra [51]. However, the excitation spectra of these systems or a paramagnetic ground state can *not* be well described by a single Slater determinant and features such as Kondo resonances, atomic multiplets, mixed valence state are still out of reach [36]. In addition,

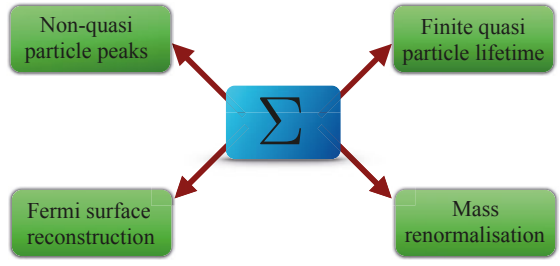

Figure 2.4. The information that one can obtain by knowing the self-energy of a system.

LDA+U focuses mainly on the inhomogeneities in the electron density and if the spin and orbital polarizations are absent, the LDA+U correction vanishes. Therefore, insulating systems with a nonmagnetic order can not be described.[4] To address these shortcomings, one needs to go beyond static mean field approaches like LDA and LDA+U, or even methods based on a perturbation expansion such as the GW approximation [52].

Spectral density functional theory was developed to deal with these problems through an interpolation between atomic physics and band theory. The dynamical mean field theory (DMFT) is a method which uses DFT as the starting point and adds dynamical effects in the form of a self-energy Σ. In this way, DMFT is able to describe both itinerant and atomic limits on equal footing [22, 23, 53].

The self-energy of correlated electrons is in general space-time dependent. In DMFT, instead it is considered to be local but still time dependent (or through a Fourier transform, frequency dependent). The self-energy is obtained from solving the Anderson impurity problem, which we will come back to later. The model Hamiltonian is the same as the one used in LDA+U. This means that the Kohn-Sham Hamiltonian is corrected with a local Coulomb repulsion, as in Eq. (2.33). Although DMFT uses DFT-LDA as the starting point, it is still quite adequate for the simulation of various systems such as rare-earth compounds [54], 3d-transition metal Mott insulators [55] and high-T_c superconductors [56, 57]. The DMFT method is exact in the limit of infinite dimensions, and for 3-dimensional systems DMFT is a reasonable approximation. In the limit of infinite dimensions, the self-energy becomes independent of the momentum ($\Sigma(k,\omega) = \Sigma(\omega)$). Therefore the interacting Green's function of the crystal becomes

$$G(k,i\omega) = \frac{1}{i\omega + \mu - \varepsilon_k - \Sigma(i\omega)}, \tag{2.44}$$

[4] In Mott insulators the energy gap is much larger than magnetic ordering temperature above which the system becomes paramagnetic but remains an insulator.

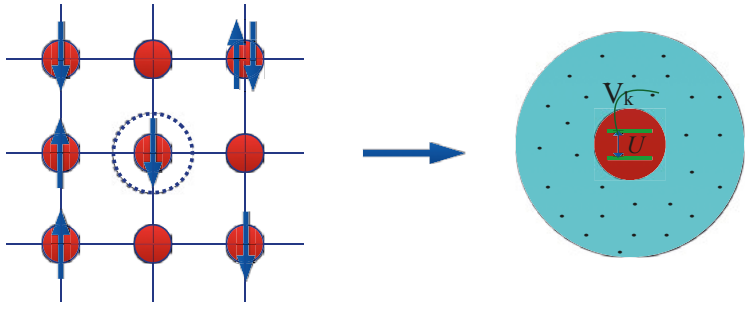

Figure 2.5. In DMFT the lattice problem is mapped into a model of a single atom embedded in a bath of electrons.

In DMFT the self-energy of the lattice is obtained by mapping the lattice problem into a model of a single atom embedded in a bath of electrons (Fig. 2.5). This system corresponds to a famous model, which is called the Anderson impurity model (AIM) [58]. It was first suggested by P. W. Anderson in order to describe a magnetic impurity atom in non-magnetic metals [58]. The Hamiltonian for a single impurity orbital reads as

$$\hat{H}_{AIM} = \sum_{\mathbf{k}}\sum_{\sigma} \varepsilon_{\mathbf{k}} \hat{n}_{\mathbf{k}\sigma} + \sum_{\sigma} \varepsilon_d \hat{n}_{\sigma} + U \hat{n}_{d\uparrow}\hat{n}_{d\downarrow} + \sum_{\mathbf{k}}\sum_{\sigma} [V_{\mathbf{k}d} c^{\dagger}_{\mathbf{k}\sigma} d_{\sigma} + h.c.]. \quad (2.45)$$

The first term is the kinetic energy of free (conduction) electrons and the second term is the kinetic energy of the electrons on the single impurity site, denoted by d. If two electrons of opposite spin occupy the same site, they will feel the Coulomb repulsion U, which is modelled by the third term. The hybridization between the electrons in the impurity site and the free conduction electrons (bath) is given by the last term, where $V_{\mathbf{k}d}$ is the matrix element for the transition between the impurity state and the free conduction states. All the features of the bath can be captured by the hybridization term $\Delta(i\omega)$ [58, 59], which enters into the non-interacting Green's function $\mathscr{G}$ through

$$\mathscr{G}^{-1} = i\omega + \mu - \Delta(i\omega), \qquad \Delta(i\omega) = \sum_{k} \frac{|V_{kd}|^2}{i\omega - \varepsilon_k}. \quad (2.46)$$

In DMFT, $\mathscr{G}$ is called the bath Green's function, since it represents the free electrons in which the impurity is embedded. The interacting Green's function can be constructed using the Dyson equation once the self-energy is known

$$G^{-1}_{imp}(i\omega) = \mathscr{G}^{-1}(i\omega) - \Sigma_{imp}(i\omega). \quad (2.47)$$

Now if we compare this equation with Eq. (2.44), we realize that the big difference between these two equations is that the Hubbard model is a *lattice* model, while the Anderson model is a *single impurity* model. Now the question is how one can relate these two models to each other. The answer

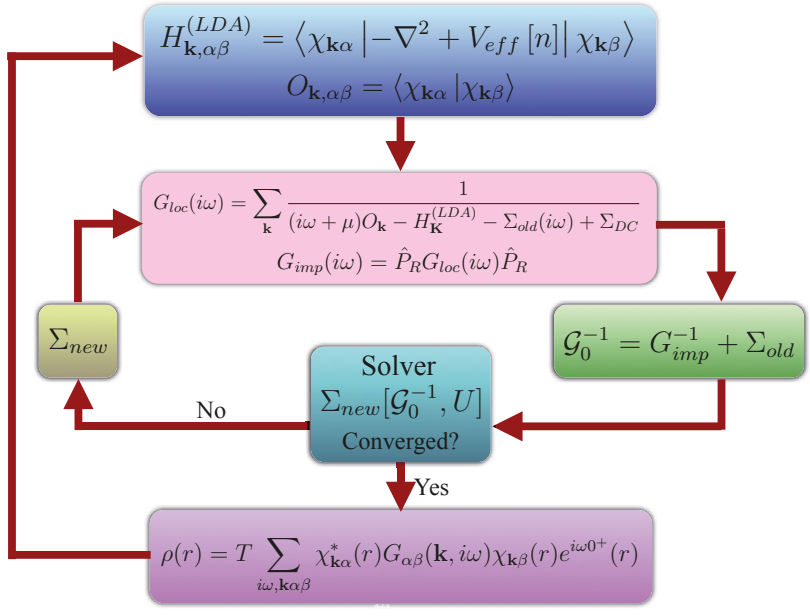

Figure 2.6. Schematic representation of the iterative procedure to follow in the LDA+DMFT scheme.

is given by the discovery of the behavior of Hubbard model at infinite dimension, which implies that one can map the lattice model to the impurity model [60, 61]. In this regard, we need to impose that both the self-energy and the the local (momentum integrated) Green's function of the lattice model should be equal to the impurity self-energy and the impurity Green's function

$$G_{imp}(i\omega) = G_{R,R'}(i\omega), \quad \Sigma_{imp}(i\omega) = \Sigma_{R,R'}(i\omega). \tag{2.48}$$

This condition leads to an approximation unless one treats an infinite dimensional systems. The *dynamical mean field theory* approximation is that the lattice self-energy is local (independent of momentum k). Then, one can rewrite the above equations as

$$\begin{aligned} G_{imp}(i\omega) &= \sum_k \frac{1}{i\omega + \mu - \varepsilon_k - \Sigma_{imp}(i\omega)} \\ &= \sum_k \frac{1}{i\omega + \mu - \varepsilon_k + G^{-1}_{imp}(i\omega) - \mathcal{G}^{-1}(i\omega)} \\ &= \sum_k \frac{1}{\Delta(i\omega) - \varepsilon_k + G^{-1}_{imp}(i\omega)}. \end{aligned} \tag{2.49}$$

This gives us an explicit self-consistency condition for the impurity Green's function. This condition is usually enforced through a DMFT cycle on top of DFT-LDA schemed in Fig. 2.6:

1. Start with solving the DFT-LDA problem and find the ground state electron density $n(r)$.
2. Construct the Kohn-Sham Hamiltonian.
3. Set up the local Green's function $G_{loc}(i\omega)$, obtained from the lattice model and a guess for the self-energy. Project it to localized orbitals.
4. Build the bath Green's function using the inverse Dyson equation $\mathcal{G}(i\omega) = [G_{loc}^{-1}(i\omega) + \Sigma(i\omega)]^{-1}$
5. Solve the local problem through one of the available "solvers" and calculate the new self-energy as a functional of $\mathcal{G}$ and U
6. Go back to the step 2 and plug the obtained self-energy into $G_{loc}(i\omega)$ and get a new chemical potential μ.
7. Repeat this procedure untill the convergence in the self-energy is obtained, then a new $n(r)$ can be calculated from $G(k, i\omega)$ which can be used in the next DFT cycle.

This is the fully self-consistent cycle and should be continued until convergence in $n(r)$, because every new density changes the H_{LDA} in Eq. (2.32).
To conclude, what DMFT does is to map a lattice problem onto a quantum impurity model subject to a self-consistency condition. The method can be used for calculations of thermodynamical properties, one-particle Green's functions, and response functions [22, 23, 53].
One issue that we have not yet discussed is how to compute the self-energy of the impurity model. Today, there exist many solvers which can calculate the self-energy in both numerical and analytical manner, and after the invention of DMFT this has become an active field of research. The reader is referred to the review articles as [22, 23, 53] for more information. In the next section, we will only discuss one of the impurity solver, namely the SPT-FLEX solver, which we have used for our studies.

2.2.3 Spin-polarized T-matrix fluctuation-exchange solver (SPT-FLEX)

Solving the quantum impurity model is one of the challenging problem in condensed matter physics. The difficulties come from the fact that the impurity models typically involve several energy scales. First, an interaction scale (U) which is often high, second; a hybridization scale (Δ), usually intermediate, and third, some dynamically generated energy scales, which in many cases are quite low compared to the former ones. In this regard, the solvers can

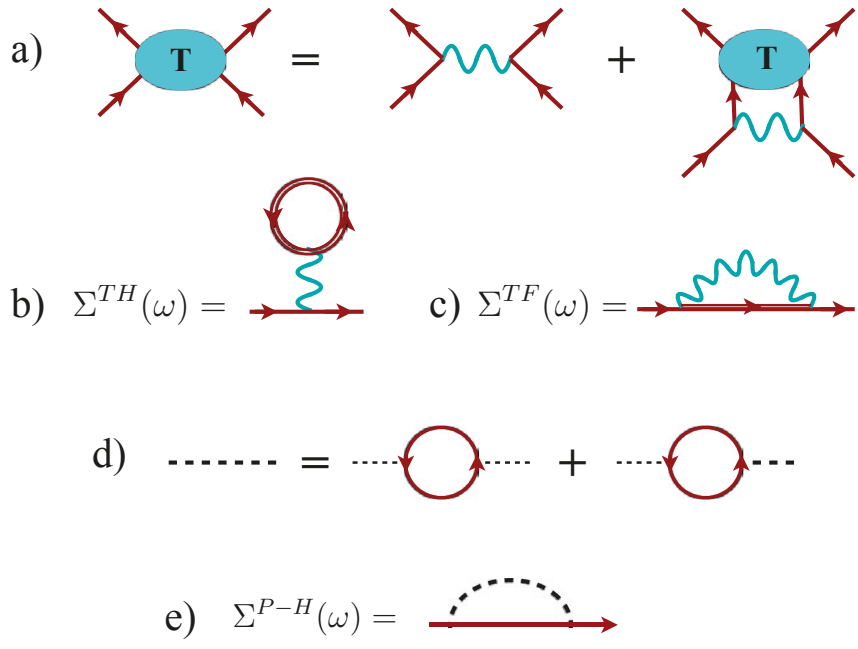

Figure 2.7. Diagrams included in the SPT-FLEX approximation. Red arrows represents the particle propagator, cyan lines are 2-particle interactions and black dashed lines which sums over all bubble diagrams is the effective interaction. (a) The PP T-matrix contribution, obtained by ladder type summations. (b) The Hartree-like and (c) the Fock-like contribution to the self-energy. (d) The RPA-like screened effective interaction. (e) The P−H self-energy. See text for detailed explanation.

be categorized into several different groups, depending on their efficiency and applicability. For instance, one group of solvers includes solvers which are numerically exact based on the quantum Monte-Carlo method [62, 63]. These solvers can handle a wide range of energy scales, but require analytical continuation of a numerical function to obtain real-time information (where observables can be found) which can be a big issue in some materials. Another group includes solvers that are based on finding an approximate answer for the self-energy of the impurity problem by the use of many-body perturbation theory [64, 65]. In this approach, the Coulomb interaction is our perturbation and the Green's function G for the whole system can be expanded in a sum of the terms consisting of products of the non-interacting Green's function G_0 and the Coulomb interaction U. These terms can be visualized by the so called Feynman diagrams (as is shown in several textbooks like Ref. [66]). However, instead of expanding G in a series of diagrams, it is usually more convenient to express the self-energy as a perturbation series. The reason is that in that case one can choose those subsets of diagrams which are more relevant to the physics of the problem under study.

One of the solvers employing this expansion of the self-energy is the fluctuation exchange (FLEX) approximation, first developed by Bickers, Scalapino and White [64, 65] to investigate high-T_c superconductivity. This solver includes the second order diagrams, but also the infinite series of bubble diagrams, which results in a screened Coulomb interaction. Also, infinite series of ladder diagrams are summed. In the original formulation of FLEX, the particle-hole (PH) and particle-particle (PP) channels are treated in an equal way, while they play different roles in magnetism. In order to have a more rigorous method, Katsnelson *et al.* [67, 68], suggests a "two-step" procedure which combines the spin polarized T-matrix and FLEX scheme (SPT-FLEX). The first step is to replace the bare matrix vertex with the T-matrix ($T(i\nu)$) in the PP interactions

$$T(i\nu) = U - U\chi^{(PP)}(i\nu)T(i\nu), \tag{2.50}$$

where $\nu = 2n\pi T$ are bosonic Matsubara frequencies for a temperature T and $\chi^{(PP)}$ is a 4-index matrix describing the bare particle-particle (PP) susceptibility. The second step is to take into account the PH channel processes using this effective interaction.
As shown in Fig. (2.7), the PP T-matrix contribution takes into account the ladder-type diagrams. The T-matrix is then used to construct the Hartree-like and the Fock-like self-energy, as illustrated in panel (b) and (c) of Fig. 2.7. These two groups of the diagrams contain all the second order contributions. For the PH channel a random-phase approximation (RPA) summation of PH bubble diagrams is needed to construct an effective interaction in (d). The PH self-energy Σ is constructed from the Fock like diagram in (e). The final expression for the full self-energy is a sum of all the above-mentioned parts

$$\Sigma(\omega) = \Sigma^{TH}(\omega) + \Sigma^{TF}(\omega) + \Sigma^{PH}(\omega). \tag{2.51}$$

Since SPT-FLEX solver is a perturbative solver, it can only be applied to systems with weak and moderate correlations, and always in the metallic regime of the Mott-Hubbard transition. It is however computationally cheap, and this fact combined with its multi-orbital formulation and the full inclusion of spin-orbit coupling makes it a good DMFT impurity solver for realistic materials, as long as care and consideration is taken.

2.2.4 Double counting

A double counting (DC) term should be subtracted from the self-energy ($\Sigma = \Sigma^{imp} - \Sigma^{DC}$) to remove the contributions that are already (wrongly) described in LDA. However, the determination of this term is one of the most serious problems in LDA+U and LDA+DMFT. This problem arises since the LDA is a functional of the electron density only, while the Hubbard correction is

a functional of the occupation numbers that are defined as projections of occupied Kohn-Sham orbitals on a localized basis set. Nevertheless, there are some suggestions for the DC term, depending on the physical limit to which the system is closer.
Here, we explain briefly some of the widely used choices of DC which can be used for metals, insulators and for the materials where the uniform occupation is still a good approximation.

- **Around mean field (AMF):**

  DFT in LDA corresponds to a sort of mean-field solution of the many-body problem. Hence, the exchange and correlation effects included in LDA are defined to be spherical, i.e., orbitally averaged within a mean field approach. This is a reasonable approach for metallic systems where LDA gives a uniform occupation. Therefore, we can define the average of the orbital occupations as [69]

  $$\bar{n} = \frac{1}{2(2l+1)} \sum_{m,\sigma} n^{\sigma}_{mm}, \tag{2.52}$$

  then the DC potential is

  $$v^{AMF}_{DC} = U(n-\bar{n}) - J(n^{\sigma} - \bar{n}), \tag{2.53}$$

  where $n(n^{\sigma})$ is the total (per spin) occupation of the correlated shell. U and J in this notation are spherically averaged Coulomb repulsion and intra-atomic exchange interaction.
  The AMF usually produces unsatisfactory results for strongly correlated insulators, but is sufficient for moderate or weakly correlated metals.

- **Fully localized limit (FLL):**

  The basic idea behind this double counting is to subtract the average effect for a localized state, with integer occupation numbers [41]. It takes the opposite approach to AMF and starts from the atomic limit. In this way, the local impurity is replaced by an isolated atom in contact with other electrons. In LDA, the energy levels of the isolated atom are degenerate. In the atomic limit, in fact, these levels are shifted depending on their occupation. For example, if these levels are empty, the FLL leads to an upward shift by $(U-J)/2$. If the levels are fully occupied, they will be moved downward by $(U-J)/2$, with the energy of

  $$E_{\mathrm{DC}} = \frac{1}{2}Un(n-1) - \frac{1}{2}J[n^{\uparrow}(n^{\uparrow}-1) + n^{\downarrow}(n^{\downarrow}-1)], \tag{2.54}$$

  and the potential of

  $$v_{\mathrm{DC},\sigma} \equiv \frac{\partial E_{\mathrm{DC}}}{\partial n^{\sigma}} = U(n-\frac{1}{2}) - J(n^{\sigma} - \frac{1}{2}), \tag{2.55}$$

This DC usually leads to integer occupation with localized electrons and therefore is only suitable for insulators.

- $\Sigma(0)$ **double counting:**

  For this choice of DC, the spin splitting in LDA+DMFT comes solely from LDA, because it considers that for separate spin channel, the orbitally averaged static part of the self-energy is quite well described by LDA. Therefore, once the self-energy is calculated in DMFT loop, one needs to remove the DC term as follows

$$\Sigma^{\sigma}_{m_1 m_2}(i\omega) = \Sigma^{\sigma}_{imp}(i\omega) - \frac{\delta_{m_1 m_2}}{2l+1} \sum_{m_3 \in \sigma} \Sigma^{\sigma}_{m_3, m_3}(0), \tag{2.56}$$

  where Σ_{imp} is the self-energy we obtain after solving the AIM and m is the correlated basis set.
  This is a good choice DC for systems with weak or intermediate correlations like transition metals. It is quite similar to what AMF does in LDA+U.

2.2.5 DMFT basis

As mentioned before, the Hubbard correction is only applied to a selected set of correlated electrons. To describe these electrons in DMFT, a basis set is required corresponding to the correlated orbitals $|\xi_i>$. This basis must be localized enough to describe local orbitals and should form an orthonormal set. If these two conditions are fulfilled, the choice of basis should not matter too much. The localization of the basis can be investigated by looking at the spectral leakage which is the overlap between the LMTO basis $|\chi_i>$ and the local basis $|\xi_i\rangle$

$$\mathcal{O}_{\xi_i \xi_j} = \sum_{\mathbf{k}, ij} \langle \xi_1 | \chi_i \rangle \, (O^{-1}_{\mathbf{k}})_{ij} \, \langle \chi_j | \xi_2 \rangle \,, \tag{2.57}$$

where $O_{\mathbf{k}}$ is the overlap matrix for LMT orbitals[5]. The new overlap in Eq. (2.57) should be ideally close to unity for a proper mapping. Afterwards, local quantities like Hamiltonian and the Green's function of the system are projected onto the basis of the correlated orbitals.
In the RSPt code, we have two different choices for correlated orbitals. A brief description is given below.

- **Orthonormalized LMTO (ORT):**
  This basis uses orthonormalized LMTO's. The orthonormalization is

[5]LDA basis in general are neither orthogonal nor normalized.

done by

$$\xi_i = \sum_{\mathbf{k},j} \chi_{\mathbf{k},j} \left[\sqrt{O_{\mathbf{k}}^{-1}} \right]_{j,i}, \tag{2.58}$$

The advantage of this basis is that there is no spectral leakage, as the overlap defined in Eq. (2.57) is one by construction. This is because the Hilbert space spanned by the ORT basis is a subspace of the Hilbert space spanned by the LMTO basis. The drawback is that the angular character is not pure, because this basis is poorly localized and it extends into the interstitial regions and even further to the neighboring MT spheres (depending on the tail energy value). Moreover, this basis strictly requires one tail (κ) for the correlated orbitals in order to have an exact correspondence between the LMTO basis and the atomic basis.

- **Muffin-tin heads (MTH):**
  This basis is extremely localized with a pure angular momentum $L = (l, m_l)$ character. It is called MT heads since it uses the radial part of LMTO inside the MT spheres while it is zero outside. It is defined as

$$\xi_{R,L}(\mathbf{r}) = \begin{cases} \mathscr{Y}_L(\hat{\mathbf{r}})\phi_l(\varepsilon_\nu, r) & r < r_{MT} \\ 0 & r > r_{MT} \end{cases} \tag{2.59}$$

  where the LMTO radial function ϕ_l is the solution of Schrödinger equation for a certain ε_ν [33] and $\mathscr{Y}_L$, as explained in Eq. (2.23), are the modified spherical harmonics. In this basis, the interstitial part is completely neglected. The main problem of this basis is that it suffers from some spectral leakage and hence the overlap matrix (2.57) is not unity. This is because the Hilbert space spanned by the correlated orbitals is not a subspace of Hilbert space produced by LMT orbitals. To decrease the spectral leakage, however, one should keep in mind that a large MT radius has to be used for this projection, e.g., never less than 90% of the maximum radius allowed by the geometry of the system.

3. Calculation of the exchange parameters and beyond

In transition metals and their compounds, the $3d$ electrons have a dual nature. While their itinerant character defines for instance charge conductivity, at the same time their localized character is responsible for the local magnetic moment formation. The latter are often described by the Heisenberg model, which in the classical limit it is written in the following way:

$$H_{eff} = -\sum_{i,j} J_{ij} \mathbf{e}_i \cdot \mathbf{e}_j, \tag{3.1}$$

where J_{ij} are the exchange parameters between atom i and atom j, and $\mathbf{e}_i$ are the unit vectors along the magnetization direction of the atom at the site i. This model successfully describes field and temperature dependence of the magnetic susceptibility, the Curie temperature and other thermodynamic properties of a wide range of magnetic materials. The values of J_{ij} can be determined from first-principle calculations. Once the J_{ij} parameters are extracted, the thermodynamic properties as well as the spin dynamics can be obtained afterwards.

In experiment, the exchange parameters can be obtained through the fitting of the inelastic neutron scattering data to the Heisenberg Hamiltonian. In theory, they can be extracted from electronic structure calculations in different ways, each of them having its own advantages and disadvantages. The simplest way is to obtain the exchange parameters from total-energy differences calculated directly from different (usually collinear) spin configurations [70]. This approach, however, has serious drawbacks. First, quite a large number of spin configurations has to be considered and second, the result is just a number, which is hard to analyze. For instance, it remains unknown which orbitals contribute more to the value of J_{ij}. In addition, there are some methodological issues which I have discussed in Paper VII, where depending on the spin polarized or non polarized DFT exchange-correlation functional one can obtain quite different results for the exchange parameters.

In this respect, several methods based on adiabatic approximation are suggested. This means that these methods are only valid under the condition that the fluctuations of spin moments are slower than the fluctuations in the electron density (due to the electron hoppings). The exchange parameters extracted from these methods usually show very good agreements with experimental founding. Here, I first give a brief description of two of these methods and later I show some of my results for different materials.

3.1 Real-space approach

In order to investigate the effective exchange interactions in *ab initio* methods, a real-space method based on multiple-scattering theory was proposed by Lichtenstein *et. al* which we refer to as LKAG approach. For more details, the reader is referred to Ref. [71, 72, 73]. Here we give a brief explanation to this method, following the derivation from Ref. [73]. According to the LKAG formalism, it is possible to calculate small total energy changes through the variations of a one-electron density by employing the Anderson local force theorem. This theorem assumes that the main contribution to the changes in the total energy comes from the changes in one-electron density. Thus under small perturbation, the variation in the total energy δE of the ground state is the sum of the one-particle energy changes of the occupied states at the fixed ground state potential. According to this theorem, one can write the first order perturbations in the charge and spin densities via the following relationship

$$\begin{aligned}\delta E &= \int_{-\infty}^{E_F} d\varepsilon\, \varepsilon\, \delta n(\varepsilon) = E_F \delta z - \int_{-\infty}^{E_F} d\varepsilon\, \delta N(\varepsilon) \\ &= -\int_{-\infty}^{E_F} d\varepsilon\, \delta N(\varepsilon),\end{aligned} \tag{3.2}$$

where E_F is the Fermi energy, $n(\varepsilon) = dN/d\varepsilon$ is the density of the electronic states and $N(\varepsilon)$ is the integrated density of states. If we only have magnetic excitations in the system, the total number of electrons must be conserved. So, the change in the number of electrons δz is zero. The density of states and the integrated density of states can be expressed via the Green's function G of the system as follows

$$\begin{aligned}n(\varepsilon) &= -\tfrac{1}{\pi}\mathrm{Im}\ \mathrm{Tr}G(\varepsilon) \\ N(\varepsilon) &= -\tfrac{1}{\pi}\mathrm{Im}\ \mathrm{Tr}\ \mathrm{Ln}(\varepsilon - H)\end{aligned} \tag{3.3}$$

in which Ln is the logarithm and $G = (\varepsilon - H)^{-1}$.
According to the above expressions, one can define the variation of the integrated density of states as

$$\delta N(\varepsilon) = -\frac{1}{\pi}\mathrm{Im}\ \mathrm{Tr}[\delta H G]. \tag{3.4}$$

Using Eq. (3.2), the first derivative of the total energy of the system takes the following form

$$\delta E = -\frac{1}{\pi}\int_{-\infty}^{E_F} d\varepsilon\, \mathrm{Im}\ \mathrm{Tr}(\delta H G) \tag{3.5}$$

and the second derivative

$$\delta^2 E = -\frac{1}{\pi}\int_{-\infty}^{E_F} d\varepsilon\, \mathrm{Im}\ \mathrm{Tr}(\delta^2 H G + \delta H G \delta H G). \tag{3.6}$$

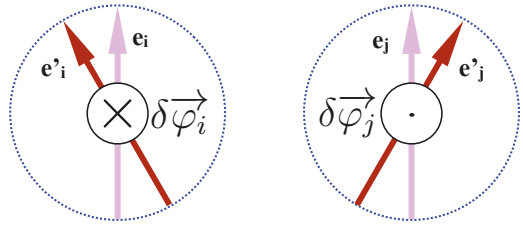

Figure 3.1. Schematic picture of infinitely small spin rotations at site i and site j.

The next step is to find the effective spin Hamiltonian as suggested by Lichtenstein *et al.* in [71, 72]. First, they proposed a system in the collinear ferromagnetic state with a unit vector of the magnetization $\mathbf{e}_i$ (Fig. 3.1), and then introduced a low-energy spin excitation to the system through small rotations of vectors $\mathbf{e}_i$ and $\mathbf{e}_j$. The operator expressing the spin rotation at the site i by an angle $|\delta\vec{\phi}|$ around direction $\mathbf{n} = \delta\vec{\phi}/|\delta\vec{\phi}|$ is given by

$$\hat{U} = e^{\frac{1}{2}i\delta\vec{\phi}\hat{\vec{\sigma}}}, \tag{3.7}$$

where $\hat{\vec{\sigma}} = (\hat{\sigma}_x, \hat{\sigma}_y, \hat{\sigma}_z)$ are the Pauli matrices. If the rotation is very small ($|\overrightarrow{\delta}\,\phi| << 1$), then we can expand the spin rotation operator in the following way:

$$\hat{U} \simeq 1 + \frac{i}{2}\delta\vec{\phi}\hat{\vec{\sigma}} - \frac{1}{8}(\delta\vec{\phi}\hat{\vec{\sigma}})^2. \tag{3.8}$$

The new Hamiltonian after this small rotation has the form

$$\hat{\tilde{H}} = \hat{U}^{\dagger}\hat{H}\hat{U}. \tag{3.9}$$

which after using Eq. (3.8), will take the following form

$$\hat{\tilde{H}} = \hat{H} + \frac{i}{2}\delta\vec{\phi}[\hat{H}, \hat{\vec{\sigma}}] - \frac{1}{8}(\delta\phi)^2[\hat{\vec{\sigma}}^2\hat{H} + \hat{H}\hat{\vec{\sigma}}^2 - 2\hat{\vec{\sigma}}\hat{H}\hat{\vec{\sigma}}] + ... \tag{3.10}$$

In the basis of some set of localized orbitals $|ilm\sigma\rangle$, the Hamiltonian matrix elements are defined as $H^{\sigma\sigma'}_{ilm,jlm'} = \langle ilm\sigma|\hat{H}|jlm'\sigma'\rangle$, where i denotes the site, l the orbital quantum number, m the magnetic quantum number and σ the spin index. For simplicity, we drop all the indices except for spin and site. Since the ground state of the system is considered to be collinear and there is no spin-orbit coupling, the Hamiltonian matrix must be diagonal in the spin subspace

$$H_{ij} = \begin{pmatrix} H^{\uparrow}_{ij} & 0 \\ 0 & H^{\downarrow}_{ij} \end{pmatrix}. \tag{3.11}$$

Using this, we can write the first variation of the Hamiltonian in the following way

$$\delta H_{jj} = i\delta\phi_j^x \begin{pmatrix} 0 & \frac{\Delta_j}{2} \\ -\frac{\Delta_j}{2} & 0 \end{pmatrix} + \delta\phi_j^y \begin{pmatrix} 0 & \frac{\Delta_j}{2} \\ \frac{\Delta_j}{2} & 0 \end{pmatrix}, \tag{3.12}$$

where $\Delta_j = H_{jj}^{\uparrow} - H_{jj}^{\downarrow}$ is the local exchange splitting. For the second derivative of the Hamiltonian we can easily obtain

$$\delta^2 H_{jj} = \delta^2\phi_j^x \begin{pmatrix} -\frac{\Delta_j}{2} & 0 \\ 0 & \frac{\Delta_j}{2} \end{pmatrix} + \delta^2\phi_j^y \begin{pmatrix} -\frac{\Delta_j}{2} & 0 \\ 0 & \frac{\Delta_j}{2} \end{pmatrix}. \tag{3.13}$$

Note that since the longitudinal fluctuations are neglected and rotation of spin moment around z axis does not change the energy of the system, no term proportional to $\delta\phi^z$ exist in the equations above.
The first derivative of the total energy δE represents the torque acting on the moments and is zero, if the state is stable. The second derivative $\delta^2 E$ is finite:

$$\begin{aligned} \delta^2 E = &-\frac{1}{\pi}\int_{-\infty}^{E_F} d\varepsilon \mathrm{Im\ Tr} \\ &\left(\frac{1}{2}\sum_i \delta^2 H_{ii} G_{ii} + \frac{1}{2}\sum_j \delta^2 H_{jj} G_{jj} + \sum_{ij} \delta H_i G_{ij} \delta H_j G_{ji}\right), \end{aligned} \tag{3.14}$$

where

$$\mathrm{Tr}(\delta^2 H_{ii} G_{ii}) = 1/2\delta^2\phi_i^x \Delta_i (G_{ii}^{\downarrow} - G_{ii}^{\uparrow}) + 1/2\delta^2\phi_i^y \Delta_i (G_{ii}^{\downarrow} - G_{ii}^{\uparrow}) \tag{3.15}$$

and

$$\begin{aligned} \mathrm{Tr}(\delta H_i G_{ij} \delta H_j G_{ji}) = &1/2\delta\phi_i^x \delta\phi_j^x (\Delta_i G_{ij}^{\downarrow} \Delta_j G_{ji}^{\uparrow}) \\ &+ 1/2\delta\phi_i^y \delta\phi_j^y (\Delta_i G_{ij}^{\downarrow} \Delta_j G_{ji}^{\uparrow}). \end{aligned} \tag{3.16}$$

The Green's function can be written as

$$G_{ii}^{\uparrow} - G_{ii}^{\downarrow} = G_{ii}^{\uparrow}\left(\frac{1}{G_{ii}^{\uparrow}} - \frac{1}{G_{ii}^{\uparrow}}\right) G_{ii}^{\downarrow} = G_{ii}^{\uparrow} \Delta_i G_{ii}^{\downarrow} = \sum_j G_{ij}^{\uparrow} \Delta_j G_{ji}^{\downarrow}. \tag{3.17}$$

Using this we can rewrite the Eq. (3.14) in the following form:

$$\delta^2 E = \frac{1}{4\pi}\int_{-\infty}^{E_F} d\varepsilon\ \mathrm{Im} \sum_{ij} (\Delta_i G_{ij}^{\downarrow} \Delta_j G_{ji}^{\uparrow}) \times [(\delta\phi_i^x - \delta\phi_j^x)^2 + (\delta\phi_i^y - \delta\phi_j^y)^2]. \tag{3.18}$$

Applying the same perturbation expansion on the classical Heisenberg Hamiltonian (Eq. 3.1), one arrives at very similar expression for $\delta^2 E$, containing the J_{ij}'s. Thus an ideal mapping of the two models is possible. Now, we reached a point where that we can have an explicit definition for the exchange interactions as follows

$$J_{ij} = \frac{1}{4\pi}\int_{-\infty}^{E_F} d\varepsilon\ \mathrm{Im}(\Delta_i G_{ij}^{\downarrow} \Delta_j G_{ji}^{\uparrow}). \tag{3.19}$$

3.2 Frozen-magnon approach (FMA)

This method is not used in this thesis. However, in order to have a complementary introduction of the ways for calculation of exchange parameters, a very brief introduction is given in this section. The interested readers are referred to Ref. [74]

In contrast to LKAG method, this method is done in reciprocal space and is based on the calculation of total energy for spin spiral [1](also called frozen magnon) magnetic configurations [74]. In this method, the spin spiral has a propagation vector ($\mathbf{q}$) defined in reciprocal space. The vectors of the magnetic moments $\mathbf{e}_m$ are localized at ionic sites with lattice vector $\mathbf{R}_m$. Then, the moment precessing around a certain axis, e.g. z, by the angle of θ can be defined as

$$\mathbf{e}_m = \sin\theta\cos(\mathbf{q}\cdot\mathbf{R}_m)\hat{\mathbf{x}} + \sin\theta\sin(\mathbf{q}\cdot\mathbf{R}_m)\hat{\mathbf{y}} + \cos\theta\hat{\mathbf{z}}. \tag{3.20}$$

Then the total energies of different spin spirals states are calculated and mapped onto Eq. (3.1). To extract meaningful exchange parameters, we are restricted to small perturbations: the cone angle θ must be as small as numerical precision permits. Then the exchange interaction for each individual site is related to the energy differences for each wave vector $\mathbf{q}$:

$$\begin{aligned}\Delta E(q,\theta) &= \sum_{j\neq 0} J_{0j}(1-\exp(\mathbf{q}\cdot(\mathbf{R}_0-\mathbf{R}_j))\sin^2\theta \\ &= [J(0)-J(\mathbf{q})]\sin^2\theta,\end{aligned} \tag{3.21}$$

where $J(\mathbf{q})$ are the Fourier transform of the exchange parameters:

$$J(\mathbf{q}) = \sum_{j\neq 0} J_{0j}\exp(i\mathbf{q}\cdot(\mathbf{R}_0-\mathbf{R}_j)), \tag{3.22}$$

where the exchange parameters can be obtained by inverse Fourier transformation of this equation. In this method, the spin spirals can be simulated in the first-principles calculations without the use of large supercells by the help of generalized Bloch theorem [75]. However, this method is only valid when spin-orbit coupling is neglected.

LKAG and FMA are formally equivalent and complementary to each other. The quantities that are calculated are J_{ij} and $E(\mathbf{q})$ in the former and latter case, respectively. In fact, these quantities are related to each other by Fourier transform and should give identical results in the limit of $\theta \to 0$ for FMA. Therefore, the advantages and disadvantages of LKAG and FMA methods refer mostly to their computational efficiency. For calculation of spin-wave dispersion curves and spin stiffness, FMA is more direct, since it does not need to

[1]Spin spiral is a magnetic configuration with moments that are rotated around specific axis by a constant angle from one atom to another along a certain direction in the crystal.

Fourier transformation. On the other hand, LKAG method seems to be more efficient for calculations of ordering temperature, since a set of calculated J_{ij} in real space, for typically 200 shells, provide an accurate parametrization for reciprocal space ($J(\mathbf{q})$). In addition, the real-space approach LKAG gives a set of pair interactions even for very distant atoms only from a single calculation. While the widely used alternative approach, FMA, relies on DFT calculations for spin spirals and then derives the coupling parameters from total energies of the spirals. Therefore, depending on the system under study, either of these methods can be applied. Again, we emphasize that the exchange parameters obtained by these two methods are formally equivalent. As an example, the J_{ij} parameters for bcc Fe bulk obtained with LKAG and FMA methods are shown in Fig. (3.2) for comparison.

In this thesis, we have used the real-space LKAG method for the calculation of exchange parameters.

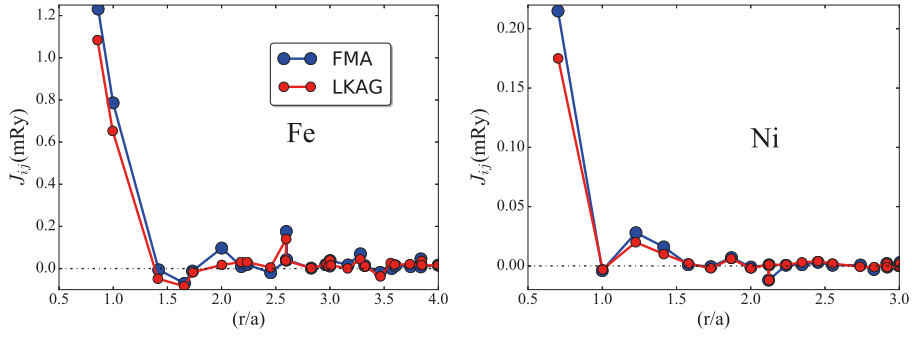

Figure 3.2. The exchange parameters (J_{ij}) calculated for bcc Fe (left panel) and fcc Ni (right panel) using two different methods; FMA and LKAG approaches [76].

3.3 Ordering temperature

Having in hand the calculated the exchange parameters, one is able to extract thermodynamic quantities such as the ordering temperature of the systems. There are several approximations that can be used.

- **Mean-field approximation (MFA)**
  In this approach, the main idea is that each spin experiences an average field of the neighboring spins and thus one can replace the spin-spin interaction by an interaction of each spin with an average magnetization of spins around it [77]. This method usually yields qualitatively correct results for three dimensional systems with long range interactions, how-

ever, it can be questionable for low dimensional systems like surfaces and for only nearest neighbor interactions. The calculated ordering temperature are usually overestimated in comparison to experimental data. For the case of a single atom per unitcell the experssion is

$$k_B T_c^{MFA} = \frac{2}{3} \sum_{j \neq 0} J_{0j}. \tag{3.23}$$

- **Random phase approximation (RPA)**
  This method goes beyond MFA and takes into account the temperature dependence when solving the Heisenberg model using Tyablikov's Green's functions method [78]. In contrast to MFA, it takes into account the collective excitations (spin waves) and provides more reliable estimates of the ordering temperatures, even though usually underestimated as compared to experiment.

- **Monte Carlo (MC)**
  The classical MC approach is the most sophisticated and computationally involved approach among the three methods. It is based on an evolutionary search of the magnetic ground states. At each MC run, a chosen spin at the lattice site j is rotated to a new random direction $\mathrm{e}_j^{\mathrm{new}}$. If this new direction lowers the energy of the system, the rotation is accepted, otherwise the old direction $\mathrm{e}_j^{\mathrm{old}}$ is kept. In this way the system is finally brought into thermal equilibrium for a given temperature [76, 79].

All these three approaches are based on mapping of magnetic moment interactions to the classical Heisenberg Hamiltonian. These moments, however, are quantum mechanical objects not classical. Therefore, one needs to somehow take into account the quantum effects. One way is to replace the classical S^2 in the Heisenberg Hamiltonian with the quantum mechanical expectation value $S(S+1)$ as suggested by Savrasov and Harrison [80, 81]. However, for large enough spin moments and at high temperatures the difference should be rather small [82].

In this thesis, the MC method has been used to extract the ordering temperature. The quantity which one can look at to extract this value is either is projected moment of the atoms when it decays to zero, or the specific heat when it reaches to its peak (see Fig. 3.3 for the case of $CaMnO_3$).

To conclude this part, stronger localization of the electrons in a system generates a larger magnetic moment and, at the same time lowers the ordering temperature, since the exchange interactions with the neighboring atoms become weaker. This is why all rare-earth metals are paramagnetic at room temperature (with the exception of Gd with T_C=289 K). On the other hand, for some of the 3*d* metals and their compound this balance is just right; among

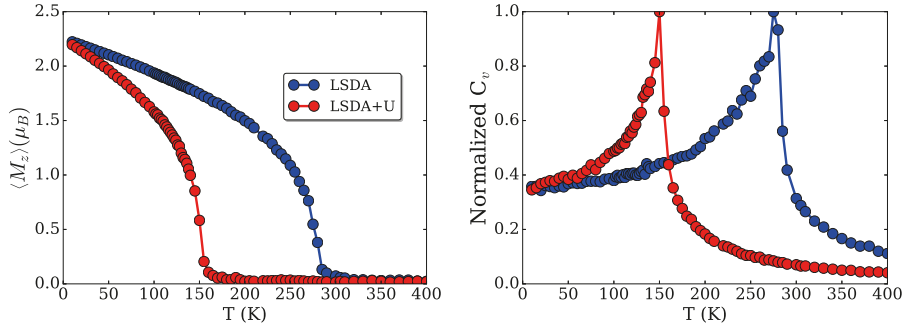

Figure 3.3. The projected spin moment (left) and the normalized specific heat (right) of $CaMnO_3$ bulk in LSDA and LSDA+U approaches, obtained from MC simulations.

them Fe, Co and Ni. In these system, the localizations of 3*d* electrons is high enough to generate a remarkable magnetic moment and still low enough to provide an overlap with the neighbors. This balance leads to significant ordering temperatures.[2]

3.4 Magnetic excitations

At zero temperature, the magnetic moments are aligned and the material has a large moment M even in the absence of an external field. At low temperature, the magnetization scales as $T^{3/2}$ according to the Bloch's law. All magnetic materials typically undergo a phase transition to a paramagnetic state when heated to sufficiently high temperatures. In a ferromagnetic materials, there exists basically two different types of magnetic excitations, called

- *Stoner excitations:*
  creation of an electron-hole pair of triplet spin which causes longitudinal fluctuations of the magnetization.
- *Magnons or spin waves:*
  collective excitations of the electrons spin responsible for transverse excitations of the magnetization.

At low temperatures and in the materials with relatively large spin splitting, one can completely ignore the Stoner excitations and only focus on the spin waves [83]. This is exactly what has been assumed in the semi-classical description of the spin dynamics where the magnetic moment is treated as a 3D vector with a fixed length. Consider a spin with magnetization **M** in the presence of an external magnetic field **B**. According to the Zeeman term in

[2]Note that Ni has a smaller moment as compared to Co and Fe and is therefore expected to be described worse by a classical vector.

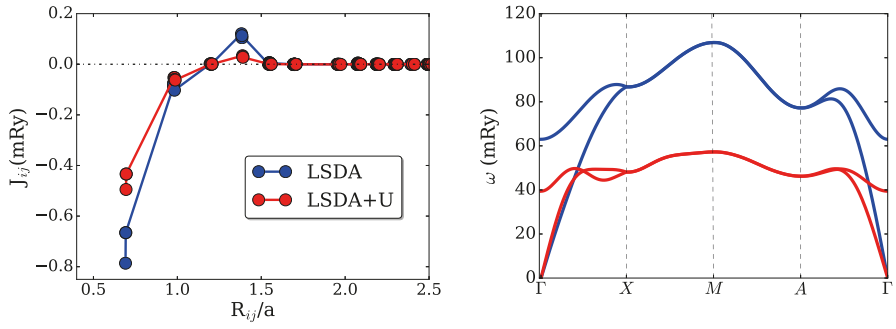

Figure 3.4. The exchange parameters (left) as well as the calculated adiabatic magnon spectra (right) of $CaMnO_3$ bulk in LSDA and LSDA+U approaches.

Eq. 1.15, the magnetization interacts with the magnetic field which exert a torque over **M** making it process around the filed axis as

$$\frac{d\mathbf{M}}{dt} = -\gamma \mathbf{M} \times \mathbf{B} \tag{3.24}$$

where γ is gyromagnetic ratio.

In reality, the **B** field should not only represent the external filed but also take into account different interactions present in the material such as exchange, anisotropy and etc. One way to model this filed is to use the Heisenberg Hamiltonian in Eq. 1.15 and define the effective field as $\mathbf{B}_{\text{eff}} = -\frac{\partial H}{\partial \mathbf{M}}$. However, in practice only the most significant terms in the Hamiltonian are taken into account.[3]

The simplest intuition to the dynamics of the system can be obtained by assuming that electron motion is much faster that the fluctuations in magnetic moments. This is referred as adiabatic approximation which gives the static spin waves by neglecting the precession motion of the moments. In this approach, one can obtain the spectra by a Fourier transform of the interatomic exchange parameters J_{ij}'s. In the case of a single atom unitcell, the energy as a function of the spin wave momentum (**q**) is

$$\omega(\mathbf{q}) = \frac{4}{M}\left[J(0) - J(\mathbf{q})\right]. \tag{3.25}$$

As an example, in Fig. 3.4 we show the adiabatic magnon spectra for $CaMnO_3$ bulk (right panel) in LSDA and LSDA+U from the obtained exchange parameters (left panel).

[3]For a more accurate description on the dynamics of the system a dissipation term needs to be added to Eq. 3.24, which finally aligns the magnetization with the magnetic filed. This is done by Landau and Lifshitz [84] for low damping and modified by Gilbert for high damping systems [85].

Some points about temperature effects:

Besides description of the ground state properties of magnetic systems which are obtained at zero temperature, it is also possible to address the dynamical properties using the temperature dependent exchange parameters. Based on the three-temperature model [86], the dynamics of the system at finite temperature is determined by the heat communicating among the spin, electron and lattice. Katsnelson and Lichtenstein have generalized the LKAG method in Eq. 3.19 for the case of DMFT [72], which can take into account the electronic temperature. In this case, the expression for the J_{ij}'s takes the following form

$$J_{ij} = \frac{1}{4}\mathrm{Tr}_{\omega,L}\left[\hat{\Sigma}_i(i\omega_n)\hat{G}^{\uparrow}_{ij}(i\omega_n)\hat{\Sigma}_j(i\omega_n)\hat{G}^{\downarrow}_{ji}(i\omega_n)\right], \tag{3.26}$$

where $\uparrow$,$\downarrow$ refer to spin, ω_n is Matsubara frequencies ($\omega = \pi(2n+1)k_BT$) and the on-site exchange is now dynamical

$$\hat{\Sigma}_i(i\omega_n) = (\hat{H}^{\uparrow}_i - \hat{H}^{\downarrow}_i) + (\hat{\Sigma}^{\uparrow}_i(i\omega_n) - \hat{\Sigma}^{\downarrow}_i(i\omega_n)), \tag{3.27}$$

with $\hat{H}$ being the local Hamiltonian matrix obtained from solving the DFT equations and $\hat{\Sigma}_i$ is the self-energy describing strong local electronic correlations. The self-energy appears for DFT+U and DFT+DMFT calculations, and also enters the expression of the Green's function as

$$\hat{G}_i(i\omega_n) = \left\langle i \left| \frac{1}{i\omega_n - \hat{H} - \hat{\Sigma}(i\omega_n)} \right| j \right\rangle. \tag{3.28}$$

This method has been used in Paper I [87], II [88] and V [89], and the results will be discussed in the next chapter. We should mention that the other temperature-driven effects such as spin disorder or lattice vibrations are not considered in this Thesis. Spin fluctuations can be captured by extracting the exchange parameters from non-collinear magnetic configurations, corresponding to a finite spin temperature. This approach has be developed in Refs. [90, 91]. To study the impact of lattice vibrations on magnetic properties, a method of the disordered local moments molecular dynamics has been employed by Alling et al. [92] which can capture the coupling of spin-lattice dynamics.

Finally, we mention that in the methods where the temperature effects are absent, like in DFT and DFT+U, one can combine *ab initio* calculations with the atomistic spin dynamics to describe the dynamics of spin systems at finite temperatures. Among them are the space and time displaced correlation function $C(\mathbf{r}-\mathbf{r}',t)$ which gives information on the correlation between two spins located at different sites $\mathbf{r}$ and $\mathbf{r}'$ and generally it is defined as

$$C^k(\mathbf{r}-\mathbf{r}',t) = \left\langle m^k(\mathbf{r},t)\, m^k(\mathbf{r}',0)\right\rangle - \left\langle m^k(\mathbf{r},t)\right\rangle \left\langle m^k(\mathbf{r}',0)\right\rangle \tag{3.29}$$

for each Cartesian component k of the moments. This function can be used to obtain the correlation length which is the measure of how long-range the magnetic order is in a given system.

In Paper IV, we discuss the correlation between the spins at different temperature where we only consider the first term of the above equation. The second term is called the connected correlation function while the first one is called the disconnected correlation function. The disconnected correlation function is the one that offers information about the ordering of the magnetic system and has been implemented in UppASD code. So for magnetic systems, the important relevant term is the disconnected correlation function.

4. Surface of 3*d* systems

Magnetism is a quantum mechanical property with no classical correspondence. This property appears to be stronger in some elements of the Periodic Table, specially for *3d* and *4f* elements, where their electronic shell is not completely occupied. Magnetism leads these materials to show quite different properties when confined to lower dimensions in comparison to their bulk structures. For instance, as a bulk, these materials present relatively strong ferromagnetism, while their thin films sometimes show non-collinear spin structures. The latter leads to the emergence of antiferromagnetic features, depending on the film thickness, the substrate used for deposition and other details [93, 94].

Density functional theory (DFT) and its formal extensions provide an excellent parameter-free description of ground-state properties of magnetic metals, including bulk structures as well as systems without three-dimensional periodicity such as surfaces, interfaces, thin films, disordered alloys, and nanoparticles. However, several studies have emphasized the importance of including strong correlation effects in the electronic structure of 3*d* systems. For instance, noncoherent features such as Hubbard bands and satellites, which appear in the excitation spectra of the photoemission experiments [95, 96], cannot be solely described by the DFT. Correlation effects in transition metals are expected to be even more pronounced for the surface atoms due to narrower bands and reduced coordination numbers. In this chapter, we report a computational study of surface magnetism of TM slabs. The main focus is on the calculations of the interatomic exchange interactions (J_{ij}).

4.1 Surface of Fe, Co and Ni

In paper I, we have studied the layer-resolved magnetic exchange interactions of the surface of late transition metals, i.e., Fe, Co and Ni [87]. The purpose of this work was to have a better understanding of magnetic exchange interactions between atoms when going from the bulk to their surfaces. In addition, the effect of correlations on the exchange parameters is studied by means of LDA+DMFT. These elements have quite high Curie temperature, which means that their magnetic moments are rather localized and robust with respect to the thermal fluctuations. Therefore, the magnetic excitations are caused mostly by transverse spin fluctuations rather than Stoner-like excitations. This approximation is actually good for ferromagnets with a large exchange splitting such as Fe, Co and less justified for Ni, that has a smaller

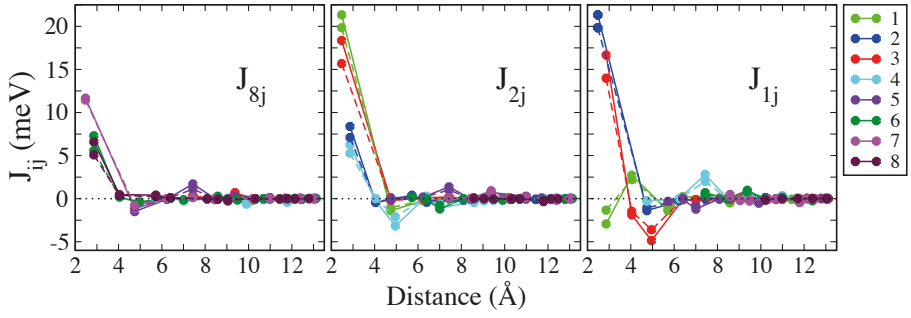

Figure 4.1. Layer-resolved exchange parameters (J_{ij}) for a 15-layer bcc Fe(001) slab for the case when atom i is located in the innermost layer (left panel), in the subsurface (middle panel), and at the surface (right panel). The solid lines indicate LDA results while the dashed lines represent the LDA+DMFT results. The layer numbering in the legend starts from the surface denoted by 1, the subsurface denoted by 2, and so on. The innermost layer is denoted by 8.

exchange splitting. Therefore, the exchange parameters obtained using DFT are not very sensitive to the details of the approximations. Here we address some of these details for the case of Fe slab.

In Fig. 4.1, we show that the interatomic exchange interactions in Fe slab present a general trend of enhanced values at the surface both in LDA (solid lines) and DMFT (dashed lines). This is driven by the larger exchange splitting of the surface states compared to the bulk states. However, the interaction between Fe surface atoms (green lines in the right panel) are rather weak, while it is opposite for Co and Ni as shown in Paper I. We argue that this (antiferromagnetic) weak interaction between the nearest neighbor atoms at the surface of Fe are due to the nesting at the Fermi surface cross-section. This nesting defines a preferable direction for a symmetry-breaking in the system and derives incommensurate magnetic ordering.

The dynamical correlations introduced within DMFT do not show drastic differences on spin moment and exchange interactions (dashed lines). This is because within the SPTF solver, which we have used in this study, the topology of the Fermi surface is unchanged. Therefore, the main effect of the dynamical correlations is the carrier mass renormalization which results in an overall slight decrease of the J_{ij}'s.

Note that the exchange parameters calculated in this work are not scaled with the moment sizes, therefore; they can directly be used to calculate the Curie temperature through MFA, RPA or MC approaches. Spin-orbit coupling in 3*d* elements is very small, which results into small orbital moments (as reported in Table II of paper I). Indeed, Dzyaloshinski-Moriya interactions are allowed by broken symmetry and they will be stronger for the surface atoms than the inner layers. To obtain substantial values for the DM interaction one

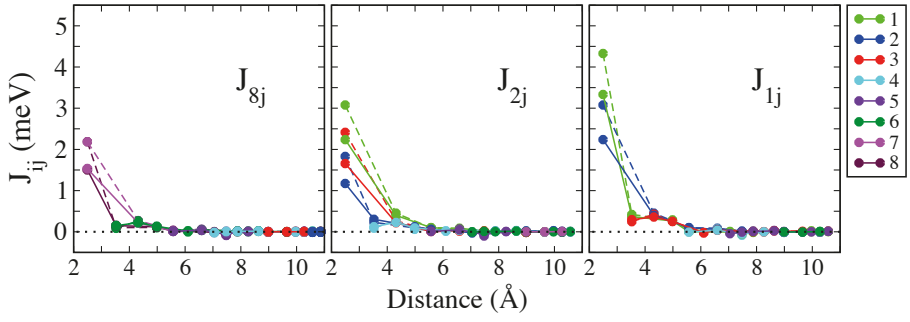

Figure 4.2. Layer-resolved exchange parameters (J_{ij}) for 15-layer fcc Ni slab for the case when atom i is located in the innermost layer (left panel), in the subsurface (middle panel) and at the surface (right panel). AMF results (solid lines) are compared with the $\Sigma(0)$ DC (dashed lines). The layer numbering in the legend starts from the surface denoted by 1, the subsurface denoted by 2, and so on.

typically requires some *4d* or *5d* substrate, which effectively enhances the SOC in the system.

Double counting effect

In our calculations, the LDA Hamiltonian is considered to be spin polarized (LSDA). In the DMFT calculations, the double counting correction has been chosen to be the static part of the self-energy (see section 2.2.4). This means that the static spin splitting in LDA+DMFT comes solely from LDA. Otherwise, one can perform non spin-polarized LDA and let all the spin polarization effects come from DMFT. In such a case, the self-energy is spin-polarized with different contribution for spin up and spin down states. Hence, one might need to make an average of these two terms before subtracting it from the LDA Hamiltonian. We did not use this approach in this paper. We, instead, considered that spin-polarized LDA already gives the correct splitting and hence the contribution coming from DMFT part at $\omega = 0$ can be canceled out as the $\Sigma(0)$ double counting.

In the case of Ni, however, it is known that the LDA splitting is overestimated when compared to experimental data. To avoid this problem, we used another widely used type of DC called around mean filed (AMF). The exchange parameters for different DC corrections are shown in Fig. 4.2, where the AMF suppresses the J_{ij}'s only slightly in comparison to $\Sigma(0)$. An analysis of the basic electronic structure revealed that the AMF corrections results in a decreased exchange splitting and consequently a reduction in the spin polarization. However, both DC methods reveal qualitatively very similar results for the exchange parameters and the difference appears mainly in the magnitude of the J_{ij}'s.

4.2 Surface of $CaMnO_3$

In paper II, we have analyzed the electronic structure as well as the magnetic properties of the bulk and surface of $CaMnO_3$ (CMO), which is a *G*-type AFM as a bulk. The motivation for this investigation came from the work by Filippetti and Pickett [97], where they investigated the surface of CMO by means of *only* density functional theory. They analyzed the band structure and calculated several magnetic configurations. Finally they found that the surface spins reverse their orientations, i.e., undergo a spin-flip (SF) process. In this way, the surface and subsurface Mn spins are coupled ferromagnetically through a double-exchange-type mechanism, while the rest of the system is still in antiferromagnetic spin configurations similar to its bulk.

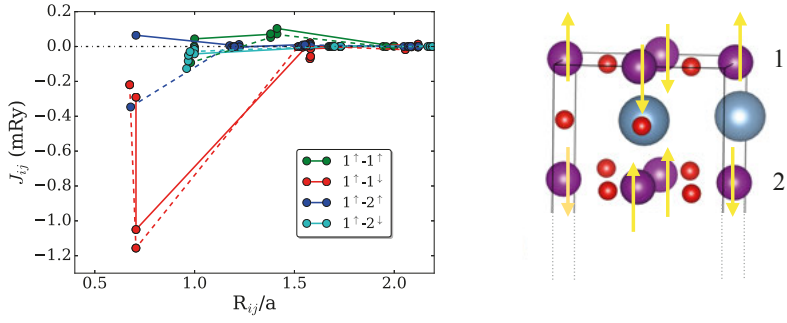

Figure 4.3. Left) The exchange interaction between an atom at the surface of CMO with the atoms at the surface (layer 1) and subsurface (layer 2) for unrelaxed (solid lines) and relaxed structure (dashed lines) within LSDA+*U* approach. Right) The obtained ground state magnetic configuration for the relaxed slab. The purple balls represent Mn atoms with yellow arrow indicating spin magnetization direction, the red balls are O and the blue ones are Ca atoms.

This finding was quite interesting. Therefore, I decided to reexamine the electronic and magnetic structure of the surface of CMO by taking into account the effect of the static on-site interaction between 3*d* electrons, within LSDA+*U* approach. The preferable magnetic order is identified by direct total-energy comparison, as well as by extracting the exchange parameters through the magnetic force theorem. While we confirmed the results reported in Ref. [97] for an non-optimizied structure, we found out that the structural relaxations play an important role and that when taken into account, the (001) surface of CMO has the same AFM ordering as the bulk, i.e., the spin-flip ordering of the surface atom disappears. These results are shown in Fig. 4.3, which indicate that a small structural displacements provides a significant modification of the interatomic exchange interaction, even to the extent of the changing the spin configuration of the system (compare the blue lines in left panels of Fig. 4.3 when they change their sign from FM to AFM after relaxation).

5. Half-metallic Heuslers alloys

In this chapter I focus on the electronic structure and magnetism in ferromagnetic Heusler compounds. Having a magnetic moment close to integer classifies these materials as rather correlated; they also show an essential feature due to many-body effects, i.e., the existence of nonquasiparticle (NQP) states [98, 99]. These states stem from the *electron-magnon* interaction and can influence the value and temperature dependence of the spin polarization in half-metal (HM) Heuslers. For instance, according to Ref. [100], at $T = 0$ the density of NQP states vanishes at the Fermi level, while for $T > 0$ these states start smearing such that their tails cross the Fermi level which results in the reduction of spin polarization. Contrarily, some other studies reported that these states have been seen above the Fermi level without crossing it [101].

Including NQP states in the electronic structure requires methods beyond standard DFT. In this work, we used DFT+DMFT to better describe the local correlation effects and possibly to observe the presence of the NQS around the Fermi level. In addition, we are interested in investigating the magnetic properties particularly exchange interaction in the presence of the strong local correlations. Below, I will address two of my papers on Heusler systems.

5.0.1 Co_2MnSi bulk

In Paper III, we have done a systematic investigation of the electronic structure and magnetic properties of a series of half-metallic Heuslers [88]. Special attention has been paid to the Heisenberg exchange parameters and the Gilbert damping. Depending on the choice of exchange correlation potentials, remarkable differences have been found in the description of the systems. Based on the obtained results, no single combination of exchange-correlation potential and shape of the KS potential geometry was able to reproduce all the experimentally measured magnetic properties of a given system simultaneously. However, we realized that the more sophisticated treatment of the geometrical shape of the potential, that is a full-potential scheme, yields results closer to experiment in comparison to the atomic sphere approximation, which excludes the nonspherical contributions.

In this work, the bulk Co_2MnSi is studied; a ferromagnetic Heusler with Mn atoms sitting at the body centres of the cubic structure and carrying most of the magnetic moment of the alloy [88]. Based on the selected Hubbard U (3 eV) and Hund's exchange J (0.8 eV) values for both Co and Mn, we

calculate the electronic structure of the system. The total density of states in LSDA, LSDA+U and LSDA+DMFT methods are shown in Paper III, Fig. 5.1. Half-metallic character and integer magnetic moment of Co_2MnSi are already predicted by DFT. While LSDA+U tends to increase the band gap of LSDA by shifting the bands far below and far above the Fermi level, DMFT (especially with Σ_0^{DC}) predicts similar spectra as for LSDA. This is due to perturbative treatment in SPTF solver where the dynamical part of the self-energy close to the Fermi level has a Fermi-liquid behavior just as in LSDA.

Our results based on LSDA+DMFT show that the NQS states appear well above the Fermi level at room temperature, as shown in Fig. 5.1, and therefore will not contribute to the spin depolarization. These states manifest themselves in the imaginary part of the self-energy (see the bottom panel of Fig. 5.1). Orbital-resolved self-energy in the cubic harmonics basis reveals that the NQP states stem from the e_g states of Mn atoms.

Finally, the exchange parameters in Co_2MnSi has been also discussed. The leading interaction is found to be the one between Mn and their nearest Co atoms. The interaction between nearest Co atoms at different sublattices also favors ferromagnetism and is stronger than the ferromagnetic interaction between the nearest Mn atoms. Overall, LSDA, LSDA+U and LSDA+DMFT deliver consistent results for the J_{ij}'s in terms of sign and global trend.

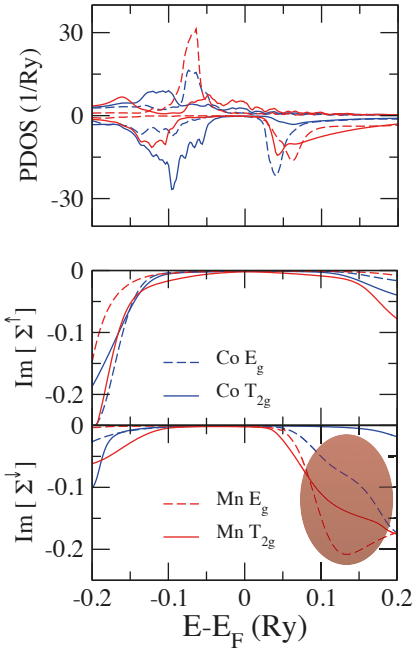

Figure 5.1. Top) partial density of states of Co and Mn 3*d* states in LSDA+DMFT using Σ_0 double-counting. Bottom) orbital-resolved spin-up and spin-down imaginary parts of the self-energy. The brown ellipse highlights the position of NQP states.

5.0.2 Co_2MnAl/CoMnVAl heterostructure

In Paper IV, we study the electronic structure of the Co_2MnAl/CoMnVAl heterostructures in the presence of the correlation effects as well as investigating their magnetic properties, particularly the exchange interactions. To analyze the role of NQP states and the tendency to noncollinear magnetism (as suggested before for this class of materials [102]), we have focused on bulk of Co_2MnAl half-metal ferromagnet (HMF) and CoMnVAl semiconductor (SC), as well as their heterostructure. Depending on the termination layers, two types of interfaces are possible [101], namely Co-Co/V-Al and Co-Mn/Mn-Al. Both of them are predicted to preserve the half-metallic character of the material.

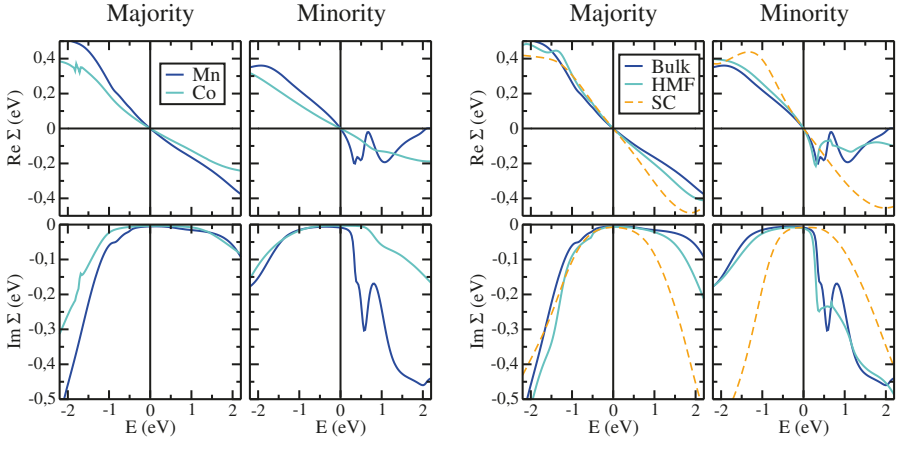

Figure 5.2. Left panel) average self-energy per orbital of the Mn and Co 3*d* states in Co_2MnAl, for majority (left panels) and minority (right panels) spin channels. Right panel) average self-energy per orbital of the Mn 3*d* states in Co_2MnAl and at the HMF side of the Co-Mn/Mn-Al interface, both for spin channels.

Similar to Co_2MnSi described in the previous section, our findings prove that Co_2MnAl is also a half-metal, whose magnetic moments and exchange couplings depend only slightly on the inclusion of strong electronic correlations (both static and dynamic). In LSDA+U, where the largest corrections are observed, the magnetic moments are increased of about 10% with respect to their values in LSDA, while the increase of the nearest neighbor exchange coupling is at most of 40%. No qualitative changes, e.g., in the sign of the magnetic moments or the interatomic exchange parameters, are observed. LSDA+DMFT simulations clearly show the appearance of NQP states within the minority-spin gap in the band structure. These states are identified to originate mainly from Mn-3*d* states and are located several hundreds meV above the Fermi level, therefore they do not seem to affect the spin polarization very much. The signature of NQP states is particularly evident in the orbitally averaged self-energy function, which is shown in the left panel of Fig. 5.2. In

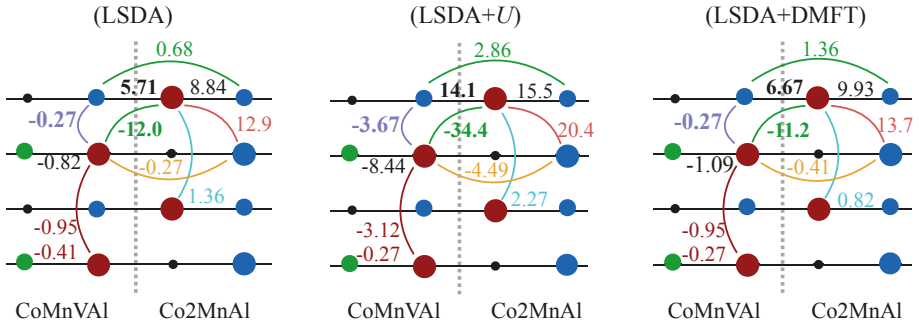

Figure 5.3. Interatomic exchange parameters J_{ij} (in meV) for the most relevant atomic pairs at Co-Mn/Mn-Al interface. Mn, Co, V, and Al atoms are, respectively, represented as red, blue, green, and small black spheres. The bonding lines and the J_{ij} values of the same color correspond to the same bond. Bigger circles represent atoms belonging to xz plane with x = 0.0, while small circles represent atoms belonging to the plane with $x = 0.5$. The z axis is perpendicular to the interface plane. Notice that two different numbers (in magenta) are reported for the Mn-Mn bond on the side of interface containing CoMnVAl. The upper and lower numbers correspond to bonds along the [100] and [010] directions, respectively.

the minority spin channel, the imaginary part of the Mn self-energy is characterized by a large peak appearing at 0.4 eV above the Fermi level, while only a small shoulder is visible for Co. This is in sharp contrast with the majority spin channel, where curves have similar shapes. One can also notice that the magnitude of the corrections induced by the self-energy is much bigger for Mn than for Co, since correlation effects are often stronger closer to half-filling.

The Co_2MnAl/CoMnVAl heterostructures are predicted to be half-metallic as well. This prediction is held by inclusion of the static corrections (LSDA+U) or the strong correlations (LSDA+DMFT). Our findings in LSDA+DMFT simulations predict the appearance of NQP states stemming from the Mn $3d$ states at the Co-Mn side of Co-Mn/Mn-Al interface. The tail due to the NQP states extends closer to the Fermi level than in the bulk HMF, resulting in a 35% reduction of the band gap with respect to its LSDA value. In the right panel of Fig. 5.2, these states are found around 0.3-0.4 eV.

The Co-Mn/Mn-Al interface is also interesting for its magnetism. The presence of two Mn atoms which are relatively close to each other leads to a strong antiferromagnetic coupling, which is stabilized by reducing the size of neighboring moments. The dominant J_{ij}'s at the Co-Mn/Mn-Al interface are shown in Fig. 5.3. Within the current magnetic configuration all the magnetic interactions seem to be satisfied, suggesting that the chosen collinear magnetic order is locally stable. However, the J_{ij}'s extracted by the magnetic force theorem are known to depend on the reference state. Thus, we believe that there are two indications that the current magnetic order might not be the ground state. First, the Co and Mn moments on the CoMnVAl side are quite small in mag-

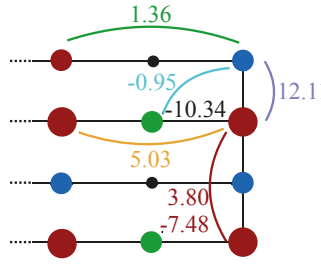

(LSDA)

Figure 5.4. Interatomic exchange parameters J_{ij} in meV for the most relevant atomic pairs at the surface of CoMnVAl. Similar pattern has been used as for Fig. 5.3 for the atom colors and etc.

nitude, 0.3 μ_B for Co and -0.6 μ_B for Mn in LSDA method. Second, the J_{ij}'s between them is also surprisingly small (bold purple numbers in Fig. 5.3).

Our interpretation is that this coupling might actually be ferromagnetic. However, since it is in competition with a strong antiferromagnetic Mn-Mn coupling (bold green) and a strong ferromagnetic Co-Mn coupling (bold black) across the interface, the system finds it energetically favorable to suppress these magnetic moments.

To verify this hypothesis we performed additional calculations by removing the HMF from the supercell. The results for the exchange parameters extracted only from LSDA approach are shown in Fig. 5.4. As can been seen, the corresponding Mn-Co magnetic coupling is ferromagnetic with their moments strongly enhanced. However, the next nearest neighbor interaction of Mn-Mn is both ferromagnetic and antiferromagnetic of the same order of magnitude (red numbers). This situation may potentially lead to a noncollinear spin order, which has already been suggested for interfaces involving Heuslers alloys [102]. A more quantitative analysis of such ordering could be done by performing calculations by including spin-orbit coupling and acount for the DM interactions. This can be then followed by atomistic spin dynamics simulations [103, 104], but this task was beyond the scope of the present study.

6. Bulk of perovskite oxides

Perovskite oxides have a variety of composition and component elements. Based on their crystal structures, there are many functions and rich application areas, namely ferroelectricity, superconductivity, catalytic activity, magnetism. In this chapter, I will discuss two perovskite systems, namely an AFM Ruddelsden-Popper double perovskite $Sr_3(Fe_{1.25}Ni_{0.75})O_{7-\delta}$, and a FM Nd_2NiMnO_6. In these studies, their electronic ground states as well as their magnetic properties are investigated, with a special focus on the pairwise exchange interactions between the magnetic atoms.

6.1 $Sr_{3-x}Y_x(Fe_{1.25}Ni_{0.75})O_{7-\delta}$ layered perovskite

In Paper V, we present a comprehensive study of the magnetic properties of the system based on our experimental and theoretical investigations [105]. Experimentally, the magnetic properties are investigated using superconducting quantum interference device (SQUID) magnetometry and neutron powder diffraction (NPD). Experimental results show an increase in the Néel temperature (T_N) with an increase of Y concentrations and O occupancy. The NPD data reveal that all samples are antiferromagnetically ordered at low temperatures. For the selected compounds, these results are in good agreement with the *ab initio* calculations using DFT+U approach based on total energy differences for different spin configurations as well as exchange parameters from magnetic force theorem (see Figs. 6.1 and 6.2). These parameters are then used to evaluate the ordering temperature via Monte Carlo simulations. The calculated magnetic moments and the ordering temperature are in good agreement with observations; e.g, for $x = 0.5\ (0.75)$ the experimental T_N is measured 275 K (310 K) while our MC simulations show a peak at 260 K (310) in the specific heat which corresponds to the ordering temperature. Including on-site magnetocrystalline anisotropy and dipole-dipole interactions in our calculations did not introduce any noticeable change of the 3D ordering in the system.

The self-consistent spin-wave theory for quasi-2D systems shows that the presence of any small interlayer exchange couplings is important and may provide 3D ordering [106, 107]. This 3D ordering can exist at low temperatures but will undergo a transition to 2D ordering upon increasing the thermal fluctuations [108]. To see this, we have performed the spin-spin correlation functions along different directions by considering only the atoms with the most relevant exchange couplings, i.e., J_1, J_2, and J_3 in Fig. 6.1. The results

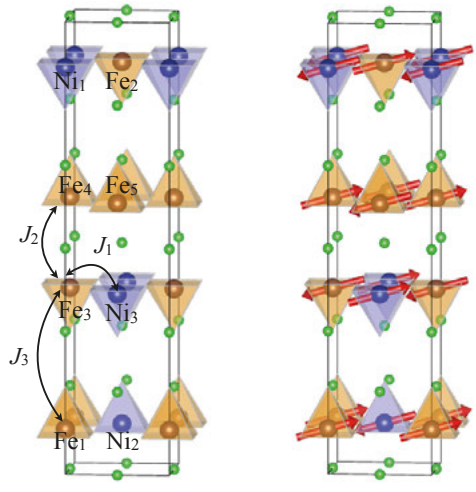

Figure 6.1. Left) The simulated supercell structure. Right) The spin configuration.

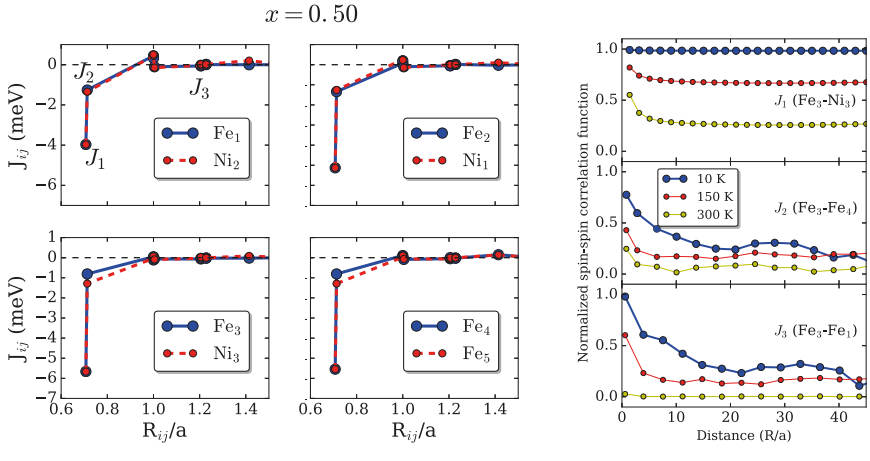

Figure 6.2. Left panel) Exchange parameters between an atom shown in the legend and all its magnetic neighbors as a function of distance for $x = 0.50$. Right panel) Temperature dependence of the normalized spin-spin correlation function as a function of distance (R) per lattice constant (a) with the intralayer (J_1) and interlayer (J_2 and J_3) exchange couplings for the case of interactions between Fe_3 and its neighbors.

for the case of Fe_3 atom in $x = 0.50$ are shown in the right panel of Fig. 6.2. As can be seen, at low temperatures where the exchange energy is larger than the thermal energy, both in-plane and out-of-plane correlation functions are finite, and the materials exhibits a 3D type of ordering. If the thermal fluctuations become larger, the correlation decays faster, especially between layers. At 150 K, the correlation between the layers is weak, and at 300 K it is vanishingly small. However, the spin-spin correlation within the plane (corresponding to the larger J_1 coupling) is finite even above T_N . Thus, we propose that there is a 3D to 2D crossover at some temperature between 150 K and the magnetic ordering temperature. This is discussed further in the Paper V [105].

6.2 Nd_2NiMnO_6 double perovskite

Paper VI is also a joint experimental and theoretical investigation of a double perovskite system. Experimentally, magnetic measurements are done based on SQUID and X-ray absorption spectroscopy (XAS) like X-ray magnetic circular dichroism (XMCD). The X-ray diffraction (XRD) characterization reveals that the system is purely monoclinic with the XAS measurements confirming 4+ and 2+ valency of Mn and Ni, respectively. The ideally ordered Nd_2NiMnO_6 double perovskite offers an ferromagnetic exchange coupling between the Ni and Mn ions.

Based on the experimental synthesized crystal structure, we have performed LSDA+U simulations, where the U correction is only applied for the Ni and Mn atoms. In the case of Nd, the spin moment has been calculated by treating the three $4f$ electrons as core states, in accordance with the standard model of the lanthanides. In rare-earth elements the spin-orbit interactions is rather strong, therefore the associated spin and orbital angular momenta combine into a total angular momentum vector $\mathbf{L} + 2\mathbf{S} = g\mathbf{J}$ moments through the following moments [109]

$$\begin{aligned} \vec{\mu}_S &= g_S \mu_B \mathbf{S}, \\ \vec{\mu}_L &= g_L \mu_B \mathbf{L}, \\ \vec{\mu}_J &= g_J \mu_B \mathbf{J}, \end{aligned} \tag{6.1}$$

where the gyromagnetic factor of electronic spin is $g_s \approx 2$, orbital $g_L = 1$ and Landé factor g_J is

$$g_J = \frac{3}{2} + \frac{S(S+1) - L(L+1)}{J(J+1)}. \tag{6.2}$$

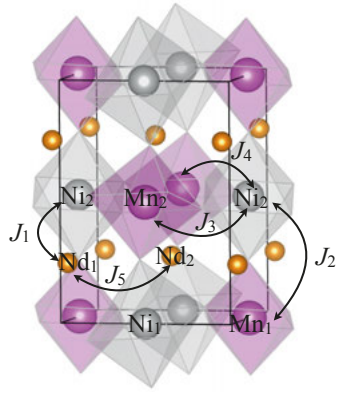

Figure 6.3. Left) The simulated structure with the labels specifying the exchange path for the case of, e.g., Ni_2. Right) The spin (red) and orbital (purple) configurations at low temperature ($\leq$50K) for the cases when the external field is 0, or bigger than α which is obtained 5T from experiment and about 30T from theory.

The magnitude of total moment is $\mu_J = g_J \mu_B \sqrt{J(J+1)}$, where the spin and orbital moment get the form of

$$\mathbf{S} = (g_J - 1)\mathbf{J}, \tag{6.3}$$

and

$$\mathbf{L} = (2 - g_J)\mathbf{J}, \tag{6.4}$$

Using the above expressions, one obtains the values of $g_J = {}^{8}/_{11}$ and $\mathbf{S}_z = 1.22$ for the $\mathbf{J} = {}^{9}/_{2}$. In the calculations of the exchange parameters only the interactions between the spins are considered. Based on that, the exchange parameters in meV are obtained as following: J_1=0.03 (0.23) between Ni (Mn) and nearest Nd atoms, J_2=5.99, J_3=4.90 and J_4=19.05. The value of J_5 which is the interaction between Nd-Nd nearest neighbors are obtained $\leq$0.01 (see Fig. 6.3 for exchange path). Empirically, one can predict that for a 180° Ni-O-Mn bridge with Ni^{2+} valence as $t_{2g}^6 e_g^2$ and Mn^{4+} valence as $t_{2g}^3 e_g^0$, the electron transfer from half-filled e_g^2 and full t_{2g}^6 manifolds of Ni^{2+} are, respectively, to empty e_g^0 and half-filled t_{2g}^3 orbitals on the Mn^{4+} ions. These electron transfers according to Goodenogh-Kanamori rules are accompanied by ferromagnetic exchange couplings [12, 10, 13].

Using MC simulations, the ordering temperature of $T_c = 225$ K is obtained based on the obtained exchange parameters. All these results are in good agreement with our experimental observations which predicts a FM coupling within Ni and Mn sublattices up to 200 K and confirms the small exchange coupling of Nd moment to its neighbors (J_1 and J_5) in consistent with random orientation of Nd moment at temperatures higher than 50 K.

7. Effect of the functional on exchange parameters

In this chapter, we discuss how the spin polarization of the DFT exchange-correlation (XC) functional influences the relative total energies of magnetic configurations and the effective exchange parameters. In the studies of transition metal oxides (TMOs), one of the most widely used methods is DFT+U. Since U is relatively large compared to bandwidths, the magnetic excitations in TMOs are expected to be well described within the Heisenberg model.

This is generally true and the calculated magnon spectra and T_c's are often in good agreement with experiment [110, 111]. However, it has been known that even in such localized systems the J_{ij}'s depend on the state they are extracted from [112]. In this work, I have performed a systematic study of this problem by addressing the influence of the spin-polarization of the underlying XC functional used to obtain the electronic structure.

In LDA+U, the XC functional of LDA is a function of only charge density, and therefore the energy contribution to the magnetism originates entirely from the Hubbard U term applied on the subset of the correlated orbitals [40]. On the other hand, in the LSDA+U the XC functional is a function of both charge and spin densities [69]. Thus the spin polarization of all orbitals contributes directly to the magnetic energy, as well as the Hubbard U term which adds further spin splitting to the correlated states.

While in LDA+U, there is no explicit dependence on the magnetization spin, LSDA+U depends explicitly on the magnetization. This difference affects the DC correction to the single-particle states, given e.g. by Eqs. 2.53 and 2.55 for AMF and FLL DC, respectively. Thus within LDA+U case, the correction is the same for both spin channels. In the case of LSDA+U, the DC correction is different for states with opposite spin projections σ. For this study, we used the FLL form of the DC and the difference between $v_{DC,\uparrow}$ and $v_{DC,\downarrow}$ is proportional to Hund's J and is supposed to completely cancel out the intrinsic Stoner I, contained in the LSDA functional. Of course, this is a strong assumption and there have been evidences that the value of this intrinsic I is overestimated by LSDA [113]. If this cancelation was perfect, LDA+U and LSDA+U would provide nearly identical results. Their difference would originate only from the effect of the spin-polarization of other "non-correlated" states, which are only taken into account in the case of LSDA+U.

7.1 Transition metal oxides

In paper VII [114], we performed a systematic study of the differences between results of LDA+U and LSDA+U calculations for the energies, band gaps, and exchange constants of the transition-metal oxide compounds $CaMnO_3$ (CMO), MnO, FeO, CoO, and NiO. We have chosen these systems, which have different crystal structures and different d-level occupancies, to ensure the generality of our conclusions.

We start with NiO. Figure 7.1 presents the total as well as the projected density of states of the d orbitals in LDA+U and in LSDA+U methods for AFM and FM states. The system is found to be insulating for both states and both methods. The gap in the FM state is slightly smaller than the gap in the AFM state in both methods. In the end of this chapter, I explain why the band gap is smaller in FM case that in AFM case for a model system.

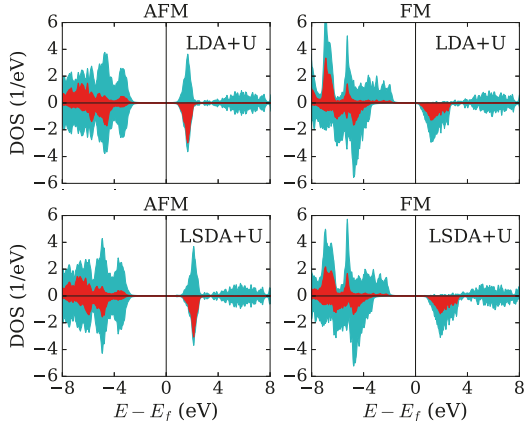

Figure 7.1. Total (cyan) as well as the projected density of states for the d orbitals (red) of NiO.

In Fig. 7.2 the exchange parameters as a function of distance are presented. The dominant interaction is the second neighbor exchange J_2. The first neighbor interaction (J_1) is extremely small because there is no superexchange path between the e_g orbitals through one anion in this geometry as can be understood from the right panel of Fig. 7.2. The exchange interactions are negative, favoring antiferromagnetism for any reference state. However the values of the exchange constants depend on the state and computational method, being strongest for ferromagnetic LDA+U ground state and weakest for antiferromagnetic LSDA+U state. This conclusion holds across the systems studied here (CMO, MnO, FeO, CoO), which suggests larger band gaps together with smaller exchange constants, for the AFM reference state compared to the FM, and for LSDA+U method compared to LDA+U (for more details see paper VII).

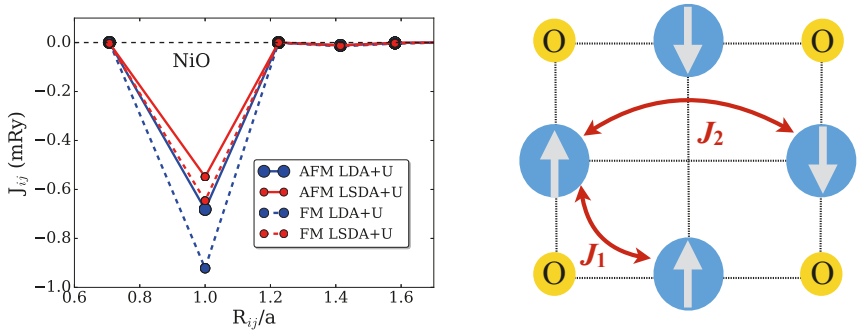

Figure 7.2. Left) Exchange parameters of NiO as a function of distance. Right) The crystal structure of TMOs. The TM atoms are shown by blue circles, whereas the oxygens are yellow balls. The grey arrow represents the spin direction in AFM TMOs.

The main focus of this work is on the obtained J_{ij}'s, which in general can be calculated using total energy difference between FM and AFM state or by use of the magnetic force theorem. The aim is to check how well the MFT-derived J_{ij}'s correspond to the DFT total energies. In Fig. 7.3, we show the comparison between these two methods. The directly computed LDA+U energy difference (red line) falls within the range of the Heisenberg-based estimate (red shaded area). For instance for NiO, the LDA+U energy difference give a value of about 0.26 which is within the range of MFT-derived J_{ij}'s: 0.30 eV and 0.22 eV for AFM and FM reference states. The trend is essentially the same for all the systems, suggesting that the LDA+U scheme indeed leads to the expected Heisenberg-like magnetic physics. On the other hand within LSDA+U approximation, the directly-derived FM-AFM energy differences (blue line) is substantially smaller than the Heisenberg-derived values (blue shaded area). It is not so easy to identify the precise reason for such a drastic differences for LSDA+U. One reasonable possibility is the magnetism of *non-correlated* orbitals. In this case, induced polarization of oxygen, which appears in the FM state, also contributes to the total energy. Assuming that this contribution is given by $E = I_O m_O^2/2$, and using values of I_O from the literature is not able to explain the discrepancies. However, there might be some inter-site TM-O interactions, but Heisenberg model in general and MFT in particular will not be able to properly address it. Hence, potentially other more sophisticated models are needed to properly account for the effect of polarization of oxygen in LSDA+U.

Sensitivity of the results to the Hund's exchange value

In order to see how sensitive our findings are to the Hund's exchange value we have done an additional set of calculations for two systems MnO and NiO by setting the J to 0.9 eV and 0.6 eV. The results are shown in Figs. 7.4. One can see that by decreasing the J value, the exchange parameters show an increase

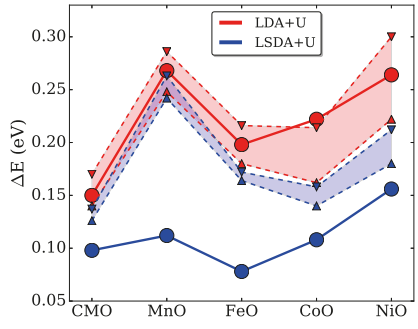

Figure 7.3. Total energy differences ($E = E_{FM} - E_{AFM}$) obtained by LDA+U (solid red line) and LSDA+U (solid blue line) with those which are obtained via J_{ij}'s. The latter results are shown with dashed lines as follows: upward (downward) triangle for AFM (FM) in red for LDA+U and blue for LSDA+U methods. The colored areas are shown as the interval in which the energy based on the J_{ij} of any reference state (FM, AFM, or a combination of both) could end up, i.e., uncertainty of the Heisenberg-based estimate.

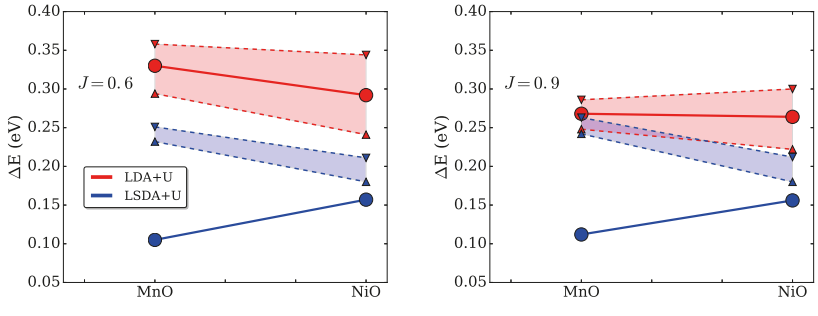

Figure 7.4. Energy difference ($\Delta E = E_{FM} - E_{AFM}$) obtained for MnO and NiO using $J = 0.9$ eV (left) and $J = 0.6$ eV (right) shown by solid lines are compared with those obtained via J_{ij}'s shown by dashed lines as follows: upward (downward) triangle for AFM (FM) in red for LDA+U and blue for LSDA+U methods. The colored areas are shown as the interval in which the energy based on the J_{ij}'s of any reference state (FM, AFM or a combination of both) could end up.

within LDA+U while a decrease within LSDA+U. This because in LDA+U the spin splitting between majority and minority d states and the corresponding band gap are reduced by reduction of the Hun'd J value, while the opposite condition is observed for LSDA+U.

However, the main conclusion remains unchanged for two different Hund's value (0.6 and 0.9 eV), and we still find a better correspondence between the DFT total energies and the parameterized Heisenberg model for LDA+U rather than for LSDA+U.

Band gaps

In FM and AFM states the predicted band gaps and the hoppings are different. To illustrate this point, in Fig. 7.5 we show a spin dimer made up of two spin sites where each site has one orbital occupied with one spin. In the FM case, both spin sites have the up-spin level lower in energy by U than the down-spin level (by convention). For the AFM arrangement, in one site the up-spin level is lower in energy by U than the down-spin level, while the opposite is true for the other site. Since only the levels of the same spin can hybrizide, in the FM case these states are of the same energy that hybridize, whereas in the AFM case they are of different energies. Thus consequently their band gaps would be very different, even if the hopping was the same while it is not.

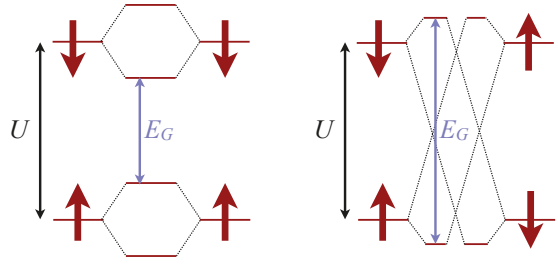

Figure 7.5. FM (left panel) and AFM (right panel) arrangement of a spin dimer with each site having one orbital occupied with one spin.

8. Local minima in L(S)DA+U

Due to the mean-field description in the heart of the standard DFT, all the electrons of a given spin direction feel similar potential (if leaving aside the crystal filed effects) and occupy almost equally each of the correlated orbitals of the same shell (d or f). For this reason, many of transition metal oxides are predicted to be metallic in the DFT level. The problem in these materials arises from the unfilled shell which possesses orbital degrees of freedom and consequently, a non-spherical charge density. This potential is overlooked by DFT. To overcome this problem, as mentioned in section 2.2.1, the Hubbard term is added to the DFT which leads to an orbital dependent shift in the potential, due to its Hartree-Fock mean-field formalism. Therefore, depending on the occupation provided by DFT part the orbital shift in the potential can be different. This leads to a well-known problem when applying the DFT+U method to study magnetic systems and that is the emergence of the metastable states, i.e., the energy landscape presents a multitude local minima. Depending on the starting points, the simulations could not be able to explore the energy landscape for the global minimum and therefore be trapped in the regions around local minima. The obstacle in the search for the ground states is that going from one minimum to other minima would involve partial occupations on the way and this requires a drastic change in the wave functions [115].

There are mainly three different sources responsible for the emergence of the local minima in the system. First, the local Hartree-Fock potential as it favours orbital anisotropy. Second, the double-counting term, which is often specifically designed to not suppress the emergence of orbital anisotropy. The widely used FLL double-counting favors integer occupation (as explained in in section 2.2.4). Therefore, degenerate orbitals which in conventional DFT have similar occupations, in DFT+U formalism would become progressively emptied or full during the charge self-consistency (CSC). Third, the crystal symmetry of the system and the presence of spin-orbit coupling which determine the local symmetries of the atomic sites. Fewer local minima can be expected if the local symmetries favour a unique integer orbital occupation. All these together can create very different density matrices m_{ij} from a given DFT density $n(r)$ (Fig. 8.1 a).

For an atom where the integer occupation is desired [115], the exact energy should follow a strain-line segments joining integer occupations of the atomic orbitals as shown in panel (b) of Fig. 8.1. While LDA predicts an

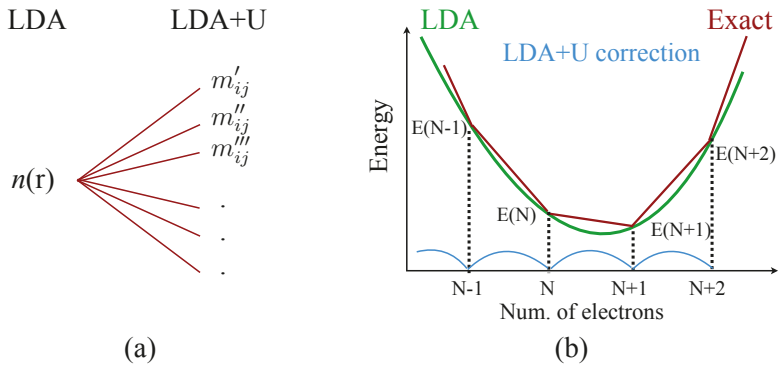

Figure 8.1. a) Initial electron density given by LDA can lead to different orbital occupations due to the sources responsible for the emergence of the local minima (see the text). b) Total energy vs the number of electron. The LDA+*U* curves is simply the difference between the other two energies, i.e., the LDA energy and the exact result for an open system [115].

unphysical curvature for noninteger occupations which only coincides with exact energy at integer occupations. In a solid the situation is more complicated. Because the fractional occupations occur due to the hybridization of the localized orbitals with the crystal environment. Therefore, it is useful to extract the unphysical curve predicted by LDA/GGA energy, which contains also hybridization effects and later polish it with the correction given by the Hubbard term. However, the term introduces the emergence of the local minima through the sources mentioned above.

How to avoid converging to a local minima

The local minima should be avoided as the properties of the system under study can be wrongly predicted, There are several ways suggested by different groups in order to explore the right ground state of the system as follows:

- *U*-ramping [116]
  The central idea of this method is to turn on the interaction from the Hubbard *U* term in an adiabatic way so that fractional orbital occupations are able to gradually converge toward integer occupations. This method works best if the system is predicted to be an insulator already in the DFT level, as the orbital anisotropy of the DFT starting point is implicitly assumed to be correct.

- Controlled symmetry reduction [117]
  In this method, a structural distortion to the system is applied to make the metastable states with similar energies undergo a splitting. The deformation

is then gradually removed. This method is useful to single-out certain minima in order to perform meaningful comparisons between different structures.

- Quasi-annealing method [118]
  In this approach an auxilliary kinetic energy is added to the system so that the simulation is able to pass over the local minima. The kinetic energy is then gradually turned off with the hope that the simulation converge to the global minimum.

- Occupation matrix control (OMC) scheme [119]
  In this method, the main idea is to constrain the DFT+U potential to identify a given minimum. Since in every strongly correlated system, the electrons in the correlated shell (d or f orbitals) are rather localized, it is possible to force them to stay in their orbitals only for the first few iterations without loosing the physics, and then allow them to move freely during CSC run.
  As an example, we consider a material of having 2 electrons in d shell. The idea is to start with several occupation matrices, with all possible configurations of having 2 electrons in 5 orbitals, i.e., 10 different configurations such as [11000], [10100], etc. The resulting local Hartree-Fock potentials are then imposed during the first few CSC iterations. This constraint is then lifted and the calculations are left to converge on their own. Depending on the starting occupation matrix, several different (metastable) states can be reached. Traditionally, the OMC method has been mostly applied for actinide oxides like UO_2, where the electrons in the f shell are quite localized.

In this thesis, we have generalized the OMC method by using random constrained density matrices to generate the seeding potential. Using this method, which we call Random Density Matrix Control (RDMC), we have studied the energy landscape of the local minima in NiO, FeO, CoO and UO_2 in a systematic way. In this approach, the occupation of each orbital can be fractional instead of only integer, which makes it more physically probable for the d electrons due to their semi-localized character.

A schematic representation of the RDMC approach is shown in Fig. 8.2. In order to have a better control on the simulation path we decided to, step by step, turn on each term in the Hamiltonian. So for the case of TMOs, the first simulations are based on a scalar relativistic approach, i.e., no SOC is taken into account. The reason is that, in these systems the orbital moment is rather small as compared to the spin moment and also excluding the SOC term for the first subset of simulations helps stabilize the orbital occupations in each spin channel. This also helps the convergency, which is sometimes quite hard to reach. Later, the SOC term is added to the simulations, in order to obtain the final metastable states. However, in the case of UO_2 the SOC is relatively

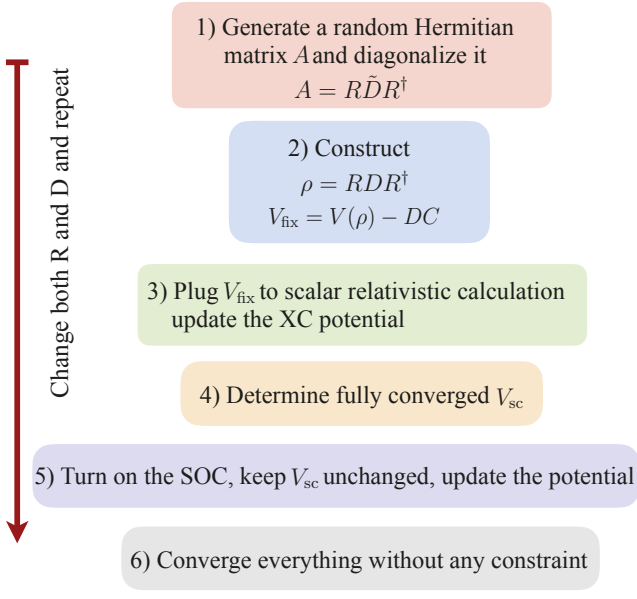

Figure 8.2. The schematic representation of the method used in this work. See the text for more details.

large as compared to the crystal field splitting. Thus, the SOC term should be taken into account from the beginning, as discussed below.

According to the scheme in Fig. 8.2, we start with generating a random (complex) Hermitian matrix A. The size of A is determined by the number of the correlated orbitals (10×10 for the d shell and 14×14 in the case of the f shell). By diagonalizing matrix A, we obtain the eigenvalues matrix $\tilde{D}$ and eigenvectors matrix R which are related to A as $A = R\tilde{D}R$. In the next step, we replace $\tilde{D}$ with a diagonal matrix D of our choice. The physical meaning of the D matrix is that it represents a density matrix of the correlated orbitals. Its trace must sum up to the number of electrons in correlated orbitals, e.g., 6 for FeO and 2 for UO_2. Using these randomly defined matrices in addition to the integer $\tilde{D}$ matrices of standard OMC, we constructed the density matrix through the expression shown in the second block of Fig. 8.2. This density matrix can then be used to estimate the corresponding DFT+U potential, which we refer to as V_{fix}. This potential is thus imposed to a particular simulation during the first few iterations until the large fluctuations in orbital occupations are quenched and the correlated electrons are rather localized in those particular states. However, the XC potential and the total density are allowed to change during this step. After a few iterations, this constraint is lifted and the electrons are allowed to move freely until convergence in both the DFT+U potential and charge density are reached. The obtained potential V_{sc} is then kept fixed and the SOC is turned on. In this way, the large fluctuations in the orbital occupations due to adding the SOC term can be suppressed. In the final step,

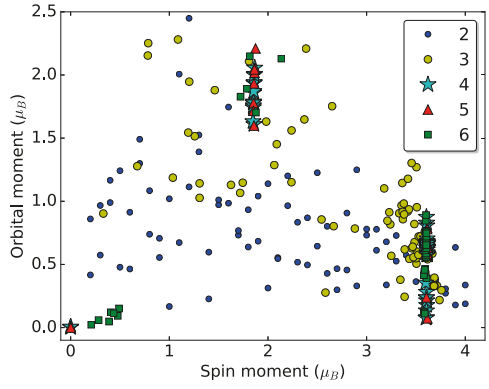

Figure 8.3. Orbital vs. spin moment of FeO obtained from different starting points in LDA+U for a k-mesh of 24×24×24. Each number in the legend corresponds to the step in Fig 8.2.

this constraint is also lifted and the simulations are left to converge on their own.

The final results are shown in Paper VIII. Here we show the case of FeO. As can bee see in Fig. 8.3, in the step 4 where the CSC run is done over the scalar relativistic approach, three different spin local minima have been observed. We refer them as: high spin (HS), the intermediate spin (IS) and the low spin (non-magnetic) solutions (LS). Each possesses several orbital local minima. Using the rather dense k-mesh of 24×24×24, most of the points keep staying in the same minimum during the later steps when the SOC is added, except that during step 6 some of the points in the LS have improved only slightly their spin and orbital moments, their relatively small starting moments could not modify to IS and HS during CSC. Using a very dense k-mesh of 40×40×40 helped all the points, even the ones with very small initial spin moments, converge to the high spin solution (see the left panel of Fig. 8.4). This k-mesh is considered to be saturated, since the further increase of the number of k-points did not modify the final results. We believe that this is due to the very complex competition between the crystal field, SOC and the Hubbard term which is not well-converged for a less dense k-mesh.

Following our study in Paper VII, we learned that the effective exchange coupling in DFT+U has contributions from the spin-dependence part of the density functional as well as the Hubbard U. For this reason we did additional simulations based on LSDA+U to see the effect of different splitting on the local minima. The results for each step of the instructions is shown in Fig. 8.4. As can be seen, finally all the points converged to a single region, with the corresponding spin moment 3.60 μ_B for LDA+U and 3.62 μ_B for LSDA+U. Similar differences has also been obtained for the orbital moments. However, the essential differences occur in the intermediate steps, when the SOC term is

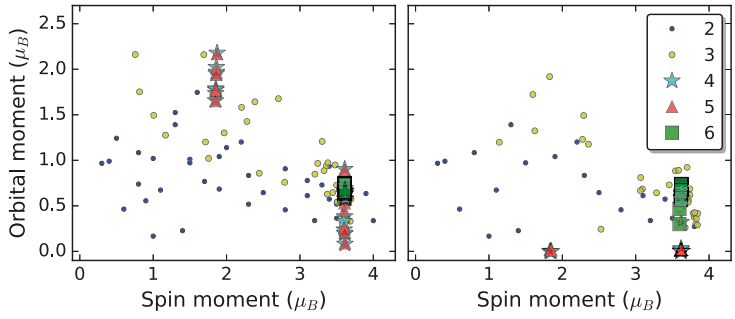

Figure 8.4. Orbital vs. spin moment of FeO obtained from different starting points in LSDA+*U* (left) and LDA+*U* (right) for a *k*-mesh of 40×40×40. Each number in the legend corresponds to the step in Fig 8.2.

still not taken into account. While the LDA+*U* predicts a finite orbital moment for the intermediate spin moment, the LSDA+*U* shows a suppressed orbital moment. Note that, these results are for a *k*-mesh of 40×40×40 where all the point finally converge to the high spin solution.

The finite orbital moments, observed in the level of scalar relativistic approach in LDA+*U* is purely induced by the Coulomb interaction. This favors states obeying the second Hund's rule. The inclusion of the SOC provides a more complete picture of the effects associated to the third Hund's rule as well.

9. Conclusions and Outlook

In this thesis, I particularly investigate electronic structure and magnetic properties of transition metal systems, including their bulk and surface and interfaces, by means of a combination of density functional theory, Hubbard term and dynamical mean-field theory. During these studies, we obtained many interesting results that could help us improve our understanding of exchange interaction in these materials.

Surface studies: In Paper I, we observed a pronounced tendency to ferromagnetism at the surface of Co and Ni, while not for Fe surface in which the surface atoms have a tendency to couple antiferromagnetically with each other, although the interaction is rather weak. Including correlation through DMFT couldn't modify the quality of the exchange interactions. In Paper II, we learn the importance of the atomic relaxation of exchange parameters, particularly for $CaMnO_3$ where the superexchange is the leading mechanism with its value extremely sensitive to the $\widehat{\text{Mn-O-Mn}}$ angle, such that the exchange can even flip its sign at the surface. In Paper III, my main result was the observation of the non-quasiparticle states in Co_2MnSi above the Fermi level at room temperature so that they can not contribute to the spin depolarization.

Double-Provskites: In Paper IV, we study the electronic and magnetic properties of heterostructure of Co_2MnAl/CoMnVAl . At the interface of Co-Mn/Mn-Al and Co-Co/V-Al the half-metallic character is preserved. Analyzing the magnetic exchange interactions at the Co-Mn/Mn-Al interface appeal that the competing magnetic interactions are likely to favor the formation of a noncollinear magnetic order, which is detrimental for the spin polarization. Next in Paper V, we had done a comprehensive study of magnetic properties of $Sr_3Y_x(Fe_{1.25}Ni_{0.75})O_{7-\delta}$. The theoretical part is done for the selected structures characterized by Y concentrations; $x = 0.5$ and 0.75 with $\delta = 1$. Our results confirmed the experimentally observed *G*-type antiferromagnetism. The calculated ordering temperature were also in agreement with measured values. While the experimental NPD results show that the magnetic state for the samples is still 3D at 300 K, the calculated spin-spin correlations through spin dynamics simulations indicate that there is a 3D to 2D cross over at some temperature between 150K and the magnetic ordering temperature. Continuing our study for double-perovskite systems, in Paper VI we investigated the exchange coupling in Nd_2NiMnO_6 where the leading one happens between $3d$ elements, e.g., between Ni-Mn, while Nd moments are randomly oriented at

temperature higher than 50 K, contributing no measurable net magnetization to the sample.

Outlook:
In the abovementioned projects, we mostly focus on Heisenberg exchange interaction term by excluding the effects of spin-orbit coupling. However, in a more accurate treatment of magnetism in transition metal compounds the higher-order magnetic interaction terms (biquadratic term and four-spin ring couplings) should also be taken into account. In the case of broken symmetry, more terms in the hamiltonian, e.g., Dzyaloshinskii-Moriya interaction and single-ion anisotropy need to be deliberated. The estimations of the exchange parameters are done for zero temperature and used for finite temperature studies as well. This means that lattice vibrations are not taken into account in case of finite temperature. One way to extract the exchange parameters at finite temperature is to start from a noncollinear spin arrangement (rather than collinear) and calculate configuration-dependent exchange parameters following the methodology described by Szilva *et. al* [120, 91].

LDA+U vs LSDA+U: In In Paper VII, we have investigated the impact of the spin polarization of exchange-correlation functional of LDA on LDA+U calculations, i.e., the difference between LDA+U and LSDA+U exchange parameters. Our results for the transition metal oxides with different d orbital occupations ($CaMnO_3$, MnO, FeO, CoO and NiO) strongly suggest that if one extracts the J_{ij} from the DFT+U total energies, the use of spin *nonpolarized* functional (e.g., LDA) is more preferable.

Outlook:
It would be interesting to reconsider the importance of higher-order exchange interactions employing spin unpolarized DFT functionals. The non-Heisenberg behavior of the MFT-derived J_{ij} is a natural consequence of the different electronic structures of the FM and AFM states. We expect that the conclusions of the present study are not restricted to the DFT+U method but also hold for DFT+DMFT, which deserves a separate study. In addition, this study is performed only for the selected family of transition metal oxides, while the generalization needs a study on more number of compounds which are traditionally accepted as good Heisenberg systems.

Local minima in L(S)DA+U: In this work, we perform a systematic study of the probable local minima in transition metal oxides in the framework of L(S)DA+U. It is an ongoing project which we hope to have a better understanding of the possible conditions where the local minima can appear. In particular, we were interested in drawing a energy landscape of the local minima and seeing how these minima can be classified in term of their spin, orbital or even higher-order multiples. Orbital moment appeared to be a good quantity

to distinguish the local minima from one another. However, single value decomposition didn't provide any further classifications in terms of higher-order multipoles.

Outlook:

Although this study has been done within L(S)DA+U approach, but it could be interesting to utilize many-body approaches such as Exact-Diagonalization or quantum Monte-Carlo methods in order to find the global minima and compare the local minima of L(S)DA+U with the global minimum and investigate their discrepancies. However, there are several technical issues in the implementation of these methods which needs special care when using, such as discretization of the hybridization function in Exact-Diagonalization and etc.

10. Populärvetenskapling sammanfattning

Ett material avsett för att användas för en specifik tillämpning kan definieras som en solid, vätska eller en annan kondenserad fas. De traditionella exemplen av material är metaller, halvledare, isolatorer, keramer och polymerer. Nya avancerade material utvecklas fortfarande och inkluderar nanomaterial, biomaterial m.m. Grunden i materialvetenskap involverar antigen studier och karakteristik av redan existerande material eller upptäcker och design av nya material och möjligen att förbättra gamla material för nya tillämpningar. När materialforskare har kartlagt ett materials egenskaper kan de fortsätta med att studera dess specifika prestanda för en viss tillämpning. Det kan erhållas genom att förstå materialets egenskaper, struktur och prestanda och hur dessa förändras över tid.

Vetenskapliga verktyg för detta innefattar delar från fysik, kemi och ingenjörskonst. Därför anses materialvetenskap vara ett tvärvetenskapligt forskningsfält. Inom ingenjörsområdet utvecklas experimentella metoder så som diffraktion med hjälp av röntgenstrålning, elektroner, eller neutroner, och olika sorters spektroskopier och kemiska analyser så som elektronmikroskopi och termisk analys. De mer forskningsinriktade aspekterna kan vara minst lika utmanande. I avdelningen för material teori vid Uppsala Universitet studerar vi olika material från atomnivå ändå upp till makroskopisk nivå. På atomnivån studeras atomer och hur de är arrangerade i form av molekyler, kristaller, etcetera. På denna längdskala, några få Ångström (en Ångström är 0,0000000001 m), bestäms mycket av de elektriska, magnetiska och kemiska egenskaperna av ett material.

Fokus på avdelningen är främst beräkningsvetenskap och teori. Med den kraftigt ökade beräkningskraften de senaste decennierna har simuleringar av material och deras egenskaper blivit möjliga. Detta innebär att materialforskare kan upptäcka egenskaper av tidigare kända material och att designa helt nya material. Fram tills nyligen hittades nya material genom tidskrävande experimentella försök och evalueringstillvägagångsätt. Men nu hoppas man kraftigt kunna reducera denna tid med hjälp av beräkningsmetoder. Detta innefattar att man simulerar material med metoder så som täthetsfunktionalteori (DFT) och dess förbättringar, molekylär dynamik, etcetera.

I denna avhandling presenterar jag elektroniska och magnetiska egenskaper av flera magnetiska fasta material. Dessa material uppvisar en stor variation av intressanta fenomen och magnetiska egenskaper. Mitt mål var att förstå hur interaktionerna mellan elektronerna på atomnivå påverkar, framförallt, de magnetiska och elektriska egenskaperna. I vissa material spelar elektron-elektron

växelverkan en stor roll och inom kondenserade materiens fysik brukar dessa kallas för starkt korrelerade material.

För dessa material kan inte den väletablerade teoretiska DFT metoden tillräckligt noggrant behandla elektron-elektron växelverkan och man behöver använda sig av mer avancerade simuleringsmetoder. De teoretiska metoderna i denna avhandling är en kombination av DFT och mer sofistikerade metoder så som DFT+U och dynamisk medelfältsteori. Från den erhållna elektronstrukturen är det möjligt att bestämma många andra materialegenskaper, antingen genom anpassning till experimentell data eller genom att transformera resultaten till en enklare modell som innehåller de fysiska storheter av intresse. I denna avhandling har jag anammat det andra sättet för att bättre förstå de magnetiska egenskaperna, framförallt den så kallade utbytesväxelverkan.

Denna växelverkan uppkommer främst mellan två magnetiska atomer med delvis ockuperade d eller f skal. Utbytesväxelverkansparametrar är de relevanta storheter för att bestämma den kritiska temperaturen, det vill säga då materialet genomgår en magnetisk fasövergång, och spinvågsdispersion. Dessa makroskopiska storheter är framförallt viktiga för tekniska tillämpningar inom till exempel spintronikminnen och logiska enheter. Därför behövs en grundläggande förståelse av de magnetiska egenskaperna i dessa material.

En intressant aspekt av detta forskningsfält är studier av låg dimensionella material. Magnetiska material kan uppvisa nya kvantmekaniska fenomen när de begränsas till två dimensioner. På grund av färre närmsta grannatomer kan lågdimensionella material kategoriseras som en bro mellan solider och enskilda atomer, med många av deras magnetiska och elektriska egenskaper bestämda av interatomära korrelationer. I denna avhandling studerar vi noggrant detta genom att jämföra spektrum och magnetiska egenskaper vid ytor och bulk för flera olika system. Detta forskningsfält är intressant inte bara för att uppnå bättre förståelse av fysiken av lågdimensionella material, men också för att kunna konstruera nya material med önskade egenskaper.

11. Acknowledgments

First, I would like to thank my supervisors Olle Eriksson, Yaroslav Kvashnin, Patrik Thunström, and Anna Delin for their outstanding supervisions. I thank Olle for giving me the opportunity to do my PhD in such an excellent research environment. Yaroslav, I specially would like to thank you for everything you have taught me during this time. PhD couldn't be done easily for me without your support and guidance. I would also like to thank Patrik for having uncountable scientific discussions, when he patiently answered to all my trivial and non trivial questions.

I want to thank Lars Nordström, Diana Iusan, Inka Locht, Oscar Grånäs, Igor Di Marco, Heike Harper and Biplab Sanyal for what I learned from them in the filed of strongly correlated physics. Manuel Periero, Anders Bergman, Jonathan Chico, Konstantinos Koumpouras and Debora Rodrigues thank you very much for teaching me how to use the UppASD code. I would like to express my appreciation to Manuel and Danny Thonig for scientific discussions on spin dynamics physics as well as non-scientific daily life discussions.

In my early PhD, I had the opportunity to share office with Henning Hammar, Kristofer Björnson and Ritwik Mondal. Thank you guys for providing a very nice and friendly environment in the office. I will definitely miss those days. Later in PhD, I shared office with Sohas, Xin and Bo, and I want to thank them as well for being lovely friends.

To all my colleagues at the materials theory division thanks for making the working environment such friendly. I will specially miss all the fika we had together. Lunchtime discussions gave me the opportunity to learn more about different countries, cultures, politics and etc. I would like to thank Lars, Olga Vekilova and Jan Rusz for nice companies during lunch and I thank Mahdi Mashkoori and Fariborz Parhizgar for our lovely Persian conversations during fika. Organising the lunch seminar gave me the opportunity to have closer interactions with almost everyone in our group. I thank those who helped me with organizing it, Susanne Mirbt, Barbara Brena and Johan Schmidt.

Now, I would like to take the opportunity to thank my family for all the support and encouragement over the years. My lovely mother who never let me feel alone and her prayers have always been with me in Sweden. Long live Manjoon. This thesis is dedicated to my beloved father who was my main supporter for going abroad and doing PhD. Unfortunately he didn't stay to see today. May you rest in peace dear pappa (Aghajoon).

Finally, I want to thank Johan Schött, my scientific and to my life partner. Thank you for being with me. Without you, I would have had a very hard time in Sweden. Thank you for everything. Dooset daram azizam.

References

[1] Walther Gerlach and Otto Stern. Der experimentelle nachweis der richtungsquantelung im magnetfeld. *Zeitschrift für Physik*, 9(1):349–352, Dec 1922.

[2] J. Stöhr, H.C.S. Joachim Stšhr, and H.C. Siegmann. *Magnetism: From Fundamentals to Nanoscale Dynamics*. Springer Series in Solid-State Sciences. Springer, 2006.

[3] I. Turek, J. Kudrnovsky, V. Drchal, and P. Bruno. Exchange interactions, spin waves, and transition temperatures in itinerant magnets. *Philosophical Magazine*, 86:1713, April 2006.

[4] M. Pajda, J. Kudrnovský, I. Turek, V. Drchal, and P. Bruno. *Ab initio* calculations of exchange interactions, spin-wave stiffness constants, and curie temperatures of Fe, Co, and Ni. *Phys. Rev. B*, 64:174402, Oct 2001.

[5] N.W. Ashcroft and N.D. Mermin. *Solid State Physics*. HRW international editions. Holt, Rinehart and Winston, 1976.

[6] S. Blundell. *Magnetism in Condensed Matter*. Oxford Master Series in Condensed Matter Physics. OUP Oxford, 2001.

[7] W. Heitler and F. London. Wechselwirkung neutraler atome und homöopolare bindung nach der quantenmechanik. *Zeitschrift für Physik*, 44(6):455–472, Jun 1927.

[8] P. Fazekas. *Lecture Notes on Electron Correlation and Magnetism*. Series in modern condensed matter physics. World Scientific, 1999.

[9] P. Bruno. Theory of interlayer magnetic coupling. *Phys. Rev. B*, 52:411–439, Jul 1995.

[10] Junjiro Kanamori. Superexchange interaction and symmetry properties of electron orbitals. *Journal of Physics and Chemistry of Solids*, 10(2):87 – 98, 1959.

[11] P. W. Anderson. Antiferromagnetism. Theory of superexchange interaction. *Phys. Rev.*, 79:350–356, Jul 1950.

[12] John B. Goodenough. Theory of the role of covalence in the perovskite-type manganites $[\mathrm{La}, \mathrm{M(II)}]\mathrm{MnO}_3$. *Phys. Rev.*, 100:564–573, Oct 1955.

[13] Junjiro Kanamori. Theory of the magnetic properties of Ferrous and Cobaltous Oxides, II. *Progress of Theoretical Physics*, 17(2):177–196, 1957.

[14] Michael P. Marder. *Condensed Matter Physics*. John Wiley and Sons, Inc., Hoboken, New Jersey, 2010.

[15] R.M. Martin. *Electronic Structure: Basic Theory and Practical Methods*. Cambridge University Press, 2004.

[16] Giuseppe Grosso and Giuseppe Pastori Parravicini. *Solid State Physics*. Academic Press, San Diego, California, 2000.

[17] P. Hohenberg and W. Kohn. *Phys. Rev.*, 136:B864, 1964.

[18] P.L. Taylor and O. Heinonen. *A Quantum Approach to Condensed Matter Physics*. Cambridge University Press, 2002.

[19] W. Kohn and L. J. Sham. Self-consistent equations including exchange and correlation effects. *Phys. Rev.*, 140:A1133–A1138, Nov 1965.
[20] John P. Perdew and Yue Wang. Accurate and simple analytic representation of the electron-gas correlation energy. *Phys. Rev. B*, 45:13244–13249, Jun 1992.
[21] R. M. Dreizler and Gross E. K. U. *Density functional theory, an approach to the quantum many-body problem*. Dover Books on Physics. Springer Berlin Heidelberg, 1990.
[22] Antoine Georges, Gabriel Kotliar, Werner Krauth, and Marcelo J. Rozenberg. Dynamical mean-field theory of strongly correlated fermion systems and the limit of infinite dimensions. *Rev. Mod. Phys.*, 68:13–125, Jan 1996.
[23] G. Kotliar, S. Y. Savrasov, K. Haule, V. S. Oudovenko, O. Parcollet, and C. A. Marianetti. Electronic structure calculations with dynamical mean-field theory. *Rev. Mod. Phys.*, 78:865–951, Aug 2006.
[24] F. Gross. *Relativistic quantum mechanics and field theory*. Wiley Science, 1999.
[25] Leslie L. Foldy and Siegfried A. Wouthuysen. On the dirac theory of spin 1/2 particles and its non-relativistic limit. *Phys. Rev.*, 78:29–36, Apr 1950.
[26] D D Koelling and B N Harmon. A technique for relativistic spin-polarised calculations. *Journal of Physics C: Solid State Physics*, 10(16):3107, 1977.
[27] Patrick Bruno. Tight-binding approach to the orbital magnetic moment and magnetocrystalline anisotropy of transition-metal monolayers. *Phys. Rev. B*, 39:865–868, Jan 1989.
[28] J. M. Wills, M. Alouani, P. Andersson, A. Delin, O. Eriksson, and O. Grechnyev. *Full-Potential Electronic Structure Method*. Springer-Verlag, Berlin, 2010.
[29] Erich Runge and E. K. U. Gross. Density-functional theory for time-dependent systems. *Phys. Rev. Lett.*, 52:997–1000, Mar 1984.
[30] N. David Mermin. Thermal properties of the inhomogeneous electron gas. *Phys. Rev.*, 137:A1441–A1443, Mar 1965.
[31] A. I. Lichtenstein, M. I. Katsnelson, and G. Kotliar. Finite-temperature magnetism of transition metals: An *ab initio* dynamical mean-field theory. *Phys. Rev. Lett.*, 87:067205, Jul 2001.
[32] J. Braun, J. Minár, H. Ebert, M. I. Katsnelson, and A. I. Lichtenstein. Spectral function of ferromagnetic 3*d* metals: A self-consistent LSDA + DMFT approach combined with the one-step model of photoemission. *Phys. Rev. Lett.*, 97:227601, Dec 2006.
[33] Alexei Grechnev, I. Di Marco, M. I. Katsnelson, A. I. Lichtenstein, John Wills, and Olle Eriksson. Theory of bulk and surface quasiparticle spectra for Fe, Co, and Ni. *Phys. Rev. B*, 76:035107, Jul 2007.
[34] S. Chadov, J. Minár, M. I. Katsnelson, H. Ebert, D. Ködderitzsch, and A. I. Lichtenstein. Orbital magnetism in transition metal systems: The role of local correlation effects. *EPL (Europhysics Letters)*, 82(3):37001, 2008.
[35] K. Yamada. *Electron Correlation in Metals*. Cambridge University Press, 2004.
[36] J. Hubbard. Electron correlations in narrow energy bands. *Proceedings of the Royal Society of London A: Mathematical, Physical and Engineering Sciences*, 276(1365):238–257, 1963.

[37] B. H. Brandow. Electronic structure of mott insulators. *Advances in Physics*, 26(5):651–808, 1977.
[38] I. G. Austin and N. F. Mott. Metallic and nonmetallic behavior in transition metal oxides. *Science*, 168(3927):71–77, 1970.
[39] V. I. Anisimov and O. Gunnarsson. Density-functional calculation of effective coulomb interactions in metals. *Phys. Rev. B*, 43:7570–7574, Apr 1991.
[40] Vladimir I. Anisimov, Jan Zaanen, and Ole K. Andersen. Band theory and Mott insulators: Hubbard *U* instead of Stoner *I*. *Phys. Rev. B*, 44:943–954, Jul 1991.
[41] Vladimir I Anisimov, F Aryasetiawan, and A I Lichtenstein. First-principles calculations of the electronic structure and spectra of strongly correlated systems: the LDA + U method. *Journal of Physics: Condensed Matter*, 9(4):767, 1997.
[42] Nicola Marzari and David Vanderbilt. Maximally localized generalized wannier functions for composite energy bands. *Phys. Rev. B*, 56:12847–12865, Nov 1997.
[43] A. I. Liechtenstein, V. I. Anisimov, and J. Zaanen. Density-functional theory and strong interactions: Orbital ordering in Mott-Hubbard insulators. *Phys. Rev. B*, 52:R5467–R5470, Aug 1995.
[44] S. L. Dudarev, G. A. Botton, S. Y. Savrasov, C. J. Humphreys, and A. P. Sutton. Electron-energy-loss spectra and the structural stability of nickel oxide: An lsda+u study. *Phys. Rev. B*, 57:1505–1509, Jan 1998.
[45] O. Gunnarsson. Calculation of parameters in model hamiltonians. *Phys. Rev. B*, 41:514–518, Jan 1990.
[46] V. I. Anisimov and O. Gunnarsson. Density-functional calculation of effective coulomb interactions in metals. *Phys. Rev. B*, 43:7570–7574, Apr 1991.
[47] Matteo Cococcioni and Stefano de Gironcoli. Linear response approach to the calculation of the effective interaction parameters in the LDA + U method. *Phys. Rev. B*, 71:035105, Jan 2005.
[48] I. V. Solovyev and M. Imada. Screening of coulomb interactions in transition metals. *Phys. Rev. B*, 71:045103, Jan 2005.
[49] M. Springer and F. Aryasetiawan. Frequency-dependent screened interaction in ni within the random-phase approximation. *Phys. Rev. B*, 57:4364–4368, Feb 1998.
[50] G.D. Mahan. *Many-Particle Physics*. Physics of Solids and Liquids. Springer US, 2010.
[51] I. V. Solovyev and K. Terakura. Effective single-particle potentials for MnO in light of interatomic magnetic interactions: Existing theories and perspectives. *Phys. Rev. B*, 58:15496–15507, Dec 1998.
[52] F Aryasetiawan and O Gunnarsson. The GW method. *Reports on Progress in Physics*, 61(3):237, 1998.
[53] Emanuel Gull, Andrew J. Millis, Alexander I. Lichtenstein, Alexey N. Rubtsov, Matthias Troyer, and Philipp Werner. Continuous-time Monte Carlo methods for quantum impurity models. *Rev. Mod. Phys.*, 83:349–404, May 2011.
[54] P. H. Dederichs, S. Blügel, R. Zeller, and H. Akai. Ground states of constrained systems: Application to cerium impurities. *Phys. Rev. Lett.*,

53:2512–2515, Dec 1984.
[55] M. R. Norman and A. J. Freeman. Model supercell local-density calculations of the 3*d* excitation spectra in NiO. *Phys. Rev. B*, 33:8896–8898, Jun 1986.
[56] O. Gunnarsson, J. W. Allen, O. Jepsen, T. Fujiwara, O. K. Andersen, C. G. Olsen, M. B. Maple, J. S. Kang, L. Z. Liu, J. H. Park, R. O. Anderson, W. P. Ellis, R. Liu, J. T. Markert, Y. Dalichaouch, Z. X. Shen, P. A. P. Lindberg, B. O. Wells, D. S. Dessau, A. Borg, I. Lindau, and W. E. Spicer. Polarized resonance photoemission for Nd_2CuO_4. *Phys. Rev. B*, 41:4811–4814, Mar 1990.
[57] A. K. McMahan, Richard M. Martin, and S. Satpathy. Calculated effective hamiltonian for La_2CoO_4 and solution in the impurity anderson approximation. *Phys. Rev. B*, 38:6650–6666, Oct 1988.
[58] P. W. Anderson. Localized magnetic states in metals. *Phys. Rev.*, 124:41–53, Oct 1961.
[59] P. Phillips. *Advanced Solid State Physics*. Advanced Solid State Physics. Cambridge University Press, 2012.
[60] Antoine Georges and Gabriel Kotliar. Hubbard model in infinite dimensions. *Phys. Rev. B*, 45:6479–6483, Mar 1992.
[61] M. Jarrell. Hubbard model in infinite dimensions: A quantum Monte Carlo study. *Phys. Rev. Lett.*, 69:168–171, Jul 1992.
[62] Masuo Suzuki, Seiji Miyashita, and Akira Kuroda. Electronic structure calculations with dynamical mean-field theory. *Progress of Theoretical Physics*, 58:1377, 1977.
[63] J. E. Hirsch, R. L. Sugar, D. J. Scalapino, and R. Blankenbecler. Monte Carlo simulations of one-dimensional fermion systems. *Phys. Rev. B*, 26:5033–5055, Nov 1982.
[64] N.E Bickers and D.J Scalapino. Conserving approximations for strongly fluctuating electron systems. i. formalism and calculational approach. *Annals of Physics*, 193(1):206 – 251, 1989.
[65] N. E. Bickers, D. J. Scalapino, and S. R. White. Conserving approximations for strongly correlated electron systems: Bethe-Salpeter equation and dynamics for the two-dimensional hubbard model. *Phys. Rev. Lett.*, 62:961–964, Feb 1989.
[66] A.L. Fetter and J.D. Walecka. *Quantum Theory of Many-particle Systems*. Dover Books on Physics. Dover Publications, 2003.
[67] Katsnelson, M. I. and Lichtenstein, A. I. Electronic structure and magnetic properties of correlated metals. *Eur. Phys. J. B*, 30(1):9–15, 2002.
[68] L. V. Pourovskii, M. I. Katsnelson, and A. I. Lichtenstein. Correlation effects in electronic structure of actinide monochalcogenides. *Phys. Rev. B*, 72:115106, Sep 2005.
[69] M. T. Czyżyk and G. A. Sawatzky. Local-density functional and on-site correlations: The electronic structure of la_2cuo_4 and $lacuo_3$. *Phys. Rev. B*, 49:14211–14228, May 1994.
[70] Hongjun Xiang, Changhoon Lee, Hyun-Joo Koo, Xingao Gong, and Myung-Hwan Whangbo. Magnetic properties and energy-mapping analysis. *Dalton Trans.*, 42:823–853, 2013.
[71] A.I. Liechtenstein, M.I. Katsnelson, V.P. Antropov, and V.A. Gubanov. Local

spin density functional approach to the theory of exchange interactions in ferromagnetic metals and alloys. *Journal of Magnetism and Magnetic Materials*, 67(1):65 – 74, 1987.

[72] M. I. Katsnelson and A. I. Lichtenstein. First-principles calculations of magnetic interactions in correlated systems. *Phys. Rev. B*, 61:8906–8912, Apr 2000.

[73] V. V. Mazurenko and V. I. Anisimov. Weak ferromagnetism in antiferromagnets: α-Fe_2O_3 and La_2CuO_4. *Phys. Rev. B*, 71:184434, May 2005.

[74] S. V. Halilov, H. Eschrig, A. Y. Perlov, and P. M. Oppeneer. Adiabatic spin dynamics from spin-density-functional theory: Application to Fe, Co, and Ni. *Phys. Rev. B*, 58:293–302, Jul 1998.

[75] L M Sandratskii. Symmetry analysis of electronic states for crystals with spiral magnetic order. I. General properties. *Journal of Physics: Condensed Matter*, 3(44):8565, 1991.

[76] L. Bergqvist. *Electronic Structure and Statistical Methods Applied to Nanomagnetism, Diluted Magnetic Semiconductors and Spintronics*. PhD dissertation, Acta Universitatis Upsaliensis, Uppsala, 2005.

[77] E. Şaşıoğlu, L. M. Sandratskii, and P. Bruno. First-principles calculation of the intersublattice exchange interactions and curie temperatures of the full heusler alloys ni$_2$Mnx ($x = \mathrm{Ga}, \mathrm{In}, \mathrm{Sn}, \mathrm{Sb}$). *Phys. Rev. B*, 70:024427, Jul 2004.

[78] S. Tyablikov. *Methods in the Quantum Theory of Magnetism*. Plenum Press, New York, 1967.

[79] D. P. Landau and K. Binder. *A Guide to Monte Carlo Simulations in Statistical Physics*. Cambridge University Press, 2014.

[80] Xiangang Wan, Quan Yin, and Sergej Y. Savrasov. Calculation of magnetic exchange interactions in mott-hubbard systems. *Phys. Rev. Lett.*, 97:266403, Dec 2006.

[81] Walter A. Harrison. Heisenberg exchange in the magnetic monoxides. *Phys. Rev. B*, 76:054417, Aug 2007.

[82] Lars Bergqvist and Anders Bergman. Realistic finite temperature simulations of magnetic systems using quantum statistics. *Phys. Rev. Materials*, 2:013802, Jan 2018.

[83] A.S. Borovik-Romanov and S.K. Sinha. Spin waves and magnetic excitations. 1 1988.

[84] 18 - on the theory of the dispersion of magnetic permeability in ferromagnetic bodies. In D. TER HAAR, editor, *Collected Papers of L.D. Landau*, pages 101 – 114. Pergamon, 1965.

[85] H. Kronmüller and M. Fähnle. *Micromagnetism and the Microstructure of Ferromagnetic Solids*. Cambridge University Press, 2009.

[86] E. Beaurepaire, J.-C. Merle, A. Daunois, and J.-Y. Bigot. Ultrafast spin dynamics in ferromagnetic nickel. *Phys. Rev. Lett.*, 76:4250–4253, May 1996.

[87] S. Keshavarz, Y. O. Kvashnin, I. Di Marco, A. Delin, M. I. Katsnelson, A. I. Lichtenstein, and O. Eriksson. Layer-resolved magnetic exchange interactions of surfaces of late 3*d* elements: Effects of electronic correlations. *Phys. Rev. B*, 92:165129, Oct 2015.

[88] Jonathan Chico, Samara Keshavarz, Yaroslav Kvashnin, Manuel Pereiro, Igor

Di Marco, Corina Etz, Olle Eriksson, Anders Bergman, and Lars Bergqvist. First-principles studies of the gilbert damping and exchange interactions for half-metallic heuslers alloys. *Phys. Rev. B*, 93:214439, Jun 2016.

[89] Igor Di Marco, Andreas Held, Samara Keshavarz, Yaroslav O. Kvashnin, and Liviu Chioncel. Half-metallicity and magnetism in the $co_2MnAl/CoMnVAl$ heterostructure. *Phys. Rev. B*, 97:035105, Jan 2018.

[90] A. Szilva, D. Thonig, P. F. Bessarab, Y. O. Kvashnin, D. C. M. Rodrigues, R. Cardias, M. Pereiro, L. Nordström, A. Bergman, A. B. Klautau, and O. Eriksson. Theory of noncollinear interactions beyond heisenberg exchange: Applications to bcc fe. *Phys. Rev. B*, 96:144413, Oct 2017.

[91] D. C. M. Rodrigues, A. Szilva, A. B. Klautau, A. Bergman, O. Eriksson, and C. Etz. Finite-temperature interatomic exchange and magnon softening in fe overlayers on ir(001). *Phys. Rev. B*, 94:014413, Jul 2016.

[92] B. Alling, F. Körmann, B. Grabowski, A. Glensk, I. A. Abrikosov, and J. Neugebauer. Strong impact of lattice vibrations on electronic and magnetic properties of paramagnetic fe revealed by disordered local moments molecular dynamics. *Phys. Rev. B*, 93:224411, Jun 2016.

[93] A. Kubetzka, P. Ferriani, M. Bode, S. Heinze, G. Bihlmayer, K. von Bergmann, O. Pietzsch, S. Blügel, and R. Wiesendanger. Revealing antiferromagnetic order of the fe monolayer on W(001): Spin-polarized scanning tunneling microscopy and first-principles calculations. *Phys. Rev. Lett.*, 94:087204, Mar 2005.

[94] M. Takada, P.L. Gastelois, M. Przybylski, and J. Kirschner. A complex magnetic structure of ultrathin fe films on Rh (001) surfaces. *Journal of Magnetism and Magnetic Materials*, 329(0):95 – 100, 2013.

[95] D. Chandesris, J. Lecante, and Y. Petroff. Two-electron resonances in transition metals. *Phys. Rev. B*, 27:2630–2635, Mar 1983.

[96] C. Guillot, Y. Ballu, J. Paigné, J. Lecante, K. P. Jain, P. Thiry, R. Pinchaux, Y. Pétroff, and L. M. Falicov. Resonant photoemission in nickel metal. *Phys. Rev. Lett.*, 39:1632–1635, Dec 1977.

[97] Alessio Filippetti and Warren E. Pickett. Magnetic reconstruction at the (001) $CaMnO_3$ surface. *Phys. Rev. Lett.*, 83:4184–4187, Nov 1999.

[98] V Yu Irkhin and M I Katsnelson. Ground state and electron-magnon interaction in an itinerant ferromagnet: half-metallic ferromagnets. *Journal of Physics: Condensed Matter*, 2(34):7151, 1990.

[99] D M Edwards and J A Hertz. Electron-magnon interactions in itinerant ferromagnetism. ii. strong ferromagnetism. *Journal of Physics F: Metal Physics*, 3(12):2191, 1973.

[100] L. Chioncel, Y. Sakuraba, E. Arrigoni, M. I. Katsnelson, M. Oogane, Y. Ando, T. Miyazaki, E. Burzo, and A. I. Lichtenstein. Nonquasiparticle states in Co_2MnSi evidenced through magnetic tunnel junction spectroscopy measurements. *Phys. Rev. Lett.*, 100:086402, Feb 2008.

[101] Stanislav Chadov, Gerhard H Fecher, Claudia Felser, Jan Minár, Jürgen Braun, and Hubert Ebert. Electron correlations in $Co_2Mn_{1-x}Fe_xSi$ heusler compounds. *Journal of Physics D: Applied Physics*, 42(8):084002, 2009.

[102] Roman Fetzer, Benjamin Stadtmüller, Yusuke Ohdaira, Hiroshi Naganuma, Mikihiko Oogane, Yasuo Ando, Tomoyuki Taira, Tetsuya Uemura, Masafumi

Yamamoto, Martin Aeschlimann, and Mirko Cinchetti. Probing the electronic and spintronic properties of buried interfaces by extremely low energy photoemission spectroscopy. *Scientific Reports*, 5:8537, 2015.

[103] B Skubic, J Hellsvik, L Nordström, and O Eriksson. A method for atomistic spin dynamics simulations: implementation and examples. *J. of Physics: Condensed Matter*, 20(31):315203, 2008.

[104] O. Eriksson, A. Bergman, L. Bergqvist, and J. Hellsvik. *Atomistic Spin Dynamics: Foundations and Applications*. Oxford University Press, Oxford, UK, 2017.

[105] Samara Keshavarz, Sofia Kontos, Dariusz Wardecki, Yaroslav O. Kvashnin, Manuel Pereiro, Swarup K. Panda, Biplab Sanyal, Olle Eriksson, Jekabs Grins, Gunnar Svensson, Klas Gunnarsson, and Peter Svedlindh. Magnetic properties of ruddlesden-popper phases $\mathbf{sr}_{3-x}\mathbf{y}_x(\mathbf{fe}_{1.25}\mathbf{ni}_{0.75})\mathbf{o}_{7-\delta}$: A combined experimental and theoretical investigation. *Phys. Rev. Materials*, 2:044005, Apr 2018.

[106] V. L. Berezinski. Destruction of long-range order in one-dimensional and two-dimensional systems having a continuous symmetry group i. classical systems. *Sov. Phys. JETP*, 32:493, 1970.

[107] V. L. Berezinski and A. Ya. Blank. *Sov. Phys. JETP*, 37:369, 1973.

[108] L. E. Svistov, A. I. Smirnov, L. A. Prozorova, O. A. Petrenko, A. Micheler, N. Büttgen, A. Ya. Shapiro, and L. N. Demianets. Magnetic phase diagram, critical behavior, and two-dimensional to three-dimensional crossover in the triangular lattice antiferromagnet $RbFe(MoO_4)_2$. *Phys. Rev. B*, 74:024412, Jul 2006.

[109] J. Jensen and A.R. Mackintosh. *Rare earth magnetism: structures and excitations*. International series of monographs on physics. Clarendon Press, 1991.

[110] Guntram Fischer, Markus Däne, Arthur Ernst, Patrick Bruno, Martin Lüders, Zdzislawa Szotek, Walter Temmerman, and Wolfram Hergert. Exchange coupling in transition metal monoxides: Electronic structure calculations. *Phys. Rev. B*, 80:014408, Jul 2009.

[111] Adam Jacobsson, Biplab Sanyal, Marjana Ležaić, and Stefan Blügel. Exchange parameters and adiabatic magnon energies from spin-spiral calculations. *Phys. Rev. B*, 88:134427, Oct 2013.

[112] R Logemann, A N Rudenko, M I Katsnelson, and A Kirilyuk. Exchange interactions in transition metal oxides: the role of oxygen spin polarization. *Journal of Physics: Condensed Matter*, 29(33):335801, 2017.

[113] Hanghui Chen and Andrew J. Millis. Spin-density functional theories and their $+u$ and $+j$ extensions: A comparative study of transition metals and transition metal oxides. *Phys. Rev. B*, 93:045133, Jan 2016.

[114] Samara Keshavarz, Johan Schött, Andrew J. Millis, and Yaroslav O. Kvashnin. Electronic structure, magnetism, and exchange integrals in transition-metal oxides: Role of the spin polarization of the functional in dft+u calculations. *Phys. Rev. B*, 97:184404, May 2018.

[115] Matteo Cococcioni and Stefano de Gironcoli. Linear response approach to the calculation of the effective interaction parameters in the LDA + U method. *Phys. Rev. B*, 71:035105, Jan 2005.

[116] B. Meredig, A. Thompson, H. A. Hansen, C. Wolverton, and A. van de Walle. Method for locating low-energy solutions within DFT + u. *Phys. Rev. B*, 82:195128, Nov 2010.

[117] Denis Gryaznov, Eugene Heifets, and Eugene Kotomin. The first-principles treatment of the electron-correlation and spin-orbital effects in uranium mononitride nuclear fuels. *Phys. Chem. Chem. Phys.*, 14:4482–4490, 2012.

[118] Hua Y. Geng, Ying Chen, Yasunori Kaneta, Motoyasu Kinoshita, and Q. Wu. Interplay of defect cluster and the stability of xenon in uranium dioxide from density functional calculations. *Phys. Rev. B*, 82:094106, Sep 2010.

[119] Gérald Jomard, Bernard Amadon, Fran çois Bottin, and Marc Torrent. Structural, thermodynamic, and electronic properties of plutonium oxides from first principles. *Phys. Rev. B*, 78:075125, Aug 2008.

[120] A. Szilva, M. Costa, A. Bergman, L. Szunyogh, L. Nordström, and O. Eriksson. Interatomic exchange interactions for finite-temperature magnetism and nonequilibrium spin dynamics. *Phys. Rev. Lett.*, 111:127204, Sep 2013.

[121] K. H. Weyrich. Full-potential linear muffin-tin-orbital method. *Phys. Rev. B*, 37:10269–10282, Jun 1988.

[122] A. G. Petukhov, I. I. Mazin, L. Chioncel, and A. I. Lichtenstein. Correlated metals and the LDA+U method. *Phys. Rev. B*, 67:153106, Apr 2003.

[123] I Galanakis, Ph Mavropoulos, and P H Dederichs. Electronic structure and Slater-Pauling behaviour in half-metallic heusler alloys calculated from first principles. *Journal of Physics D: Applied Physics*, 39(5):765, 2006.

[124] P. J. Webster and K. R. A. Ziebeck. *In Alloys and Compounds of d-Elements with Main Group Elements. Part 2*. Springer-Verlag, Berlin, 1988.

[125] Y. O. Kvashnin, O. Grånäs, I. Di Marco, M. I. Katsnelson, A. I. Lichtenstein, and O. Eriksson. Exchange parameters of strongly correlated materials: Extraction from spin-polarized density functional theory plus dynamical mean-field theory. *Phys. Rev. B*, 91:125133, Mar 2015.

[126] Ph. Mavropoulos, K. Sato, R. Zeller, P. H. Dederichs, V. Popescu, and H. Ebert. Effect of the spin-orbit interaction on the band gap of half metals. *Phys. Rev. B*, 69:054424, Feb 2004.

[127] S. Picozzi, A. Continenza, and A. J. Freeman. Co_2MnX (X=Si,Ge, Sn) heusler compounds: An *ab initio* study of their structural, electronic, and magnetic properties at zero and elevated pressure. *Phys. Rev. B*, 66:094421, Sep 2002.

[128] M. P. Raphael, S. F. Cheng, B. N. Das, B. Ravel, B. Nadgorny, G. Trotter, E. E. Carpenter, and V. G. Harris. *MRS Proceedings*. Spring Meeting, 2001.

[129] L. Chioncel, E. Arrigoni, M. I. Katsnelson, and A. I. Lichtenstein. Majority-spin nonquasiparticle states in half-metallic ferrimagnet Mn_2VAl. *Phys. Rev. B*, 79:125123, Mar 2009.

[130] J. Kübler. Proceedings of the 4th general conference of the condensed matter division of the eps first principle theory of metallic magnetism. *Physica B+C*, 127(1):257 – 263, 1984.

[131] L. Makinistian, Muhammad M. Faiz, Raghava P. Panguluri, B. Balke, S. Wurmehl, C. Felser, E. A. Albanesi, A. G. Petukhov, and B. Nadgorny. On the half-metallicity of Co_2FeSi heusler alloy: Point-contact Andreev reflection spectroscopy and *ab initio* study. *Phys. Rev. B*, 87:220402, Jun 2013.

[132] M. Jourdan, J. Minár, J. Braun, A. Kronenberg, S. Chadov, B. Balke, A. Gloskovskii, M. Kolbe, H.J. Elmers, G. Schönhense, H. Ebert, C. Felser, and M. Kläui. Direct observation of half-metallicity in the heusler compound Co_2MnSi. *Nat Commun*, 5, 2014.
[133] Claudia Felser and Atsufumi Hirohata. *Heusler Alloys: Properties, Growth, Applications*. Physics of Solids and Liquids. Springer US, 2016.
[134] J. H. van Vleck. On the anisotropy of cubic ferromagnetic crystals. *Phys. Rev.*, 52:1178–1198, Dec 1937.
[135] Tôru Moriya. Anisotropic superexchange interaction and weak ferromagnetism. *Phys. Rev.*, 120:91–98, Oct 1960.
[136] Alessio Filippetti and Warren E. Pickett. Magnetic reconstruction at the (001) $CaMnO_3$ surface. *Phys. Rev. Lett.*, 83:4184–4187, Nov 1999.
[137] Alessio Filippetti and Warren E. Pickett. Double-exchange-driven spin pairing at the (001) surface of manganites. *Phys. Rev. B*, 62:11571–11575, Nov 2000.
[138] R. A. de Groot, F. M. Mueller, P. G. van Engen, and K. H. J. Buschow. New class of materials: Half-metallic ferromagnets. *Phys. Rev. Lett.*, 50:2024–2027, Jun 1983.
[139] S. Keshavarz, Y. O. Kvashnin, D. C. M. Rodrigues, M. Pereiro, I. Di Marco, C. Autieri, L. Nordström, I. V. Solovyev, B. Sanyal, and O. Eriksson. Exchange interactions of $camno_3$ in the bulk and at the surface. *Phys. Rev. B*, 95:115120, Mar 2017.
[140] J. Kübler, G. H. Fecher, and C. Felser. Understanding the trend in the curie temperatures of co_2-based heusler compounds: Ab initio calculations. *Phys. Rev. B*, 76:024414, Jul 2007.
[141] Erik R. Ylvisaker, Warren E. Pickett, and Klaus Koepernik. Anisotropy and magnetism in the LSDA + U method. *Phys. Rev. B*, 79:035103, Jan 2009.
[142] T. N. Casselman and F. Keffer. Right-angled superexchange. *Phys. Rev. Lett.*, 4:498–500, May 1960.

Acta Universitatis Upsaliensis

Digital Comprehensive Summaries of Uppsala Dissertations from the Faculty of Science and Technology 1720

Editor: The Dean of the Faculty of Science and Technology

A doctoral dissertation from the Faculty of Science and Technology, Uppsala University, is usually a summary of a number of papers. A few copies of the complete dissertation are kept at major Swedish research libraries, while the summary alone is distributed internationally through the series Digital Comprehensive Summaries of Uppsala Dissertations from the Faculty of Science and Technology. (Prior to January, 2005, the series was published under the title "Comprehensive Summaries of Uppsala Dissertations from the Faculty of Science and Technology".)

Distribution: publications.uu.se
urn:nbn:se:uu:diva-357525

ACTA
UNIVERSITATIS
UPSALIENSIS
UPPSALA
2018